RIDE COMFORT IMPROVEMENT BY APPLICATION OF TUNED MASS DAMPERS AND LEVER TYPE VIBRATION ISOLATORS

A THESIS SUBMITTED TO
THE GRADUATE SCHOOL OF NATURAL AND APPLIED SCIENCES
OF
MIDDLE EAST TECHNICAL UNIVERSITY

BY

GÖKSU AYDAN

IN PARTIAL FULFILLMENT OF THE REQUIREMENTS
FOR
THE DEGREE OF MASTER OF SCIENCE
IN
MECHANICAL ENGINEERING

JULY 2010

Approval of the Thesis:

RIDE COMFORT IMPROVEMENT BY APPLICATION OF TUNED MASS DAMPERS AND LEVER TYPE VIBRATION ISOLATORS

submitted by **GÖKSU AYDAN** in partial fulfillment of the requirements for the degree of **Master of Science in Mechanical Engineering Department, Middle East Technical University** by,

Prof. Dr. Canan Özgen _____
Dean, Graduate School of **Natural and Applied Sciences**

Prof. Dr. Süha Oral _____
Head of Department, **Mechanical Engineering**

Assist. Prof. Dr. Ender Ciğeroğlu _____
Supervisor, **Mechanical Engineering Dept., METU**

Inst. Dr. S. Çağlar Başlamışlı _____
Co-Supervisor, **Mechanical Engineering Dept., Hacettepe U.**

Examining Committee Members:

Prof. Dr. Y. Samim Ünlüsoy _____
Mechanical Engineering Dept., METU

Assist. Prof. Dr. Ender Ciğeroğlu _____
Mechanical Engineering Dept., METU

Inst. Dr. S. Çağlar Başlamışlı _____
Mechanical Engineering Dept., Hacettepe University

Assoc. Prof. Dr. Serkan Dağ _____
Mechanical Engineering Dept., METU

Inst. Dr. Can Ulaş Doğruer _____
Mechanical Engineering Dept., Hacettepe University

Date: 09.07.2010

I hereby declare that all information in this document has been obtained and presented in accordance with academic rules and ethical conduct. I also declare that, as required by these rules and conduct, I have fully cited and referenced all material and results that are not original to this work.

Name, Last name : Göksu, Aydan

Signature :

ABSTRACT

RIDE COMFORT IMPROVEMENT BY APPLICATION OF TUNED MASS DAMPERS AND LEVER TYPE VIBRATION ISOLATORS

Aydan, Göksu

M.Sc., Department of Mechanical Engineering

Supervisor : Assist. Prof. Dr. Ender Ciğeroğlu

Co-Supervisor: Inst. Dr. S. Çağlar Başlamışlı

July 2010, 103 pages

In this study, the efficiency of linear and rotational tuned mass dampers (TMD) and lever type vibration isolators (LVI) in improving ride comfort is investigated based on a vehicle quarter-car model. TMDs reduce vibration levels by absorbing the energy of the system, especially at their natural frequencies. Both types of TMDs are investigated in the first part of this study. Although linear TMDs can be implemented more easily on suspension systems, rotational TMDs show better performance in reducing vibration levels; since, the inertia effect of rotational TMDs is higher than the linear TMDs. In order to obtain better results with TMDs, configurations with chain of linear TMDs are obtained in the second part of the study without changing the original suspension stiffness and damping coefficient. In addition to these, the effect of increasing the number of TMDs used in the chain configuration is investigated. Results show that performance deterioration at lower frequencies than wheel hop is reduced by using chain of TMDs. In the third part of this study, various configurations of LVIs with different masses are considered and significant attenuation of vibration amplitudes at both body bounce and wheel hop frequencies is achieved. Results show that TMDs improve ride comfort around wheel hop frequency while LVIs are quite efficient around body bounce frequency. Finally,

parameter uncertainty due to aging of components and manufacturing defects are investigated.

Keywords: Tuned Mass Damper, Tuned Vibration Absorber, Lever Type Vibration Isolator, Suspension Optimization, Ride Comfort

ÖZ

AYARLANABİLİR KÜTLELİ VE KALDIRAÇ TİPLİ SÖNÜMLEYİCİLER KULLANILARAK SÜRÜŞ KONFORUNUN ARTIRIMI

Aydan, Göksu

Yüksek Lisans, Makine Mühendisliği Bölümü

Tez Yöneticisi : Yrd. Doç. Dr. Ender Ciğeroğlu

Ortak Tez Yöneticisi: Öğr. Gör. Dr. S. Çağlar Başlamışlı

Temmuz 2010, 103 sayfa

Bu çalışmada, doğrusal ve açısal ayarlanabilir kütleli sönümleyiciler (AKS) ve kaldıraç tipli sönümleyiciler (KTS) kullanılarak, çeyrek araba modeli üzerinde sürüş konforunun iyileştirilmesi hedeflenmiştir. AKS'ler sistemin enerjisini, özellikle kendi doğal frekanslarında emerek titreşim seviyelerini azaltır. Çalışmanın ilk aşamasında iki tip AKS üzerinde çalışılmıştır. Doğrusal AKS'ler daha az yer kapladığından, süspansiyon sistemine daha rahat uygulanabilmesine rağmen, açısal AKS'ler titreşim düzeyini bastırmada daha iyi performans göstermiştir. Bunun sebebi, açısal AKS'lerin atalet etkisinin daha fazla olmasıdır. AKS uygulamalarından daha iyi performans alabilmek için, çalışmanın ikinci aşamasında, toplam süspansiyon direngenliğini ve sönümleme katsayısını değiştirmeden doğrusal AKS'lerden oluşan zincir, çeyrek araba modeline uygulanmıştır. Bu yeni konfigürasyonda, zincirde kullanılan AKS sayısının etkisi de incelenmiştir. Elde edilen sonuçlara göre, daha düşük frekanslardaki ivme artışı en aza indirilmiştir. Çalışmanın üçüncü aşamasında, çeşitli konfigürasyonlarda ve çeşitli kütlelerde KTS uygulamaları yapılmış ve gövde sıçrama ve tekerlek sıçrama frekanslarında önemli iyileştirme sağlanmıştır. Elde edilen sonuçlara göre, AKS'ler sürüş konforunu tekerlek sıçrama frekansında iyileştirirken, KTS'ler gövde sıçrama frekansında daha fazla etkili olmuştur. Son

olarak, üretim hatalarından ve bileşenlerin eskimesinden kaynaklanan parametre belirsizlikleri incelenmiştir.

Anahtar Kelimeler: Ayarlanabilir Kütleli Sönümleyici, Ayarlanabilir Titreşim Emici, Kaldıraç Tipli Sönümleyici, Süspansiyon Optimizasyonu, Sürüş Konforu

to my dear family

ACKNOWLEDGEMENTS

First, I would like to express my deepest appreciation to my supervisor Asst. Prof. Dr. Ender Ciğeroğlu and to my co-supervisor Inst. Dr. S. Çağlar Başlamışlı for their guidance, support, supervision and encouragement throughout my thesis study. Additionally, I would like to thank Prof. Dr. Y. Samim Ünlüsoy who has shared his experience with me.

I am very grateful to my closest colleague Caner Boral for his assistance and support in my thesis study. Also, financial support of Münir Birsel Foundation is also gratefully acknowledged.

I would like to express my deepest gratitude to my parents Mahser and Dündar Aydan and my sister Gözde Aydan for their unconditional support and encouragement throughout my life. I would also like to express my deepest appreciation to Seda Öztürk for her endless support and giving me the strength to carry on my study in all my hard times.

TABLE OF CONTENTS

LIST OF FIGURES

FIGURES

LIST OF TABLES

TABLES

LIST OF SYMBOLS

$[C]$	Damping Matrix
$[K]$	Stiffness Matrix
$[M]$	Mass Matrix
$[\alpha(\omega)]$	Receptance Matrix
$\{X(\omega)\}$	State Vector in Frequency Domain
$\{x\}$	Position Vector
$\{x_{LTMD}\}$	State Vector of Single LTMD under Random Input
$\{x_{qc}\}$	State Vector of Quarter-Car Model under Random Input
$\{y_0\}$	Position Vector
A	Area under Sprung Mass Acceleration vs Frequency Plot
A_i	i^{th} Area under Sprung Mass Acceleration vs Frequency Plot
A_T	Sum of Areas Multiplied by Their Weighting Coefficients
a	Sprung Mass Acceleration
c_i	Damping Coefficient of i^{th} TMD's Viscous Damper
c_s	Damping Coefficient of Suspension Viscous Damper
c_{si}	Damping Coefficient of i^{th} Suspension Viscous Damper
F_r	Force Input due to Tyre Deflection
F	Force due to Road Irregularities
k_i	Stiffness Constant of i^{th} TMD's Spring
k_s	Stiffness Constant of Suspension Spring
k_{si}	Stiffness Constant of i^{th} Suspension Spring
k_t	Tire Stiffness
l_1	Length of Lever of LVI 1
l_2	Distance between Pins in LVI 1

l_3	Length of Lever of LVI 2
l_4	Distance between Pins in LVI 2
l_{r1}	Length of Lever in RTMD
l_{r2}	Distance between Pin and Spring in RTMD
m_i	Mass of i^{th} TMD and LVI
m_p	Mass of Plate in LVI Configuration
m_{pi}	Mass of i^{th} Plate in Chain of LTMD Configuration
m_s	Sprung Mass
m_{us}	Unsprung Mass
n	Total Number of Building Blocks in Chain of LTMD Configuration
V	Forward Velocity
v_i	Displacement of i^{th} LVI
w_i	Displacement of i^{th} LTMD in Chain of LTMD Configuration
$w(t)$	White Noise Input
$y(t)$	Road Surface Displacement Profile
$\dot{y}(t)$	Road Surface Velocity Profile
z_i	Weighting Coefficient of i^{th} Area
α_i	Ratio of Length of Lever to the Distance between Pins in i^{th} LVI
β	Breakaway Frequency
σ^2	Variance of the Road Irregularities
θ_1	Rotation Angle of Lever in RTMD
ξ_{LTMD}	Damping Ratio of LTMD
ξ_{RTMD}	Damping Ratio of RTMD
ξ_{TMD}	Damping Ratio of TMD
ω	Frequency
ω_{LTMD}	Natural Frequency of LTMD
ω_{RTMD}	Natural Frequency of LTMD

LIST OF ABBREVIATIONS

DOF	Degrees of Freedom
fr	Frequency Range (Area Boundary)
LTMD	Linear Tuned Mass Damper
LVI	Lever Type Vibration Isolator
RTMD	Rotational Tuned Mass Damper
TMD	Tuned Mass Damper

CHAPTER 1

INTRODUCTION

One major source of discomfort for automobile passengers consists of road irregularities. Passive suspension systems and tires can adequately isolate passengers from road inputs only at specific frequency ranges. At some frequencies, such as "body bounce" and "wheel hop", the classical passive suspension system increases vibration amplitudes due to resonance. These vibrations reduce not only the ride comfort of passengers, but also the quality of the ride.

In the literature, many active suspension systems have been designed to attenuate vibrations especially at "body bounce" frequency [1,2]. Nevertheless this type of suspensions indirectly increases fuel consumption due to high energy consumption of sensors and actuators. Furthermore their initial and maintenance costs are high. Therefore, as far as fuel consumption and cost is concerned, passive systems are advantageous over active systems.

The performance of suspension system is identified by three important parameters; a) ride comfort, b) suspension stroke, c) road holding. In literature, ride comfort is measured by sprung mass acceleration when the velocity input from road surface is considered. Ride comfort is an important criteria for passengers especially travelling long distances without feeling tired. Suspension stroke is a constraint in design process in order not to have packaging problems and road holding characteristic of a

vehicle is measured by variations in the tire-road contact. Decreasing the variations of the tire-road contact force from its static value increases road holding.

1.1 TRADITIONAL LIMITATIONS OF PASSIVE SUSPENSION OPTIMIZATION

Formerly, it was thought that, ride comfort increases as the stiffness constant of suspension decreases [3]. However, there exist several constraints while identifying suspension stiffness coefficient. Firstly, stiffness constant cannot be lower than a certain value in order to limit static deflection. Fully loaded conditions of vehicle should also be considered for static deflection. Moreover as the suspension spring constant is reduced, the body bounce frequency is reduced and discomfort of passengers increases due to the coincidence of heart beat frequency with wheel hop frequency around 1 Hz. Further reduction of body bounce frequency (around 0.5 Hz) causes sea sickness. Therefore, body bounce frequency is generally settled at around 1.2 Hz.

In this thesis, passive TMDs and LVIs are implemented on a quarter car vehicle model in order to assess the abilities of each isolator type in attenuating sprung mass vibrations around "wheel hop" and "body bounce" frequencies.

1.2 QUARTER-CAR MODEL

The quarter-car model is a basic vehicle ride model including the tire, the unsprung mass (mass below the suspension) and the share of the sprung mass (mass above the suspension) on a single suspension (Figure 1.1). Although it is quite a simple model, it gives considerably accurate results at the beginning stage of the suspension design process for automobiles. In the present study, the sprung and the unsprung masses are denoted by m_s and m_{us} respectively. The tire stiffness and suspension springs are k_t and k_s respectively and damping coefficient of the suspension viscous damper

is c_s. The road input due to irregularities is taken as y. Tire damping is small; therefore, it is neglected. The parameters of a typical quarter-car model for a mid-sized saloon passenger car obtained from Ünlüsoy [3] are given in Table 1.1.

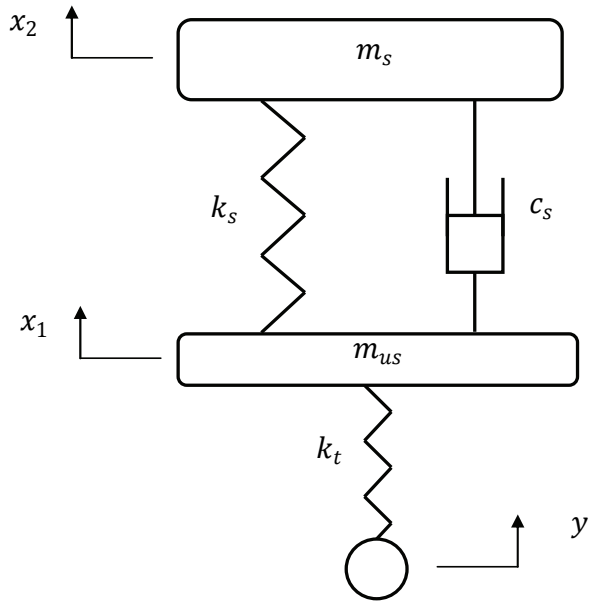

Figure 1.1 Quarter-Car Model

Table 1.1 Parameter Values of Quarter-Car Model [3]

Parameters	Values
$\boldsymbol{m_s}$	320 kg
$\boldsymbol{m_{us}}$	46 kg
$\boldsymbol{c_s}$	980 Ns/m
$\boldsymbol{k_s}$	15000 N/m
$\boldsymbol{k_t}$	145000 N/m

1.3 TUNED MASS DAMPERS AND LEVER TYPE VIBRATION ISOLATORS

TMDs are narrowband vibration absorbers which can suppress the vibrations of the structures at their natural frequencies. A TMD is simply modeled by a mass which is connected to the main structure with a spring and a viscous damper (Figure 1.2). Generally, TMDs are connected to the points where the displacement is maximum. When the structure vibrates around the natural frequency of the TMD, TMD absorbs some of the energy of the system and dissipates it with the help of the viscous damper on it.

Lever type vibration isolators (Figure 1.3) are generally utilized in aerospace industry because vibration isolation can be obtained with a small mass attached on a lever. Lever is pinned between two platforms and attenuates the vibrations in case a relative motion occurs between the two platforms.

1.4 LITERATURE SURVEY

The TMD was firstly patented by Frahm in 1911 (U.S. Patent No. 989,958) and the application was related to the decrease of the rolling motion and vibration reduction of ship hulls [5,6]. The theory behind the vibration absorption properties of TMDs was first given in the papers of Ormondroyd and Den Hartog [5]. Den Hartog discusses the optimal tuning of TMDs in his book [5]. Later on TMDs were mostly involved in the suppression of wind induced vibrations of buildings [7-11] and in the attenuation of seismic responses of structures [8,10-14]. There exists several real life applications of TMD applied on buildings for the reduction of the vibrations due to wind and earthquakes. It is reported that the vibration response of Sydney Tower is reduced approximately by 40-50% through the application of TMDs [0,16]. Another example in Japan is Higashimyama Sky Tower, where the vibration response is reduced by 30-50% through the application of TMDs [0,17]. Furthermore, there are

several application examples of TMDs on bridges and especially on high speed railway bridges [18,19]. Lin et. al. [20] applied TMDs for suppressing the coupled flexural and torsional buffeting response of long-span bridges. Matsumoto et al [21], used TMDs made up of steel plates and suspended by springs on a footbridge to attenuate vibrations due to walking [6]. Moreover, there are numerous examples of TMD applications in the literature for suppressing floor vibrations [21-23]. Setareh et. al. [6], used a pendulum-type TMD, also called rotational TMD, to control floor vibrations.

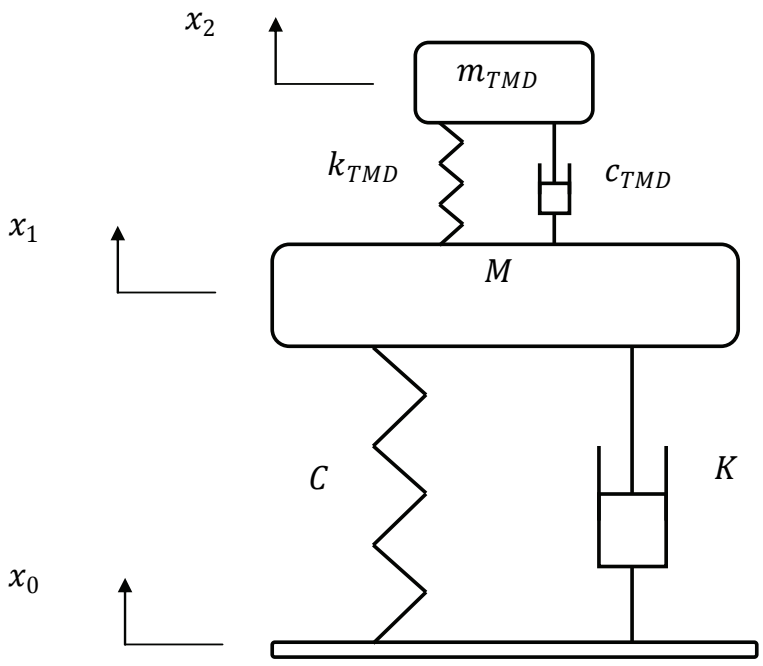

Figure 1.2 Tuned Mass Damper Model is Assessed on Structure

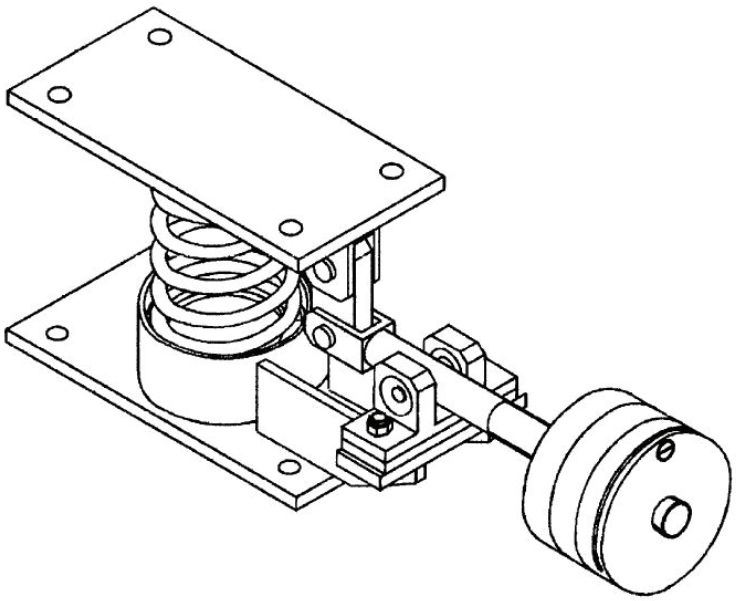

Figure 1.3 Lever Type Vibration Isolator [4]

TMDs are also used for the mitigation of rail rutting corrugation [25], on the hard disc actuators to reduce vibrations [26,27], on flexible marine structures when a ship is berthed [28], on turning machines to reduce chattering [29]. It is possible to see examples of TMDs in the nature. Yolk, albumen and shell of an egg is an example of TMD to protect the embryo [6,24]. In the aerospace industry, TMDs have been used in DC-9 aircraft in order to suppress the internal noise of the aircraft to an acceptable value [5]. Another example consists of a TMD is placed on Pratt & Whitney's R-1820 aircraft engine to reduce excessive vibration causing failure of the engine [5]. There exists a patent on the application of TMD on integrally bladed turbine rotor [30]. Since TMDs are narrow band vibration absorbers, multiple TMD applications on structures are presented in [31-35] in order to increase the effective frequency range of TMDs. Igusa [34] and Jangid [35] have shown that multiple TMDs are more robust and less sensitive to system parameters. In the literature semi-active and active

TMD application are also available to increase the effectiveness of TMDs [5,22,36,37].

Although TMDs are widely used on structures such as buildings and bridges, studies on the implementation of TMDs on road vehicles for the purpose of ride improvement are extremely scarce in literature. Chen et. al. [38] investigated the performance of TMD implemented on a truck, a bridge and finally on both a truck and a bridge under windy conditions. Another study of TMD application on trucks is done by Muluka [39], for the reduction of dynamic tire loads and the improvement of trucks' road friendliness.

Application areas of TMDs on automobiles are exhaust hangers, steering systems, engine frames and mirrors [40], which are by no means related to ride comfort improvement. In the automobile steering system, a torsional tuned mass damper is generally connected in series to the steering column to eliminate the first mode of vibration of the steering column [41-44]. In the patent owned by Goetchius [45], it is mentioned that a small TMD may be used in brake assembly to reduce brake induced vibrations. In the slip phase of clutches, the alternating torque generated by the engine causes chatter vibrations and a torsional friction dependent TMD on clutches is prone to suppress chatter vibrations [46]. Furthermore the patent owned by Cerri et al. proposes multidimensional TMD for the suspension links of automobiles [47]. It is known that TMDs were first used as a major element of the automobile suspension by the Citroen 2CV [48]. Furthermore it was also used in Formula 1 by the Renault Team in 2005 in order to increase the road holding especially on the kerbs; but it was forbidden by FIA [49].

Dynamic anti-resonant vibration isolators (also called LVI) were firstly patented by Flannelly in 1967 [50]. The objective was to create an isolator which had considerably lower static deflection than other isolators and also provided isolation for low frequency excitations. Theoretically, hundred percent isolation is provided at

a tuned anti-resonant frequency and practically very close to hundred percent isolation is then obtained [50]. Since isolation is provided by a very small mass compared to the isolated mass, dynamic anti-resonant vibration isolators are useful for systems where weight reduction is important such as aircrafts. Goodwin [51] and Halwes [52] provided hydraulic equivalents of dynamic anti-resonant vibration isolator [53]. It is possible to observe the applications of dynamic anti-resonant vibration isolators in the aerospace industry. An application example of a dynamic anti-resonant vibration isolator on an Army furnished UH-1H helicopter for rotor isolation is proposed by Rita et al [54] and significant results in the reduction of fuselage vibrations were obtained. In Jones' study [55], fuselage is isolated from the vibrations due to rotor induced shear forces and moments. Similar studies on rotor isolation are available in the literature [56,57]. Hydraulic engine mounts [58,59] that have inertia-track, have the same working principle with LVI systems proposed by Goodwin [51] and Halwes [52].

In order to make a proper comparison between the standard quarter-car model and the LVI added model, the total stiffness and damping coefficients of the suspension are taken as constant in this study. Therefore a viscous damper is added on the LVI to satisfy the equivalent damping coefficient. Since a damper is added on the isolator, there will be no anti-resonance created at any frequency. In the study by Yilmaz et al. [2], a two degree of freedom model of a dynamic anti-resonant vibration isolator is applied on the quarter-car model to reduce the tire induced noise and vibration. However, in the model, the total stiffness constant and damping coefficient of the suspension were not fixed.

Although it has been stated that the single degree of freedom model for dynamic anti-resonant vibration isolator is not the ideal design [4,61], both single and two degree of freedom models are investigated in this study with different configurations.

1.5 SCOPE OF THESIS

The purpose in this study, is to investigate the efficiency of linear and rotational TMDs and LVIs in improving ride comfort based on a vehicle quarter-car model. Linear and rotational TMDs, chain of linear TMDs and LVIs with different configurations and with different masses are investigated on quarter model and their performance in reducing sprung mass acceleration are compared. Furthermore, in the dilemma of restriction of additional mass to the car and increase of efficiency of TMDs/LVIs with higher masses, an optimization problem rises. Therefore all the configurations in the study are optimized in order to get optimal ride comfort with a small mass as much as possible. Moreover the optimization results obtained under harmonic input are verified under random road input. Finally, parameter uncertainty due to aging of components, manufacturing defects and change of sprung mass according to loading conditions, are investigated.

1.6 OUTLINE

In chapter 2, linear and rotational TMDs on quarter car model are investigated. Linear and rotational TMDs are assessed on unsprung mass separately and optimized for the reduction of sprung mass acceleration. Comparison between linear and rotational TMDs are made.

In chapter 3, a model with chain of linear TMDs is prepared. Total suspension stiffness and damping values are taken as constant. According to the optimized results the effect of number of linear TMDs, total additional mass and weighting coefficients of optimization are investigated.

In chapter 4, the effect of LVI on sprung mass acceleration is investigated with six different configurations. Parameters of LVI are optimized and comparison between configurations are made. Effect of mass of LVI is also investigated.

In chapter 5, the performance of chain of linear TMD and a LVI configuration is tested under random input. Analysis are made on both frequency and time domain.
In chapter 6, Monte Carlo simulations are made for different configurations in order to see the effects of parameter change due to aging, manufacturing defect and loading conditions.

In chapter 7, discussion, conclusion and future work are given.

CHAPTER 2

SINGLE LINEAR AND ROTATIONAL TUNED MASS DAMPER APPLICATION

2.1 INTRODUCTION

TMD application on buildings and bridges is an accustomed process since the additional mass on structures do not cause significant problems. As far as the application of TMDs on automobiles is concerned, added masses must be very small compared to the total vehicle mass, since extra mass increases fuel consumption and decreases overall performance of the vehicle. On the contrary, it is known that TMDs are more effective when the ratio of additional mass to the system mass is large. Therefore decreasing the sprung mass acceleration by adding a small mass on sprung mass is not feasible.

It is known that there are two resonance frequencies of quarter car model called wheel hop and body bounce. Since it is not possible to decrease sprung mass acceleration by using a small mass at body bounce frequency, reduction of sprung mass acceleration can be achievable at wheel hop frequency by using a small mass added on the unsprung mass. As the vibration of unsprung mass is attenuated, the transmitted force from unsprung mass to the sprung mass can be reduced around wheel hop frequency. Consequently sprung mass acceleration can be reduced.

2.2 MODELLING WITH SINGLE LINEAR TMD

The configuration with a single linear TMD (LTMD) added on the unsprung mass can be seen in Figure 2.1. Displacements of the unsprung mass, the sprung mass and the LTMD are x_1, x_2 and x_3, respectively. The input to the model due to road irregularities is:

$$F_r = (y - x_1)k_t. \tag{2.1}$$

Equations of motion of the 3-DOF system are given by:

$$[M]\{\ddot{x}\} + [C]\{\dot{x}\} + [K]\{x\} = k_t\{y_0\}, \tag{2.2}$$

where the mass, damping and stiffness matrices and position vector are:

$$[M] = \begin{bmatrix} m_{us} & 0 & 0 \\ 0 & m_s & 0 \\ 0 & 0 & m_1 \end{bmatrix}, \tag{2.3}$$

$$[C] = \begin{bmatrix} c_s + c_1 & -c_s & -c_1 \\ -c_s & c_s & 0 \\ -c_1 & 0 & c_1 \end{bmatrix}, \tag{2.4}$$

$$[K] = \begin{bmatrix} k_s + k_t + k_1 & -k_s & -k_1 \\ -k_s & k_s & 0 \\ -k_1 & 0 & k_1 \end{bmatrix}, \tag{2.5}$$

$$\{x\} = \begin{Bmatrix} x_1 \\ x_2 \\ x_3 \end{Bmatrix}, \tag{2.6}$$

$$\{y_0\} = \begin{Bmatrix} y \\ 0 \\ 0 \end{Bmatrix}. \tag{2.7}$$

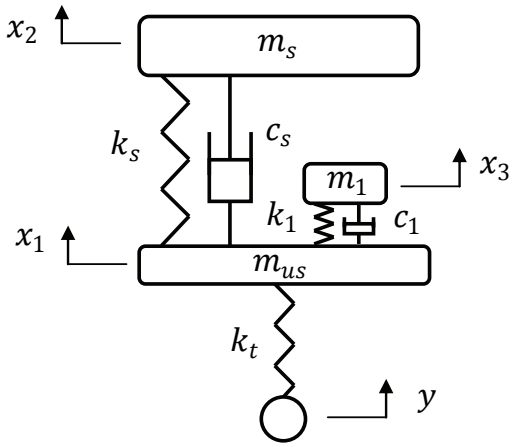

Figure 2.1 Quarter-Car Model with Single LTMD on Unsprung Mass

The natural frequency of the LTMD is $\omega_{LTMD} = \sqrt{k_1/m_1}$ and the damping ratio is $\xi_{LTMD} = c_1/2m_1\omega_{LTMD}$.

2.3 MODELLING WITH SINGLE ROTATIONAL TMD

In this model, the performance of a rotational TMD (RTMD) added on the sprung mass is analyzed (Figure 2.2). The lever can rotate around a pinned support and the angle of rotation of the lever is denoted by θ_1. The angle of the lever is assumed to be small; therefore, linear theory is used. Displacements of the unsprung mass and the sprung mass are x_1 and x_2, respectively. The mass of the lever is neglected. The viscous damper with a damping coefficient of c_1 is attached between m_1 and unsprung mass where the velocity of the lever is maximum. The RTMD spring is connected to the lever at a distance l_{r2} from the support, which is half of l_{r1}. In addition, the length of the lever is limited to 0.3 m.

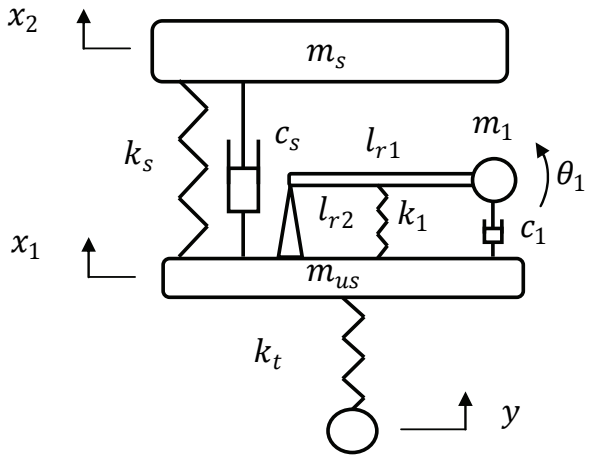

Figure 2.2 Quarter-Car Model with Single RTMD on Unsprung Mass

The equations of motion of the system are given by equation (2.2) where the mass, damping and stiffness matrices and the position vectors are as follows:

$$[M] = \begin{bmatrix} m_s & 0 & 0 \\ 0 & m_{us} + m_1 & m_1 l_{r1} \\ 0 & m_1 l_{r1} & m_1 l_{r1}^2 \end{bmatrix}, \tag{2.8}$$

$$[C] = \begin{bmatrix} c_s & -c_s & 0 \\ -c_s & c_s & 0 \\ 0 & 0 & c_1 l_{r1}^2 \end{bmatrix}, \tag{2.9}$$

$$[K] = \begin{bmatrix} k_s & -k_s & 0 \\ -k_s & k_s + k_t & 0 \\ 0 & 0 & k_1 l_{r2}^2 \end{bmatrix}, \tag{2.10}$$

$$\{x\} = \begin{Bmatrix} x_2 \\ x_1 \\ \theta \end{Bmatrix}, \tag{2.11}$$

$$\{y_0\} = \begin{Bmatrix} 0 \\ y \\ 0 \end{Bmatrix}. \tag{2.12}$$

The natural frequency of the RTMD is $\omega_{RTMD} = (l_{r2}/l_{r1})\sqrt{k_1/m_1}$ and the damping ratio is $\xi_{RTMD} = c_1/2m_1\omega_{RTMD}$

2.4 OPTIMIZATION PROBLEM

The optimization parameters for the single LTMD and RTMD systems consist of the concentrated mass m_1, TMD stiffness constant k_1 and damping ratio of TMDs.

In the literature, ride comfort is commonly assessed through sprung mass acceleration under road velocity input. Hence, the objective is to reduce sprung mass acceleration as much as possible with minimum performance deterioration. For an harmonic input, the receptance matrix and state vector can be found as follows:

$$[\alpha(\omega)] = \left[[K] - \omega^2[M] + i\omega[C]\right]^{-1}, \tag{2.13}$$

$$\{X(\omega)\} = [\alpha(\omega)]\,\{F(y)\}. \tag{2.14}$$

If the harmonic velocity input to the tire from road surface is taken as:

$$\dot{y}(t) = Ae^{i\omega t}, \tag{2.15}$$

displacement can be found as:

$$y(t) = \frac{A}{i\omega}e^{i\omega t}, \tag{2.16}$$

Then the force input to the unsprung mass can be calculated as

$$F(t) = k_t y(t) = k_t \frac{A}{i\omega} e^{i\omega t}. \tag{2.17}$$

After finding the displacement of the sprung mass $X(\omega)$ in frequency domain, it is easy to find the acceleration of the sprung mass.

$$|a(\omega)| = \omega^2 |\{x(\omega)\}|. \tag{2.18}$$

The objective function is selected as the area under the sprung mass acceleration vs frequency plot curve.

$$A = \int_{0\ Hz}^{24\ Hz} |a(\omega)| d\omega. \tag{2.19}$$

In order not to deteriorate performance of the system at any frequency, total area is divided into several parts and optimization function is redefined as the sum of areas multiplied by selected weighting coefficients.

$$A_i = \int_{fr_i} |a(\omega)| d\omega, \tag{2.20}$$

where fr_i (Table 2.1) is the frequency range that area under sprung mass acceleration vs frequency curve is calculated.

$$\sum_{i=1}^{n} A_i z_i = A_T. \tag{2.21}$$

A typical area division consisting of six parts is given in Figure 2.3. In the present problem, areas are divided according to the frequency ranges given in Table 2.1. The coefficients obtained for the best performance of each configuration, are given in Table 2.2.

A lower limit to the damping ratios of TMDs is imposed in order not to deteriorate performance of the system at frequencies lower than the natural frequency of TMDs.

Table 2.1 Area Boundaries

Area	Frequency Range (fr) [Hz]
A_1	0 – 1
A_2	1 – 1.5
A_3	1.5 – 3
A_4	3 – 4
A_5	4 – 5
A_6	5 – 6
A_7	6 – 7
A_8	7 – 8
A_9	8 – 9
A_{10}	9 – 10
A_{11}	10 – 11
A_{12}	11 – 24

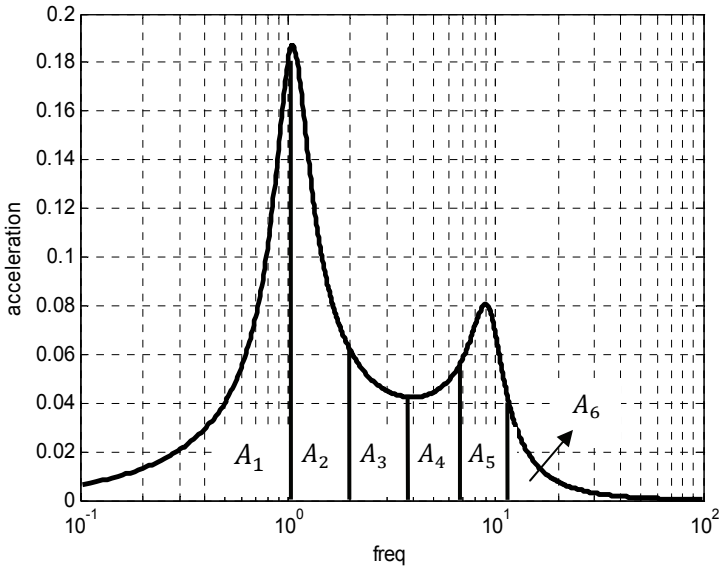

Figure 2.3 Sample Area Division

The statement of the optimization problem is:

$$\text{minimize} \qquad A_T = \sum_{i=1}^{n} \left(z_i \int_{fr_i} |a(\omega)| d\omega \right), \tag{2.22}$$

subject to

$$m_1 \leq 3\ kg, \tag{2.23}$$

$$\xi_{\text{TMD}} < 1. \tag{2.24}$$

Pattern Search command of MATLAB® is utilized in optimization and details of Pattern Search are given in Appendix.

Table 2.2 Weighting Coefficients

Coefficients	Single LTMD	Single RTMD
z_1	1	1
z_2	1	1
z_3	1	1
z_4	4	1
z_5	7	1
z_6	7	3
z_7	6	3
z_8	4	3
z_9	4	3
z_{10}	3.5	3
z_{11}	1	1
z_{12}	0	0

2.5 RESULTS

The optimization results obtained for LTMD and RTMD configurations are given below. In order to keep the system inside practical limits, the total additional mass is limited to 3 kg. Optimal parameter values are given in Table 2.3.

The natural frequencies of LTMD and RTMD are:

$$\omega_{LTMD} = \sqrt{\frac{k_1}{m_1}} = 7.72\ Hz, \tag{2.25}$$

$$\omega_{RTMD} = \left(\frac{l_{r2}}{l_{r1}}\right)\sqrt{\frac{k_1}{m_1}} = 8.08\ Hz, \tag{2.26}$$

which are slightly lower than the wheel hop frequency.

Table 2.3 Optimization Results for Single LTMD and Single RTMD Configurations

	Single RTMD	**Single LTMD**
$\boldsymbol{m_1}$ [kg]	3	3
$\boldsymbol{k_1}$ [N/m]	30943	7056
$\boldsymbol{\xi_1}$	0.20	0.20

2.5.1 COMPARISON OF SINGLE LTMD AND SINGLE RTMD

The performance comparison of a single LTMD and a single RTMD in reducing sprung mass acceleration can be seen in Figure 2.4. Both types of TMDs suppress the vibrations around "wheel hop" frequency. The percent improvements in sprung mass acceleration of both types of TMDs are given in Figure 2.5. The plot is obtained by dividing the difference of sprung mass acceleration of modified system and standard quarter car model to the acceleration of the sprung mass of the standard quarter car model. It can be seen that the percent improvement achieved by the RTMD is higher than 25% around 9 Hz; whereas the percent improvement of the LTMD is slightly lower than 25%. The reason is that the inertia effect of the RTMD is higher than that of the LTMD. One must make a compromise between the inertia effect which increases with the arm length of the RTMD and the space available for mounting the RTMD. In this study the arm length of the RTMD is taken as 0.3 m. If the length is increased, obviously the inertia effect will increase, but, in practice, it is very difficult to use higher lengths in automobiles. For the present case, the superiority of an RTMD over an LTMD is not significant. Therefore it is more suitable to use an LTMD rather than an RTMD in automobiles. Moreover, in Figure 2.5, it can be seen

that the application of TMDs deteriorates the performance around 6 Hz, however deterioration is not more than 8%.

The road holding characteristics of quarter car model is measured by tire deflection. Higher deflection of tire generates more normal force on the tire-road contact surface whereas if the deflection is in the reverse direction it decreases the road holding characteristics of a car. Therefore, decreasing the variations of the tire deflection from its static value increases road holding. In Figure 2.6, the road holding characteristics of systems equipped with RTMDs and LTMDs can be observed. Around 9 Hz where the ride comfort is significantly improved, road holding is also improved since the tire deflection variations around static value decreases. On the other hand, road holding is slightly degraded at frequencies smaller than 8 Hz.

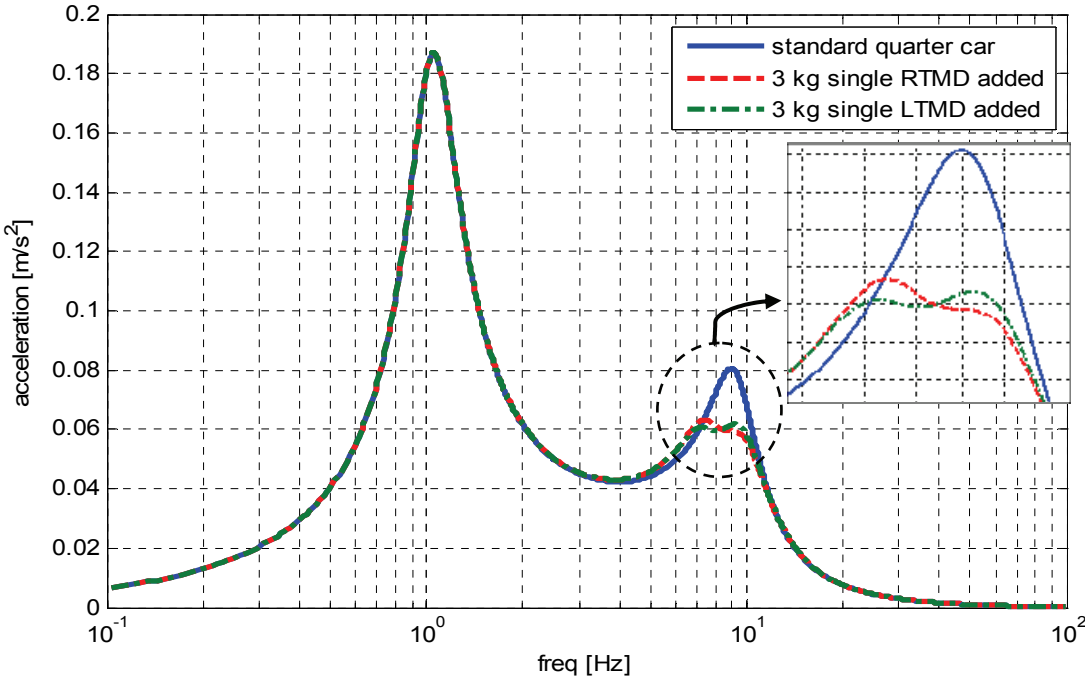

Figure 2.4 Comparison of Single LTMD and Single RTMD on Sprung Mass Acceleration vs Frequency Graph

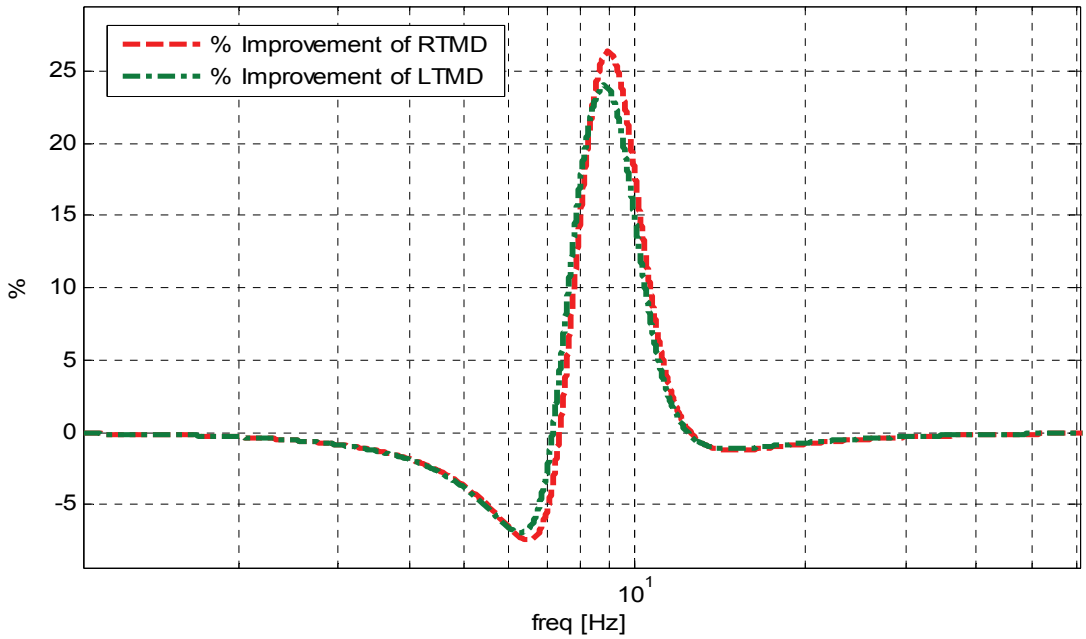

Figure 2.5 Improvement Comparison of Sprung Mass Acceleration of Single LTMD and Single RTMD

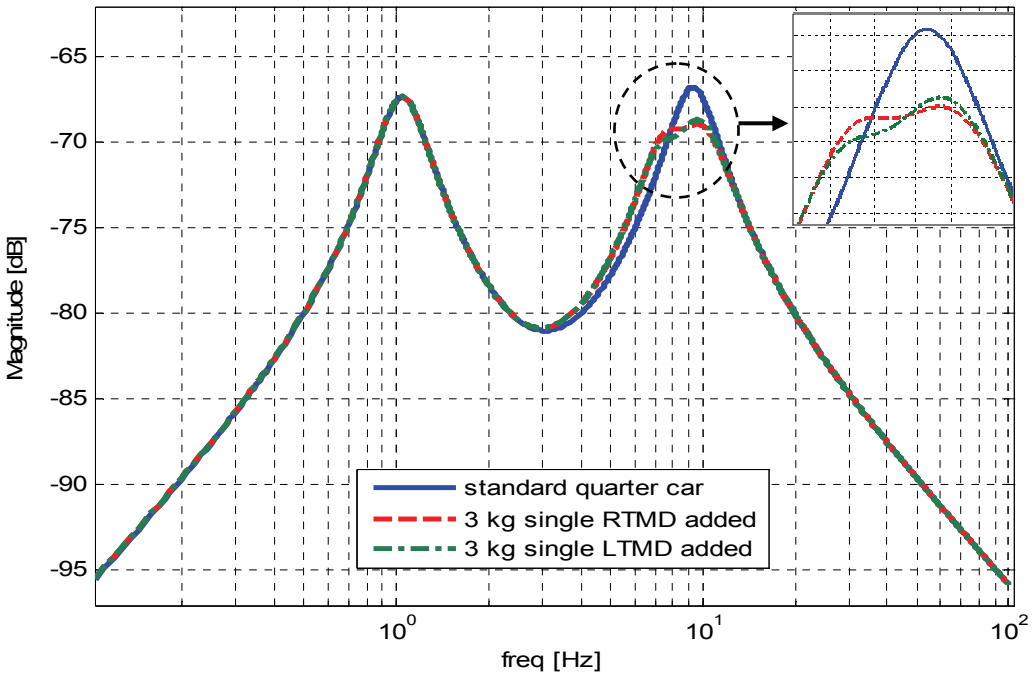

Figure 2.6 Comparison of Single LTMD and Single RTMD on Tyre Deflection vs Frequency Graph

2.5.2 RESULTS WITH RESPECT TO ISO 2631 STANDARDS

In ISO 2631 standards, ride comfort boundaries defines the maximum time that passengers can travel without feeling tiredness. If a boundary is exceeded at a frequency value, then passengers in that vehicle cannot travel more than the time limit specified by the boundary. ISO 2631 ride comfort limits that define the boundaries are given in Table 2.4. The piecewise linear boundaries in logarithmic scale are converted into linear scale in vertical axis.

In Figure 2.7, the performances of Single LTMD and Single RTMD configuration with 3 kg additional mass are compared with a standard quarter-car model with respect to ISO 2631 ride comfort boundaries for a harmonic input of 0.025 m/s. It can be seen on Figure 2.7 that the standard quarter-car model exceeds the 4 hours boundary around wheel hop frequency. Since the sprung mass acceleration is attenuated in the single LTMD and single RTMD configurations, 4 hours boundary is satisfied. Hence, the passengers can travel for 4 hours in a vehicle on which TMD is implemented around wheel hop frequency.

Table 2.4 ISO 2631 Ride Comfort Boundaries for Vertical Vibrations [3]

Frequency $[Hz]$	**Acceleration** $[m/s^2]$						
	1 min	16 mins	25 mins	1 hr	2.5 hrs	4 hrs	8 hrs
1	1.778	1.349	1.127	0.749	0.444	0.337	0.200
4	0.889	0.673	0.571	0.375	0.225	0.168	0.100
8	0.889	0.673	0.571	0.375	0.225	0.168	0.100
80	8.89	6.73	5.71	3.75	2.25	1.68	1.00

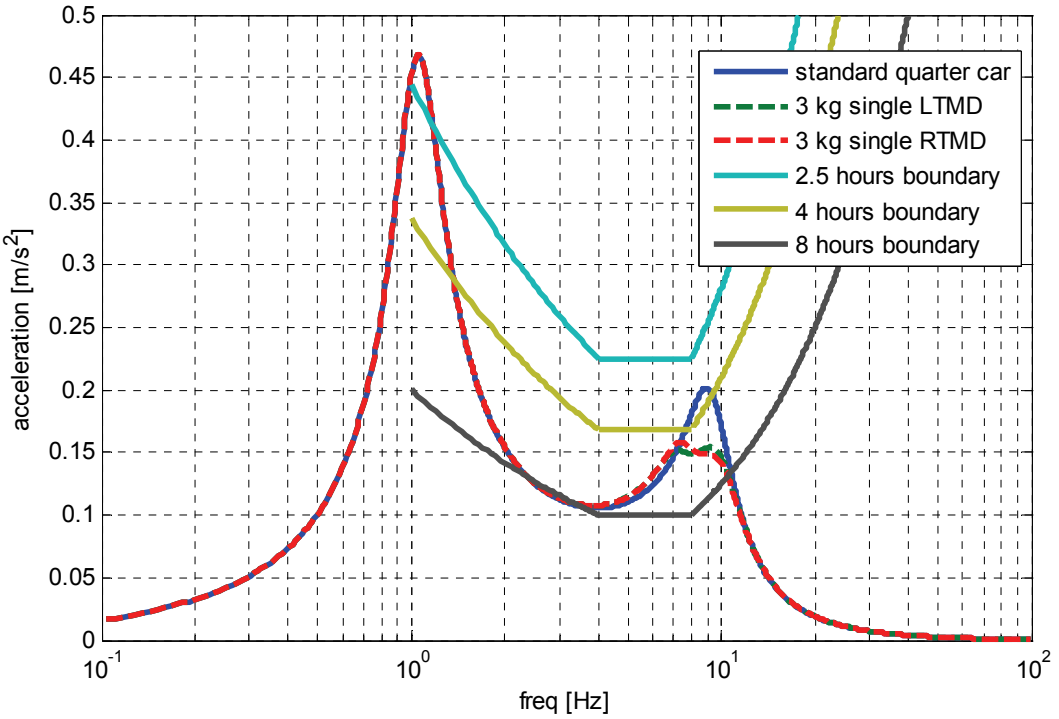

Figure 2.7 Comparison of Performances of Single LTMD and Single RTMD Configurations with Quarter-Car Model on ISO 2631 Curves

CHAPTER 3

CHAIN OF LINEAR TUNED MASS DAMPERS APPLICATION

3.1 INTRODUCTION

The application of TMDs on unsprung mass reduces the sprung mass acceleration around wheel hop frequency as shown in chapter 2. However performance deterioration is observed at frequencies lower than natural frequency of TMDs. In order to decrease the deterioration, a new model is proposed. Chain of LTMDs are utilized to absorb more energy from the system. Suspension spring and viscous damper are divided into several parts by inserting additional plates between the sprung and unsprung masses and LTMDs are added on these plates. The vibration due to road irregularities and the resonance of unsprung mass is not directly transmitted to the sprung mass. At every plate, the LTMDs suppress the vibrations and better performance can be observed with respect to a single LTMD application.

3.2 MODELLING

The proposed chain of LTMDs consists of n building blocks. A single building block is given in Figure 3.1 and a suspension system consisting of n building blocks is given in Figure 3.2. The single LTMD configuration is obviously a chain of LTMD with n=1.

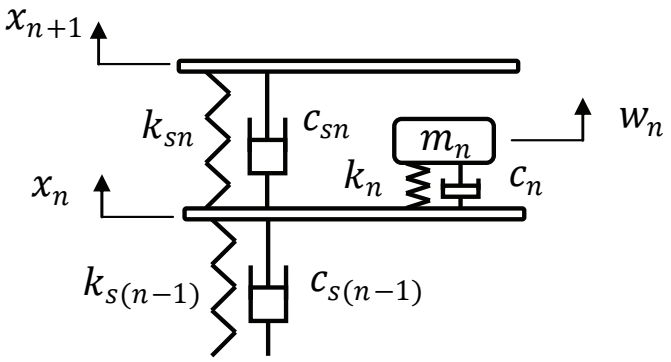

Figure 3.1 Single Building Block used in the LTMD Chain

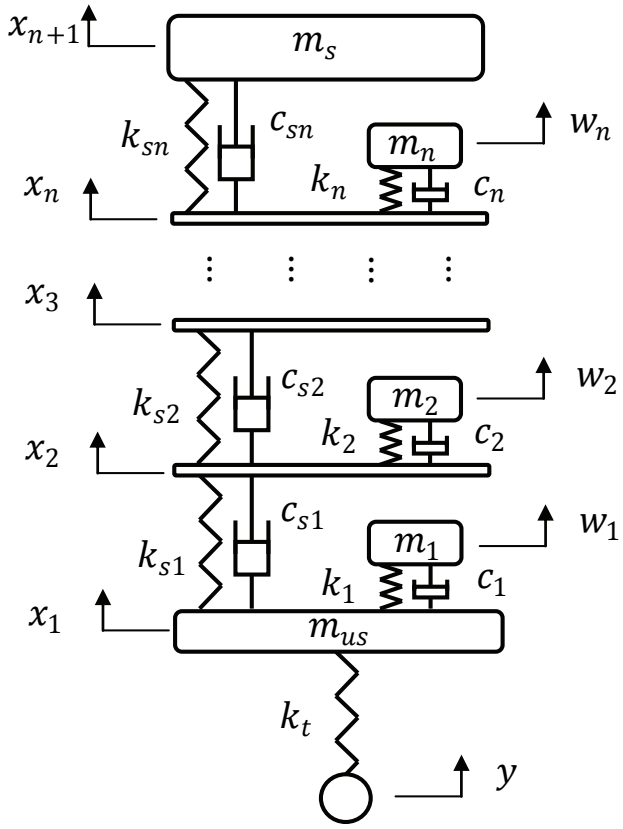

Figure 3.2 Quarter-Car Model with n-block LTMD Chain

Plates placed between sprung and unsprung masses, support the LTMDs. The masses of the plates (m_p) are assumed to be very small compared to the mass of the TMDs. The masses indicated by m_i stand for the mass of i^{th} TMD. The spring constants and the viscous damping coefficients of i^{th} TMD are k_i and c_i respectively. Equivalent suspension spring constant and viscous damping coefficient are obtained by serially connected springs (k_{si}) and viscous dampers (c_{si}) between the plates. The positions of i^{th} plate and i^{th} TMD are denoted by x_i and w_i, respectively. The displacements of the unsprung mass and the sprung mass are x_1 and x_{n+1}, respectively.

The equations of motion of the system is given in equation (2.2) and the mass, damping, stiffness matrices are as follows.

$$[M] = \begin{bmatrix} m_{us} & 0 & \cdots & \cdots & \cdots & \cdots & \cdots & 0 \\ 0 & m_{p1} & 0 & \cdots & \cdots & \cdots & \cdots & 0 \\ \vdots & 0 & \ddots & 0 & \cdots & \cdots & \cdots & 0 \\ \vdots & \vdots & 0 & m_{p(n-1)} & 0 & \cdots & \cdots & 0 \\ \vdots & \vdots & \vdots & 0 & m_s & 0 & \cdots & 0 \\ \vdots & \vdots & \vdots & \vdots & 0 & m_1 & 0 & 0 \\ \vdots & \vdots & \vdots & \vdots & \vdots & 0 & \ddots & 0 \\ 0 & 0 & 0 & 0 & 0 & 0 & 0 & m_n \end{bmatrix}. \quad (3.1)$$

M is $(2n+1) \times (2n+1)$ matrix.

The stiffness matrix

$$[K] = \begin{bmatrix} [K_1] & [K_2] \\ [K_3] & [K_4] \end{bmatrix}, \quad (3.2)$$

is a $(2n+1) \times (2n+1)$ matrix where:

$$[K_1] = \begin{bmatrix} k_t + k_{s1} + k_1 & -k_{s1} & \cdots & 0 & 0 \\ -k_{s1} & k_{s1} + k_{s2} + k_2 & \cdots & 0 & 0 \\ \vdots & \vdots & \ddots & -k_{s(n-1)} & 0 \\ 0 & 0 & -k_{s(n-1)} & k_{s(n-1)} + k_{sn} + k_n & -k_{sn} \\ 0 & 0 & 0 & -k_{sn} & k_{sn} \end{bmatrix}, \quad (3.3)$$

is $(n+1) \times (n+1)$ matrix,

$$[K_2] = \begin{bmatrix} -k_1 & 0 & \cdots & 0 \\ 0 & -k_2 & \cdots & 0 \\ \vdots & \vdots & \ddots & 0 \\ 0 & 0 & 0 & -k_n \\ 0 & 0 & 0 & 0 \end{bmatrix}, \quad (3.4)$$

is $(n+1) \times n$ matrix,

$$[K_3] = \begin{bmatrix} -k_1 & 0 & \cdots & 0 & 0 \\ 0 & -k_2 & \cdots & 0 & 0 \\ \vdots & \vdots & \ddots & 0 & 0 \\ 0 & 0 & 0 & -k_n & 0 \end{bmatrix}, \quad (3.5)$$

is $n \times (n+1)$ matrix,

$$[K_4] = \begin{bmatrix} k_1 & 0 & \cdots & 0 \\ 0 & k_2 & \cdots & 0 \\ \vdots & \vdots & \ddots & 0 \\ 0 & 0 & 0 & k_n \end{bmatrix}, \quad (3.6)$$

is $n \times n$ matrix.

The damping matrix,

$$[C] = \begin{bmatrix} [C_1] & [C_2] \\ [C_3] & [C_4] \end{bmatrix}, \quad (3.7)$$

is a $(2n+1) \times (2nx1)$ matrix where:

$$[C_1] = \begin{bmatrix} c_{s1} + c_1 & -c_{s1} & \cdots & 0 & 0 \\ -c_{s1} & c_{s1} + c_{s2} + c_2 & \cdots & 0 & 0 \\ \vdots & \vdots & \ddots & -c_{s(n-1)} & 0 \\ 0 & 0 & -c_{s(n-1)} & c_{s(n-1)} + c_{sn} + c_n & -c_{sn} \\ 0 & 0 & 0 & -c_{sn} & c_{sn} \end{bmatrix}, \tag{3.8}$$

is a $(n+1) \times (nx1)$ matrix

$$[C_2] = \begin{bmatrix} -c_1 & 0 & \cdots & 0 \\ 0 & -c_2 & \cdots & 0 \\ \vdots & \vdots & \ddots & 0 \\ 0 & 0 & 0 & -c_n \\ 0 & 0 & 0 & 0 \end{bmatrix}, \tag{3.9}$$

is a $(n+1) \times n$ matrix

$$[C_3] = \begin{bmatrix} -c_1 & 0 & \cdots & 0 & 0 \\ 0 & -c_2 & \cdots & 0 & 0 \\ \vdots & \vdots & \ddots & 0 & 0 \\ 0 & 0 & 0 & -c_n & 0 \end{bmatrix}, \tag{3.10}$$

is a $n \times (n+1)$ matrix

$$[C_4] = \begin{bmatrix} c_1 & 0 & \cdots & 0 \\ 0 & c_2 & \cdots & 0 \\ \vdots & \vdots & \ddots & 0 \\ 0 & 0 & 0 & c_n \end{bmatrix}, \tag{3.11}$$

is a $n \times n$ matrix.

Position vectors are:

$$\{x\} = \begin{Bmatrix} x_1 \\ x_2 \\ \vdots \\ x_n \\ x_{n+1} \\ w_1 \\ \vdots \\ w_n \end{Bmatrix}, \tag{3.12}$$

$$\{y_0\} = \begin{Bmatrix} y \\ 0 \\ \vdots \\ 0 \end{Bmatrix}. \tag{3.13}$$

3.3 OPTIMIZATION PROBLEM

Optimization parameters for the chain of LTMD system consist of the concentrated masses m_i, TMD stiffness constants k_i and damping ratios of TMDs. Moreover, each stiffness constant k_{si} and each viscous damping coefficient c_{si} of the suspension are also allowed to assume different values for different values of the index "i" in order to provide a greater flexibility in the ensuing optimization process.

The objective function is again defined as sum of the areas under sprung mass acceleration vs frequency curve multiplied by selected weighting coefficients (Equation 2.19). The same weighting coefficients with single LTMD configuration are utilized in chain of LTMD configuration.

Some constraints are imposed on the system so as to satisfy the pre-selected total suspension stiffness and damping coefficient. In addition, a lower limit to the damping ratios of TMDs is imposed in order not to deteriorate performance of the system at frequencies lower than the natural frequency of TMDs.

The statement of the optimization problem is:

$$\text{minimize} \qquad A_T = \sum_{i=1}^{n} \left(z_i \int_{fr_i} |a(\omega)| d\omega \right), \tag{3.14}$$

subject to

$$\sum_{i=1}^{n} \frac{1}{k_{si}} = \frac{1}{k_s}, \tag{3.15}$$

$$\sum_{i=1}^{n} \frac{1}{c_{si}} = \frac{1}{c_s}, \tag{3.16}$$

$$\sum_{i=1}^{n} m_i = m_T, \tag{3.17}$$

$$\xi_{TMD_i} < 1. \tag{3.18}$$

3.4 RESULTS

The optimization results obtained, for chain of LTMD are given Table 3.1. In order to keep the system in practical limits, the total additional mass for all configurations are limited to 3 kg initially.

The natural frequencies of LTMDs are:

$$\omega_1 = \sqrt{\frac{k_1}{m_1}} = 8.42\ Hz, \tag{3.19}$$

$$\omega_2 = \sqrt{\frac{k_2}{m_2}} = 7.87\ Hz, \tag{3.20}$$

Table 3.1 Optimization Results

	Single LTMD (n=1)	**Chain of LTMD (n=3)**	**Chain of LTMD (n=5)**
$\boldsymbol{m_1}$ [kg]	3	0.675	1.349
$\boldsymbol{m_2}$ [kg]	-	2.225	0.851
$\boldsymbol{m_3}$ [kg]	-	0.100	0.600
$\boldsymbol{m_4}$ [kg]	-	-	0.100
$\boldsymbol{m_5}$ [kg]	-	-	0.100
$\boldsymbol{k_1}$ [N/m]	7056	1890	3680
$\boldsymbol{k_2}$ [N/m]	-	5442	2113
$\boldsymbol{k_3}$ [N/m]	-	232	1197
$\boldsymbol{k_4}$ [N/m]	-	-	203
$\boldsymbol{k_5}$ [N/m]	-	-	244
$\boldsymbol{\xi_1}$	0.20	0.15	0.15
$\boldsymbol{\xi_2}$	-	0.15	0.15
$\boldsymbol{\xi_3}$	-	0.15	0.15
$\boldsymbol{\xi_4}$	-	-	0.15
$\boldsymbol{\xi_5}$	-	-	0.15
$\boldsymbol{k_{s1}}$ [N/m]	15000	45000	75000
$\boldsymbol{k_{s2}}$ [N/m]	-	45000	75000
$\boldsymbol{k_{s3}}$ [N/m]	-	45000	75000
$\boldsymbol{k_{s4}}$ [N/m]	-	-	75000
$\boldsymbol{k_{s5}}$ [N/m]	-	-	75000
$\boldsymbol{c_{s1}}$ [Ns/m]	980	2940	4900
$\boldsymbol{c_{s2}}$ [Ns/m]	-	2940	4900
$\boldsymbol{c_{s3}}$ [Ns/m]	-	2940	4900
$\boldsymbol{c_{s4}}$ [Ns/m]	-	-	4900
$\boldsymbol{c_{s5}}$ [Ns/m]	-	-	4900

$$\omega_3 = \sqrt{\frac{k_3}{m_3}} = 7.67\ Hz, \tag{3.21}$$

which are slightly lower than wheel hop frequency.

3.4.1 EFFECT OF NUMBER OF PLATFORMS

In this section the effect of the number of platforms on the overall ride comfort is investigated. In Figure 3.3, the performance of chain of LTMDs with $n = 1, 3$ and 5 are investigated on sprung mass acceleration vs frequency plot. In the enlarged part of the figure, it can be seen that the performance deterioration is large at frequencies below 7 Hz, for $n = 1$. As the number of platforms increases, the deterioration is reduced. It is easier to compare the three configurations in the improvement plots of Figure 3.4. The deterioration at frequencies lower and higher than wheel hop frequency is maximum with single LTMD configuration. In addition to the reduction of performance deterioration, ride comfort improvement is higher at wheel hop frequency when the number of platforms is five. Moreover, the road holding capability of configuration with $n = 1$ is the worst among the analyzed chain configurations at frequencies lower than resonance frequency of TMD as seen in Figure 3.5.

3.4.2 EFFECT OF WEIGHTING COEFFICIENTS

In this section, the effect of weighting coefficients is investigated. The number of platforms in the chain and the total mass added on the system are kept constant. The number of platforms is taken as three and the total mass added on the system is again taken as 3 kg. Three sets of weighting coefficients are given in Table 3.2. The optimization results of parameters obtained for three different sets of weighting coefficients are given in Table 3.3.

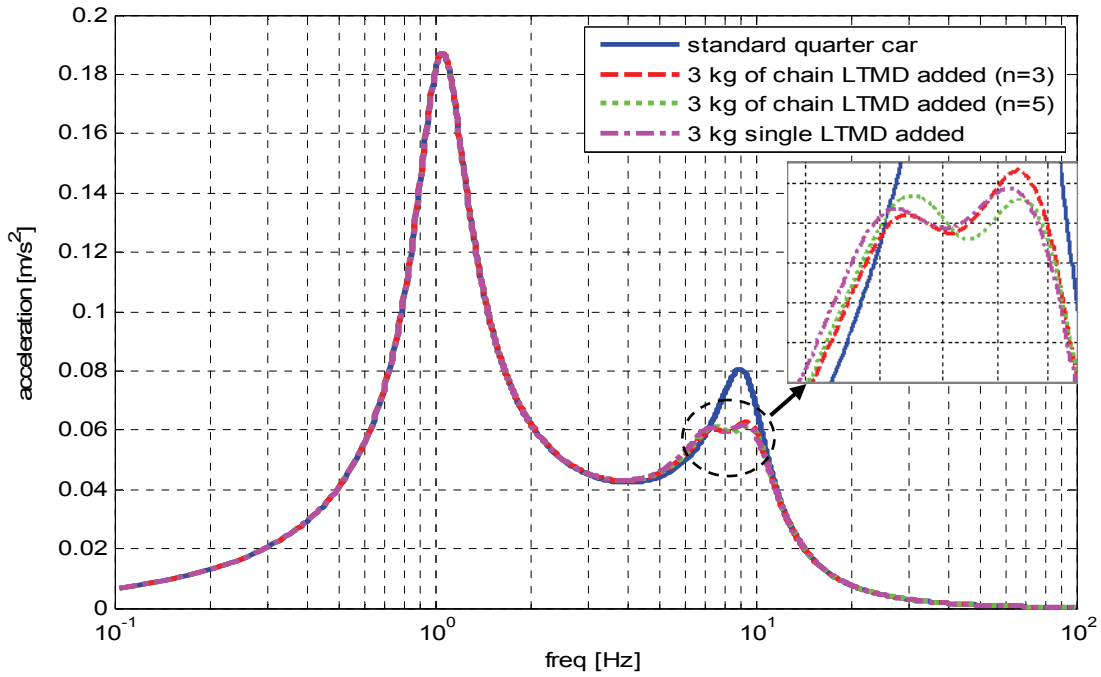

Figure 3.3 Effect of Number of Platform on Sprung Mass Acceleration

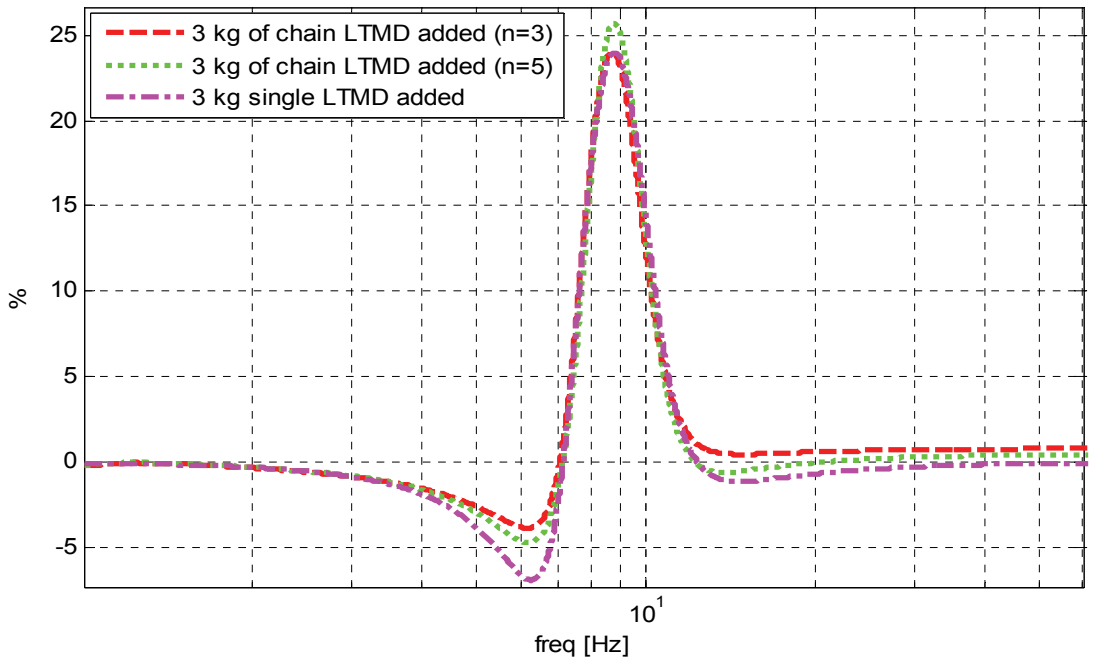

Figure 3.4 Effect of Number of Platforms on the Improvement of Sprung Mass Acceleration

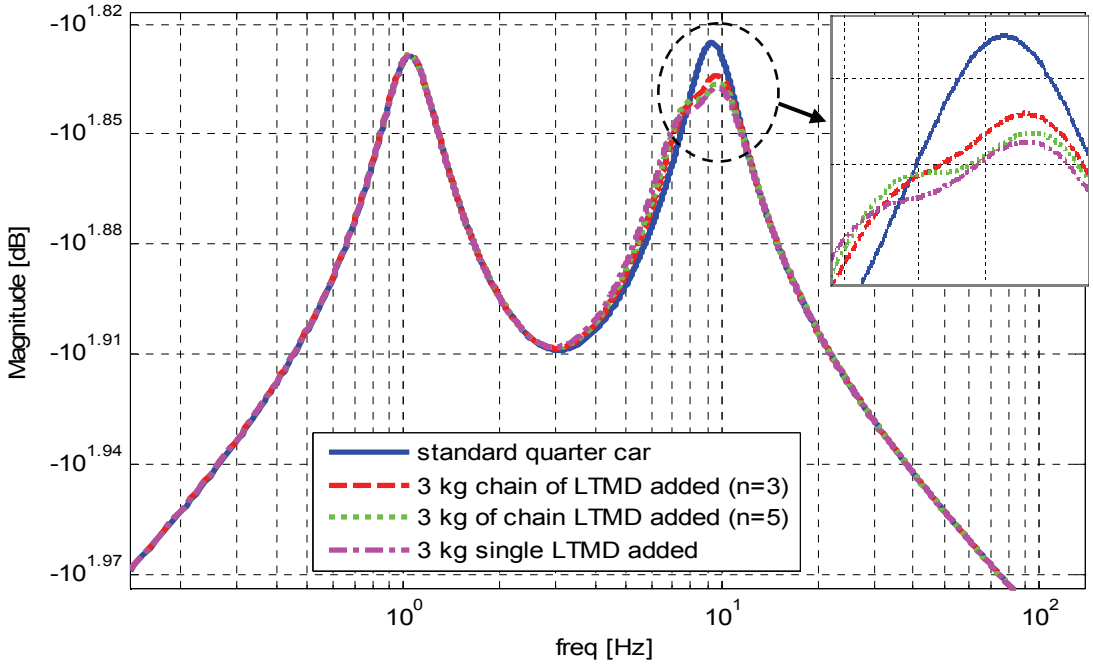

Figure 3.5 Effect of Number of Platforms on Road Holding

Table 3.2 Different Sets of Weighting Coefficients for Chain of LTMD

Weighting Coefficients	LTMD Chain Set-1	LTMD Chain Set-2	LTMD Chain Set-3
z_1	1	1	1
z_2	1	1	1
z_3	1	1	1
z_4	4	4	4
z_5	7	7	7
z_6	7	8	8
z_7	6	7	8
z_8	4	5	6
z_9	4	4	4
z_{10}	3.5	3.5	3.5
z_{11}	1	1	1
z_{12}	0	0	0

The weighting coefficients between 5-8 Hz are gradually increased in the sets and the changes in responses are observed. As can be seen from Table 3.3, the mass of LTMD attached to the unsprung mass decreased while the mass of the second LTMD increased in set-2 and set-3.

According to the optimization results, the sprung mass acceleration is attenuated around 6-8 Hz as the coefficients around these frequencies are increased (Figure 3.6). Set-3 gives best results up to 8 Hz. For this case, the improvement in ride comfort starts approximately at 6 Hz. However, the improvement about 8-10.5 Hz is less than that observed for the other two sets of coefficients (Figure 3.7). These masses can be selected according to the frequency range that is desired to be suppressed.

Table 3.3 Optimization Results for Different Sets of Weighting Coefficients

Parameters	Set-1	Set-2	Set-3
$\boldsymbol{m_1}$ [kg]	0.674	0.612	0.112
$\boldsymbol{m_2}$ [kg]	2.226	2.288	2.787
$\boldsymbol{m_3}$ [kg]	0.100	0.100	0.101
$\boldsymbol{k_1}$ [N/m]	1890	1650	265
$\boldsymbol{k_2}$ [N/m]	5442	4561	5346
$\boldsymbol{k_3}$ [N/m]	232	205	201
$\boldsymbol{\xi_1}$	0.15	0.15	0.15
$\boldsymbol{\xi_2}$	0.15	0.15	0.15
$\boldsymbol{\xi_3}$	0.15	0.15	0.15
$\boldsymbol{k_{s1}}$ [N/m]	45000	45000	45000
$\boldsymbol{k_{s2}}$ [N/m]	45000	45000	45000
$\boldsymbol{k_{s3}}$ [N/m]	45000	45000	45000
$\boldsymbol{c_{s1}}$ [Ns/m]	2940	2940	2940
$\boldsymbol{c_{s2}}$ [Ns/m]	2940	2940	2940
$\boldsymbol{c_{s3}}$ [Ns/m]	2940	2940	2940

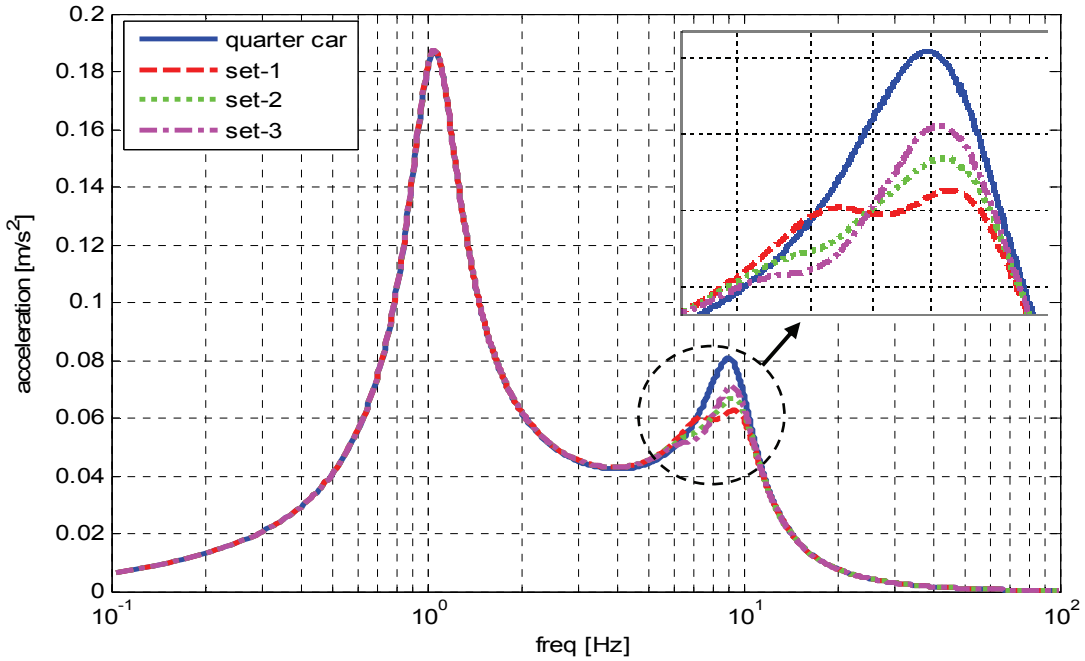

Figure 3.6 Comparison of Different Sets of Weighting Coefficients on Sprung Mass Acceleration for Chain of LTMD Configuration (n=3)

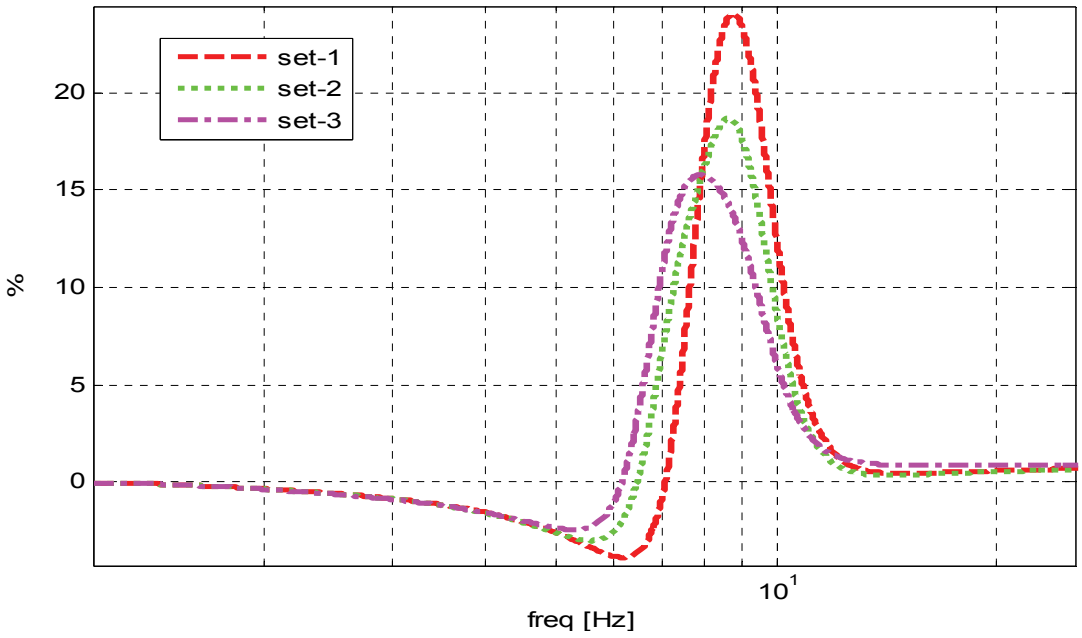

Figure 3.7 Effect of Weighting Coefficients on the Improvement of Sprung Mass Acceleration for Chain of LTMD Configuration (n=3)

3.4.3 EFFECT OF TOTAL TMD MASS

In this part of the study, the effect of the total mass of chain of LTMDs is investigated. The number of platforms is taken as three (n=3) and set-1 weighting coefficients are used. As can be seen in Figure 3.8, more attenuation is obtained by utilizing higher masses. The increased mass results in more improvement on the sprung mass acceleration at frequencies higher than 5.5 Hz for the chain of LTMD case ($n = 3$) as can be seen in Figure 3.9. As the mass is increased up to 8 kg, the improvement approaches 30 percent around wheel hop frequency. The increased mass also attenuates sprung mass acceleration at higher frequencies. The disadvantages of mass increase are a) slightly more deterioration around 2-5 Hz and b) higher fuel consumption. If it is considered that the fuel tank of a standard family car is generally larger than 50 liters or just a driver increases the mass of the car more than 60 kg, slightly higher masses for LTMDs can be accepted.

3.4.4 RESULTS WITH RESPECT TO ISO 2631 STANDARDS

In Figure 3.10, the performances of chain of LTMD configuration ($n = 3$) with 3 kg additional mass and quarter-car model are compared with respect to ISO 2631 ride comfort boundaries for a harmonic input of 0.025 m/s. It can be seen that the standard quarter-car model exceeds the 4 hours boundary around 8 Hz. However in chain of LTMD configuration the 4 hours boundary is satisfied around wheel hop frequency due to suppression of acceleration by TMD application. Therefore, passengers can travel 4 hours without feeling tiredness around wheel hop frequency in TMD implemented system.

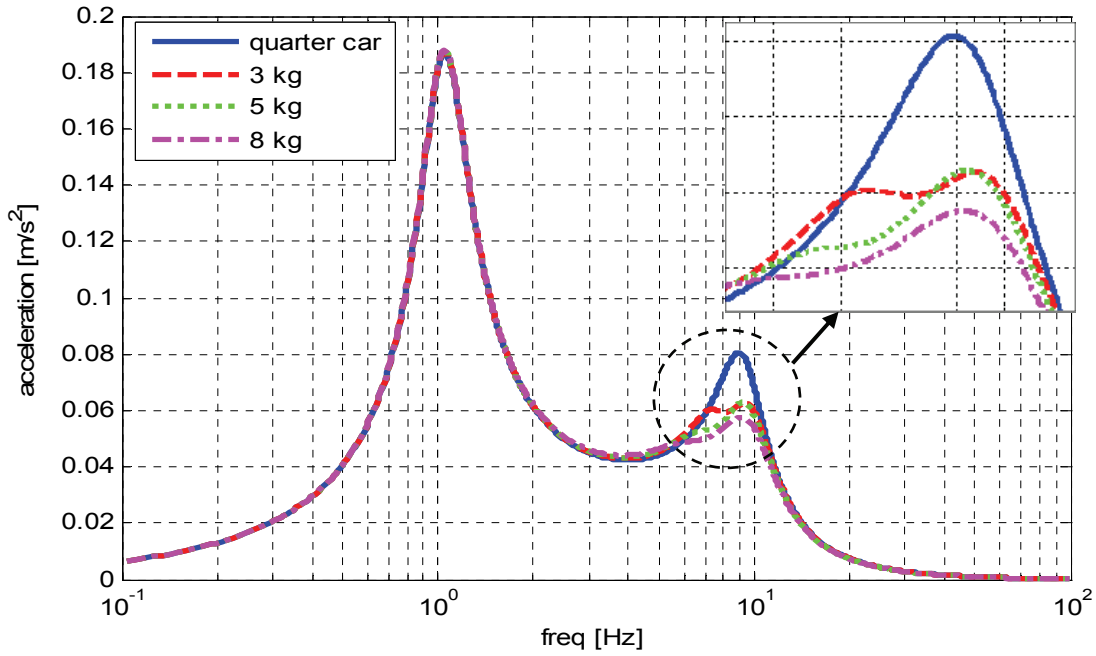

Figure 3.8 Effect of TMD Mass on Sprung Mass Acceleration for Chain of LTMD Configuration (n=3)

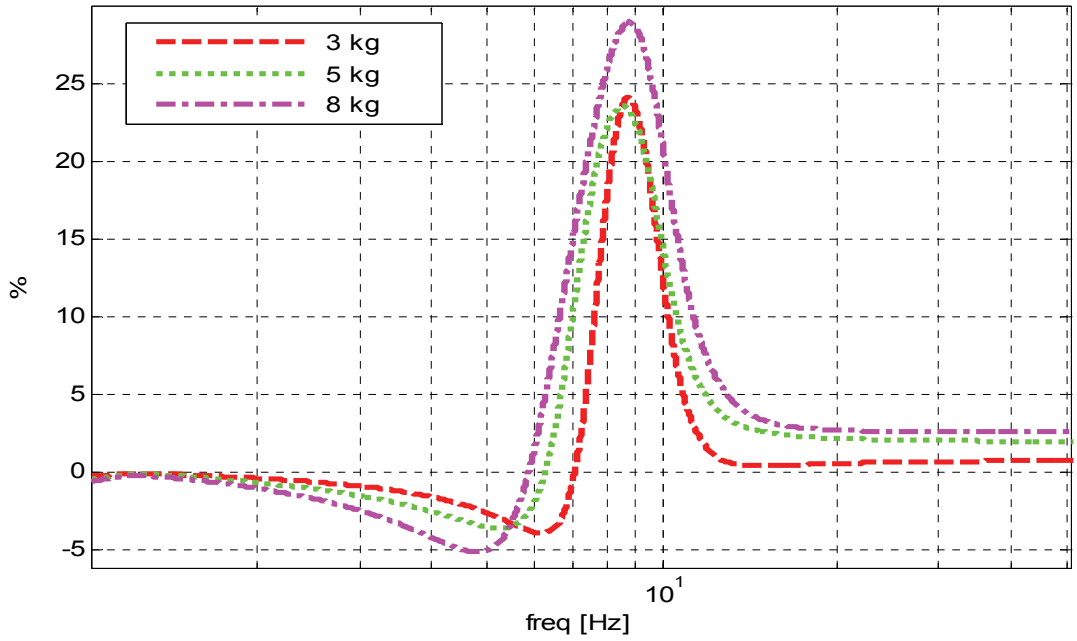

Figure 3.9 Effect of TMD Mass on the Improvement of Sprung Mass Acceleration for Chain of LTMD Configuration (n=3)

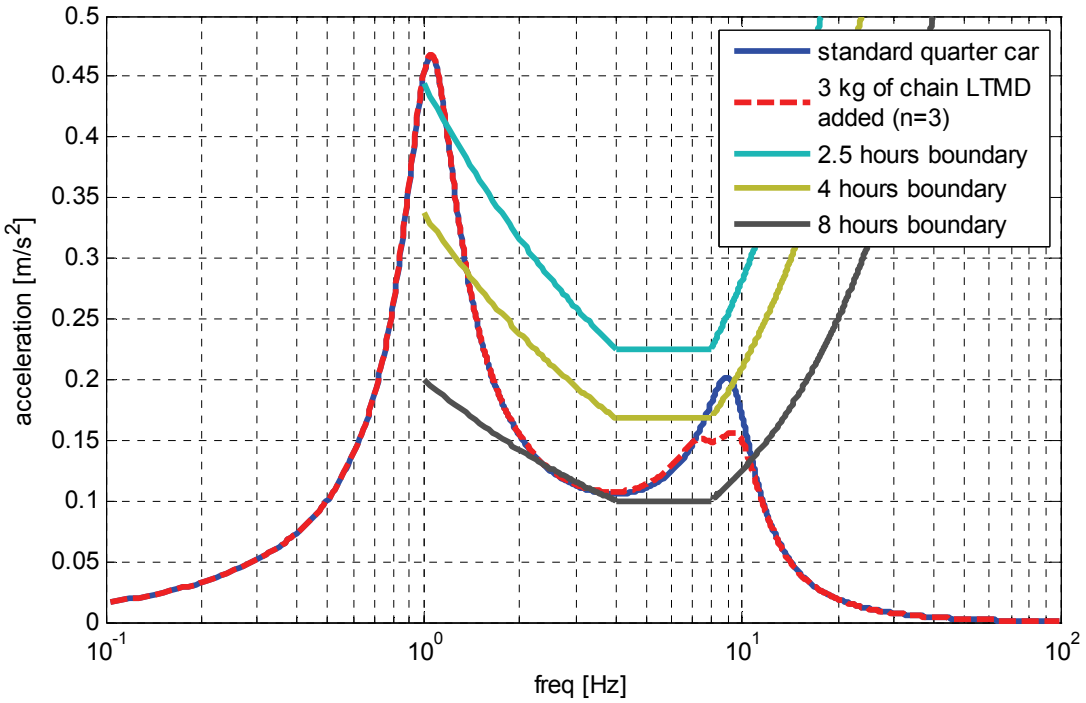

Figure 3.10 Comparison of Performances of Chain of LTMD Configuration ($n = 3$) and Quarter-Car Model with Respect to ISO 2631 Curves

CHAPTER 4

LEVER TYPE VIBRATION ISOLATOR APPLICATION

4.1 INTRODUCTION

LVIs are generally utilized in aerospace industry due to their effectiveness with a comparatively small mass than other isolators. LVIs attenuates the vibration levels by the counter motion of attached mass at the tip of the lever. By attaching the concentrated mass at the tip of the lever, rotational inertia of the lever is increased. Creating an anti-resonance is possible by using LVIs without a damper. However, in suspension applications, energy dissipation is as well important. Hence application of LVIs on quarter car model with viscous damper is investigated.

4.2 MODELLING

There exists two lumped mass models of lever type vibration isolator which are given in Figure 4.1 and Figure 4.2 [62,63]. The lever is pinned on two plates and rotates due to the relative motion between the plates.

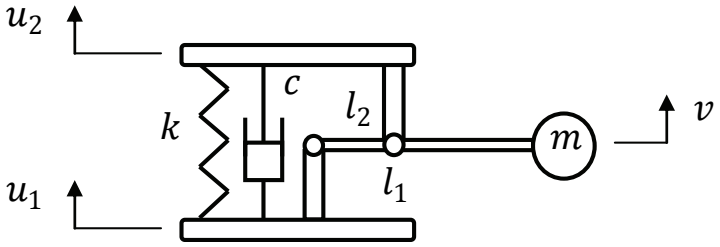

Figure 4.1 Lever Type Vibration Isolator, Type-1

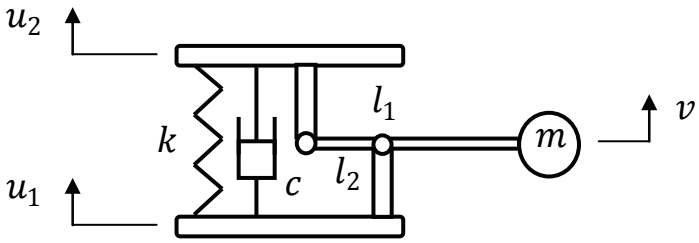

Figure 4.2 Lever Type Vibration Isolator, Type-2

The difference between the two types lies in the connection points between the lever and the plates. When the spring k is compressed, the concentrated mass m at the tip of the lever moves in negative v direction in type-1 and in positive v direction in type-2. The mass of the lever rod is assumed to be negligibly small. Moreover the angle of rotation of the lever is assumed to be small; hence linear theory is applicable. The total length of the lever rod is l_1 and the length of the rod in between the two pins is l_2.

The displacement v can be defined in terms of plate displacements u_1 and u_2 as follows:

$$v = \begin{cases} \alpha u_2 - (\alpha - 1)u_1 & \text{for type-1,} \quad (4.1) \\ \alpha u_1 - (\alpha - 1)u_2 & \text{for type-2,} \quad (4.2) \end{cases}$$

where

$$\alpha = l_1/l_2 > 1. \tag{4.3}$$

Both types of lever type vibration isolators are investigated on the quarter car model with different configurations

4.2.1 LVI CONFIGURATION 1

In this configuration, type-1 LVI is connected between the sprung and the unsprung masses (Figure 4.3). Since the displacement v depends on x_1 and x_2, a two degree of freedom model is obtained. Equations of motion of the system are given in Equation (2.2), where $[M]$, $[C]$ and $[K]$ are mass, damping and stiffness matrices.

$$[M] = \begin{bmatrix} m_{us} + m_1(\alpha_1 - 1)^2 & -m_1\alpha_1(\alpha_1 - 1) \\ -m_1\alpha_1(\alpha_1 - 1) & m_s + m_1\alpha_1^2 \end{bmatrix}, \tag{4.4}$$

$$[C] = \begin{bmatrix} c_s & -c_s \\ -c_s & c_s \end{bmatrix}, \tag{4.5}$$

$$[K] = \begin{bmatrix} k_s + k_t & -k_s \\ -k_s & k_s \end{bmatrix}. \tag{4.6}$$

The position vectors defined above are:

$$\{x\} = \begin{Bmatrix} x_1 \\ x_2 \end{Bmatrix}, \tag{4.7}$$

$$\{y_0\} = \begin{Bmatrix} y \\ 0 \end{Bmatrix}. \tag{4.8}$$

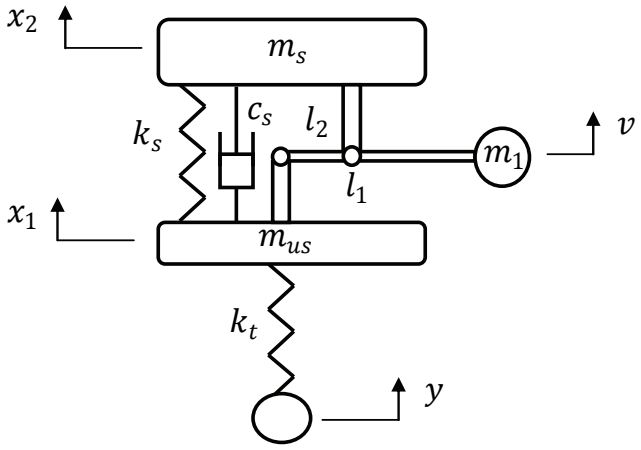

Figure 4.3 LVI Configuration 1

4.2.2 LVI CONFIGURATION 2

In the second configuration, type-2 LVI is connected between the sprung and the unsprung mass (Figure 4.4). Mass, damping and stiffness matrices of this configuration are.

$$[M] = \begin{bmatrix} m_{us} + m_1{\alpha_1}^2 & -m_1\alpha_1(\alpha_1 - 1) \\ -m_1\alpha_1(\alpha_1 - 1) & m_s + m_1(\alpha_1 - 1)^2 \end{bmatrix}, \tag{4.9}$$

$$[C] = \begin{bmatrix} c_s & -c_s \\ -c_s & c_s \end{bmatrix}, \tag{4.10}$$

$$[K] = \begin{bmatrix} k_s + k_t & -k_s \\ -k_s & k_s \end{bmatrix}. \tag{4.11}$$

The position vectors are:

$$\{x\} = \begin{Bmatrix} x_1 \\ x_2 \end{Bmatrix}, \tag{4.12}$$

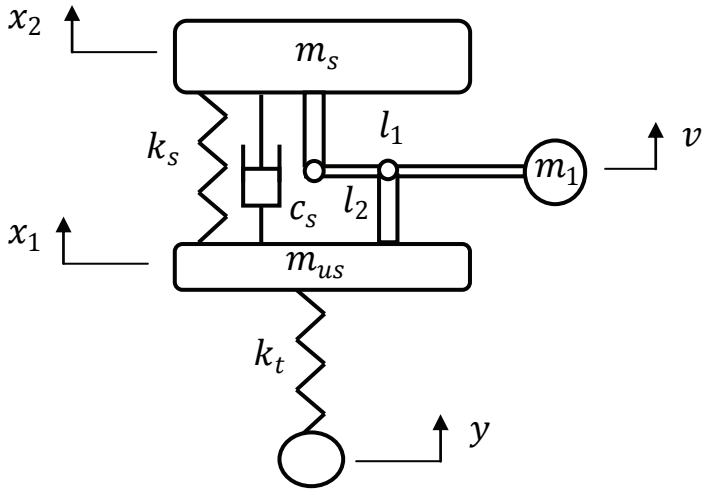

Figure 4.4 LVI Configuration 2

$$\{y_0\} = \begin{Bmatrix} y \\ 0 \end{Bmatrix}. \tag{4.13}$$

4.2.3 LVI CONFIGURATION 3

In configuration 3 (Figure 4.5), a combination of both types of LVI is considered. An extra plate with mass m_p is added to the system. The plate is connected to the unsprung mass and the sprung mass with springs having stiffnesses k_{s1} and k_{s2} and with dampers having coefficients c_{s1} and c_{s2} respectively. Type-1 LVI is connected between the sprung mass and the plate and type-2 LVI is connected between the plate and the unsprung mass. The total lengths of the levers in type-1 and type-2 isolators are l_1 and l_3 and lever lengths between pins are l_2 and l_4 respectively. The concentrated masses at the tip of the levers of type-1 and type-2 isolators are m_1 and m_2 and the displacements of m_1 and m_2 are denoted by v_1 and v_2 respectively. The displacements v_1 and v_2 can be written in terms of x_1, x_2 and x_3 as

$$v_1 = \alpha_1 x_1 - (\alpha_1 - 1)x_2, \tag{4.14}$$

$$v_2 = \alpha_2 x_3 - (\alpha_2 - 1)x_2, \tag{4.15}$$

where

$$\alpha_1 = l_1/l_2, \tag{4.16}$$

$$\alpha_2 = l_3/l_4. \tag{4.17}$$

The mass, damping and stiffness matrices are:

$$[M] = \begin{bmatrix} m_{us} + m_1{\alpha_1}^2 & -m_1\alpha_1(\alpha_1 - 1) & 0 \\ -m_1\alpha_1(\alpha_1 - 1) & m_p + m_1(\alpha_1 - 1)^2 + m_2(\alpha_2 - 1)^2 & -m_2\alpha_2(\alpha_2 - 1) \\ 0 & -m_2\alpha_2(\alpha_2 - 1) & m_s + m_2{\alpha_2}^2 \end{bmatrix}, \tag{4.18}$$

$$[C] = \begin{bmatrix} c_{s1} & -c_{s1} & 0 \\ -c_{s1} & c_{s1} + c_{s2} & -c_{s2} \\ 0 & -c_{s2} & c_{s2} \end{bmatrix}, \tag{4.19}$$

$$[K] = \begin{bmatrix} k_t + k_{s1} & -k_{s1} & 0 \\ -k_{s1} & k_{s1} + k_{s2} & -k_{s2} \\ 0 & -k_{s2} & k_{s2} \end{bmatrix}. \tag{4.20}$$

The displacement vectors are:

$$\{x\} = \begin{Bmatrix} x_1 \\ x_2 \\ x_3 \end{Bmatrix}, \tag{4.21}$$

$$\{y_0\} = \begin{Bmatrix} y \\ 0 \\ 0 \end{Bmatrix}. \tag{4.22}$$

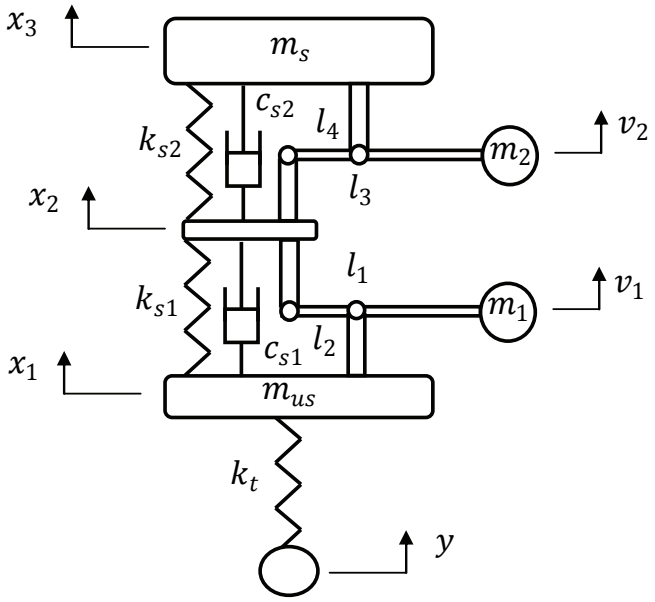

Figure 4.5 LVI Configuration 3

4.2.4 LVI CONFIGURATION 4

Configuration 4 is obtained by interchanging the two types of LVIs in configuration 3. Here the type-2 LVI is placed between the sprung mass and plate and type-1 LVI is placed between plate and the unsprung mass (Figure 4.6). Therefore positions of concentrated masses at the tip of the levers are as follows:

$$v_1 = \alpha_1 x_2 - (\alpha_1 - 1)x_1, \tag{4.23}$$

$$v_2 = \alpha_2 x_2 - (\alpha_2 - 1)x_3. \tag{4.24}$$

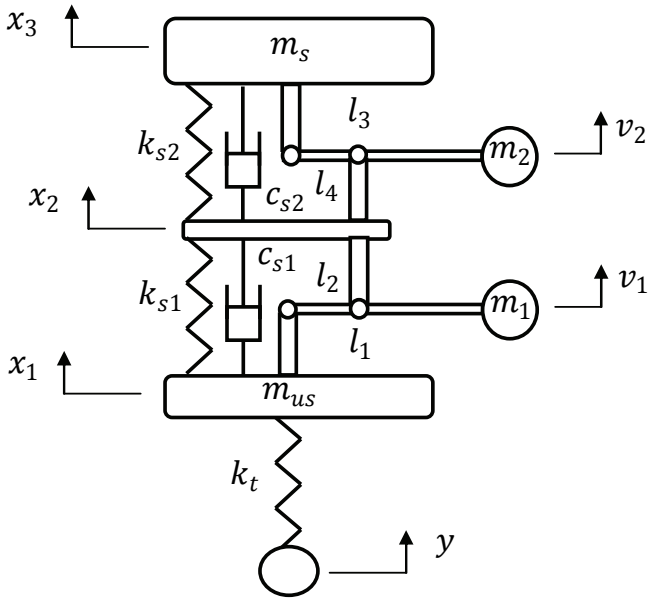

Figure 4.6 LVI Configuration 4

Mass, damping and stiffness matrices are:

$$[M] = \begin{bmatrix} m_{us} + m_1(\alpha_1 - 1)^2 & -m_1\alpha_1(\alpha_1 - 1) & 0 \\ -m_1\alpha_1(\alpha_1 - 1) & m_p + m_1{\alpha_1}^2 + m_2{\alpha_2}^2 & -m_2\alpha_2(\alpha_2 - 1) \\ 0 & -m_2\alpha_2(\alpha_2 - 1) & m_s + m_2(\alpha_2 - 1)^2 \end{bmatrix}, \tag{4.25}$$

$$[C] = \begin{bmatrix} c_{s1} & -c_{s1} & 0 \\ -c_{s1} & c_{s1} + c_{s2} & -c_{s2} \\ 0 & -c_{s2} & c_{s2} \end{bmatrix}, \tag{4.26}$$

$$[K] = \begin{bmatrix} k_t + k_{s1} & -k_{s1} & 0 \\ -k_{s1} & k_{s1} + k_{s2} & -k_{s2} \\ 0 & -k_{s2} & k_{s2} \end{bmatrix}. \tag{4.27}$$

and the position vectors are:

$$\{x\} = \begin{Bmatrix} x_1 \\ x_2 \\ x_3 \end{Bmatrix}, \tag{4.28}$$

$$\{y_0\} = \begin{Bmatrix} y \\ 0 \\ 0 \end{Bmatrix}. \tag{4.29}$$

4.2.5 LVI CONFIGURATION 5

In configuration 5, two type-1 LVIs are utilized (Figure 4.7). An extra plate with mass m_p is added to the system as in configuration 3 and 4. The positions of concentrated masses are:

$$v_1 = \alpha_1 x_2 - (\alpha_1 - 1)x_1, \tag{4.30}$$

$$v_2 = \alpha_2 x_3 - (\alpha_2 - 1)x_2. \tag{4.31}$$

Mass, damping and stiffness matrices are:

$$[M] = \begin{bmatrix} m_{us} + m_1(\alpha_1 - 1)^2 & -m_1\alpha_1(\alpha_1 - 1) & 0 \\ -m_1\alpha_1(\alpha_1 - 1) & m_p + m_1{\alpha_1}^2 + m_2(\alpha_2 - 1)^2 & -m_2\alpha_2(\alpha_2 - 1) \\ 0 & -m_2\alpha_2(\alpha_2 - 1) & m + m_2{\alpha_2}^2 \end{bmatrix}, \tag{4.32}$$

$$[C] = \begin{bmatrix} c_{s1} & -c_{s1} & 0 \\ -c_{s1} & c_{s1} + c_{s2} & -c_{s2} \\ 0 & -c_{s2} & c_{s2} \end{bmatrix}, \tag{4.33}$$

$$[K] = \begin{bmatrix} k_t + k_{s1} & -k_{s1} & 0 \\ -k_{s1} & k_{s1} + k_{s2} & -k_{s2} \\ 0 & -k_{s2} & k_{s2} \end{bmatrix}. \tag{4.34}$$

and the position vectors are:

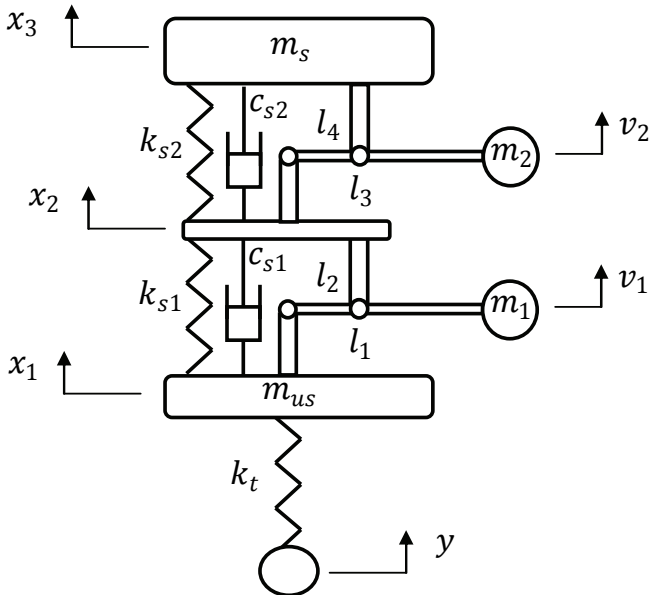

Figure 4.7 LVI Configuration 5

$$\{x\} = \begin{Bmatrix} x_1 \\ x_2 \\ x_3 \end{Bmatrix}, \tag{4.35}$$

$$\{y_0\} = \begin{Bmatrix} y \\ 0 \\ 0 \end{Bmatrix}. \tag{4.36}$$

4.2.6 LVI CONFIGURATION 6

In configuration 6, only type 1 LVI is utilized with an extra plate (Figure 4.8). The isolator is connected between the sprung mass and the plate. The mass, damping and stiffness matrices and the displacement vectors are given as follows:

$$[M] = \begin{bmatrix} m_{us} & 0 & 0 \\ 0 & m_1(\alpha-1)^2 & -m_1\alpha(\alpha-1) \\ 0 & -m_1\alpha(\alpha-1) & m_s + m_1\alpha^2 \end{bmatrix}, \tag{4.37}$$

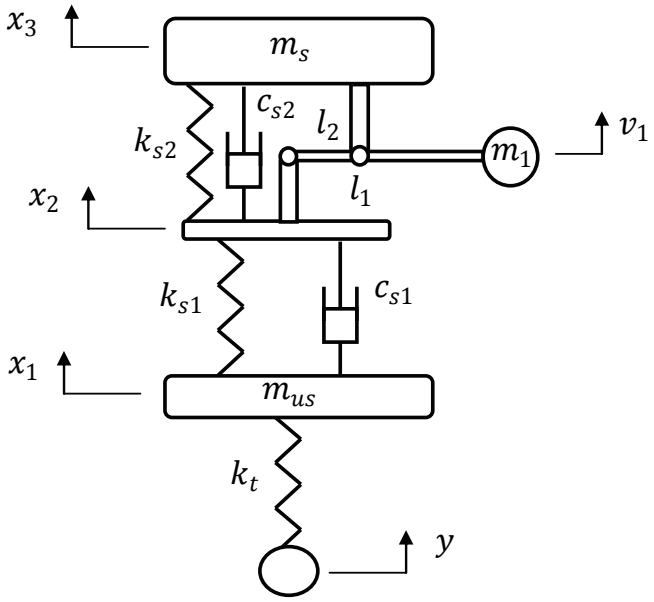

Figure 4.8 LVI Configuration 6

$$[C] = \begin{bmatrix} c_{s1} & -c_{s1} & 0 \\ -c_{s1} & c_{s1} + c_{s2} & -c_{s2} \\ 0 & -c_{s2} & c_{s2} \end{bmatrix}, \tag{4.38}$$

$$[K] = \begin{bmatrix} k_{s1} + k_t & -k_{s1} & 0 \\ -k_{s1} & k_{s2} + k_{s1} & -k_{s2} \\ 0 & -k_{s2} & k_{s2} \end{bmatrix}, \tag{4.39}$$

$$\{x\} = \begin{Bmatrix} x_1 \\ x_2 \\ x_3 \end{Bmatrix}, \tag{4.40}$$

$$\{y_0\} = \begin{Bmatrix} y \\ 0 \\ 0 \end{Bmatrix}. \tag{4.41}$$

4.3 OPTIMIZATION PROBLEM

Optimization parameters for configurations including a single LVI consists of the concentrated mass m_i and length ratio α_i. For the configurations including 2 LVIs each stiffness constant k_{si} and each viscous damping coefficient c_{si} are as well included in the optimization parameters.

The objective function is defined as the sum of the areas multiplied by selected weighting coefficients as mentioned in Chapter 2 (Equation 2.19). The weighting coefficients determined for all the LVI configurations are given in Table 4.1. For configuration 4, two sets of coefficients are obtained, both giving satisfactory results.

The statement of the optimization problem is:

minimize $$A_T = \sum_{i=1}^{n} \left(z_i \int_{fr_i} |a(\omega)| d\omega \right), \tag{4.42}$$

subject to

$$\sum_{i=1}^{n} \frac{1}{k_{si}} = \frac{1}{k_s}, \tag{4.43}$$

$$\sum_{i=1}^{n} \frac{1}{c_{si}} = \frac{1}{c_s}, \tag{4.44}$$

$$\sum_{i=1}^{n} m_i = m_T, \tag{4.45}$$

$$1 < \alpha_i \leq 5. \tag{4.46}$$

Table 4.1 Weighting Coefficients of LVI Configurations

Coefficients	Configuration						
	1	**2**	**3**	**4 (I)**	**4 (II)**	**5**	**6**
z_1	1	1	1	1	1	1	2
z_2	1	1	19	1	20	18	2
z_3	5	1	1	1	1.5	1.5	3
z_4	6	1	1	1	2	2	1
z_5	8	1	2	1	2	2	1
z_6	5	3	2	2	2	2	1
z_7	4	3	3	4	2	2	4
z_8	5	4	3	3	2.6	2	5
z_9	5	4	3	10	2.6	2	6
z_{10}	3	1	1	2	1	1	3
z_{11}	1	1	1	1	1	1	1
z_{12}	0.1	1	1	1	1	1	1

4.4 RESULTS

Optimization results are obtained using the weighting coefficients given in Table 4.1. For practical purposes, the additional total LVI mass is limited to 3 kg and the value of α for each LVI configuration is limited to 5. Also each stiffness constant and damping coefficient are optimized by keeping the total stiffness and damping of the suspension constant. The values of parameters obtained throughout optimization are given in Table 4.2.

Table 4.2 Optimization Results for LVI Configurations

Parameters	Configuration						
	1	**2**	**3**	**4 (I)**	**4 (II)**	**5**	**6**
$\boldsymbol{m_1}$ [kg]	3	1	0.418	1.74	1.74	1.99	3
$\boldsymbol{m_2}$ [kg]	-	-	2.572	1.26	1.26	1.01	-
$\boldsymbol{\alpha_1}$	1.7	2.0	5.0	2.8	4.0	3.6	2.27
$\boldsymbol{\alpha_2}$	-		2.6	5.0	5.0	4.9	-
$\boldsymbol{k_{s1}}$ [N/m]	15000	15000	30000	30000	20580	30000	30000
$\boldsymbol{k_{s2}}$ [N/m]	-	-	30000	30000	55326	30000	30000
$\boldsymbol{c_{s1}}$ [Ns/m]	980	980	2189	1475	1903	1960	3287
$\boldsymbol{c_{s2}}$ [Ns/m]	-	-	1774	2921	2020	1960	1396

4.4.1 COMPARISON OF SINGLE LVI CONFIGURATIONS

As mentioned before, the single degree of freedom model for dynamic anti-resonant vibration isolator is not the ideal design [4,61]. The reason behind the application of LVIs without plate is just to show the inadequate performance of LVIs without using plates. Another reason is to compare the performances of both types of LVIs (type-1 and type-2).

As can be seen in Figure 4.9, both types of LVIs give inadequate results. However, type-1 LVI (configuration 1) has a better performance than type-2 LVI, especially between 1-8 Hz. It is easier to compare both LVIs in the improvement plot (Figure 4.10). It is observed that, type-1 LVI attenuates vibrations at a wider frequency range. Also the performance deterioration of type-1 LVI is less than type-2.

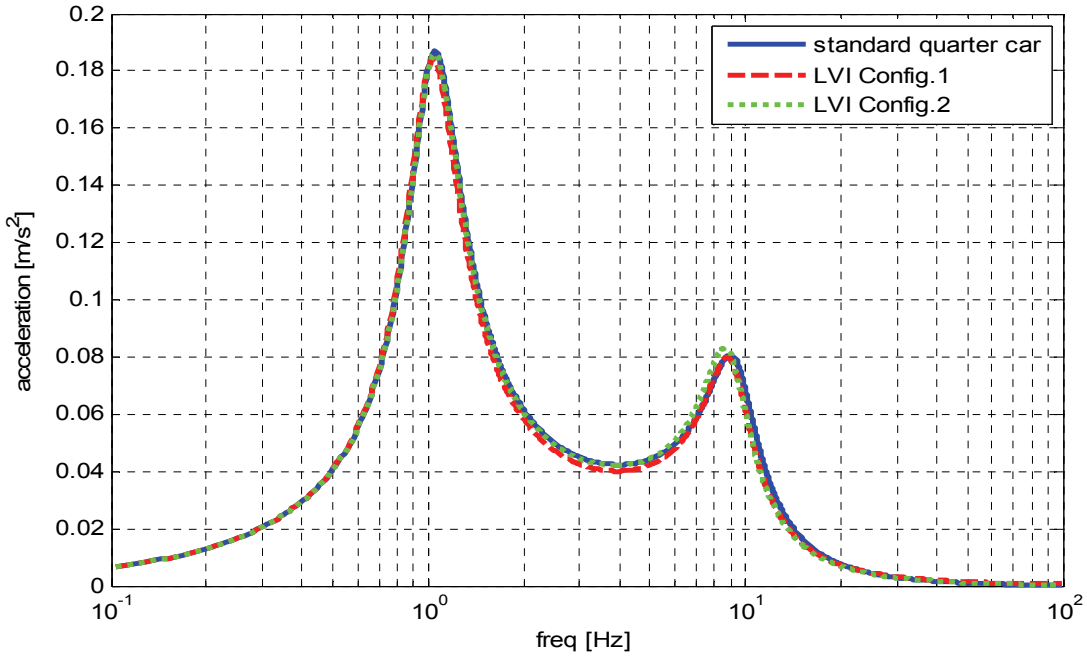

Figure 4.9 Comparison of Performance of LVI Configurations 1 and 2 on Sprung Mass Acceleration Plot

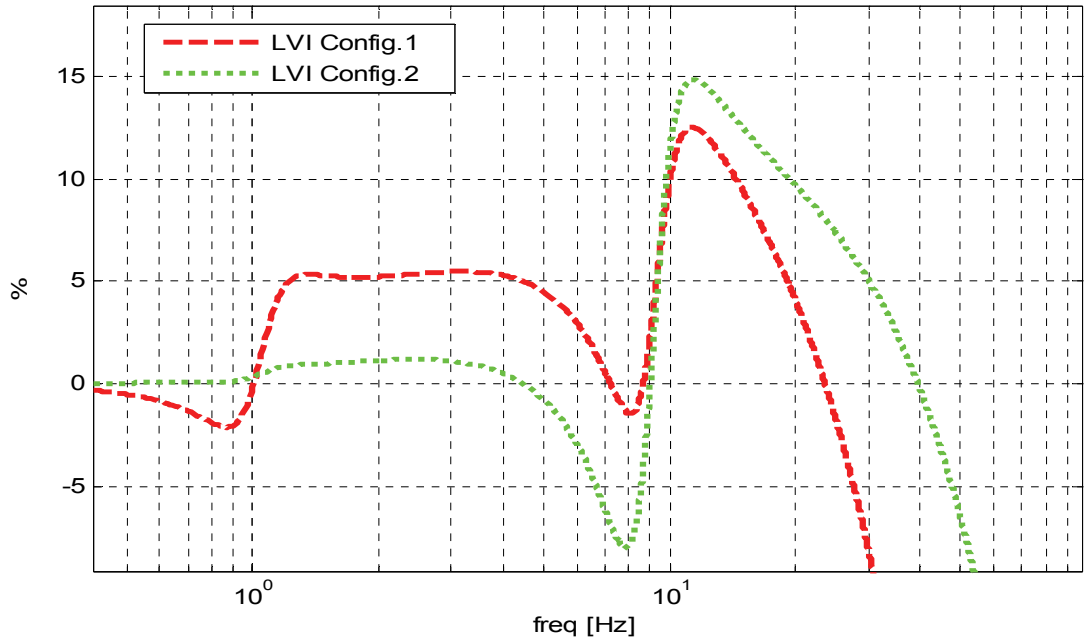

Figure 4.10 Improvement Comparison of LVI Configurations 1 and 2 on Sprung Mass Acceleration

4.4.2 COMPARISON OF CHAIN OF LVI CONFIGURATIONS

The results obtained by using the optimum values in Table 4.2 are given in Figure 4.11 - Figure 4.13. Performance comparison of four different configurations on sprung mass acceleration vs frequency plot is given in Figure 4.11. It is observed that the LVI application reduces the vibration at body bounce, wheel hop frequencies, and at frequencies around 5 Hz.

At the wheel hop frequency configuration 4 with weighting coefficients of set-2 gives the best result. At frequencies lower than wheel hop frequency, configuration 4 with weighting coefficients of set-1 and configuration 6 show better performance than others (Figure 4.12).

In the frequency range of 1 Hz to 8 Hz, configuration 3, 4 with set-2 and configuration 5 are more effective than other configurations. The wheel hop frequency of the quarter-car model is slightly shifted to the lower frequency range for some configurations as can be seen in Figure 4.12.

The tyre deflection curves of LVI configurations 3 to 6 are given in Figure 4.13. At frequencies between 2 Hz and 9 Hz, road holding characteristic of standard quarter car model show better performance than LVI configurations. However at frequencies lower than 2 Hz, less variation of tire deflection is observed for all LVI configurations. Therefore road holding is improved around body bounce frequency.

To sum up, configurations can be selected according to the desired attenuation. Furthermore the improvement provided by a selected configuration can be slightly changed by altering the weighting coefficients. Obviously, more improvement can be achieved using higher masses.

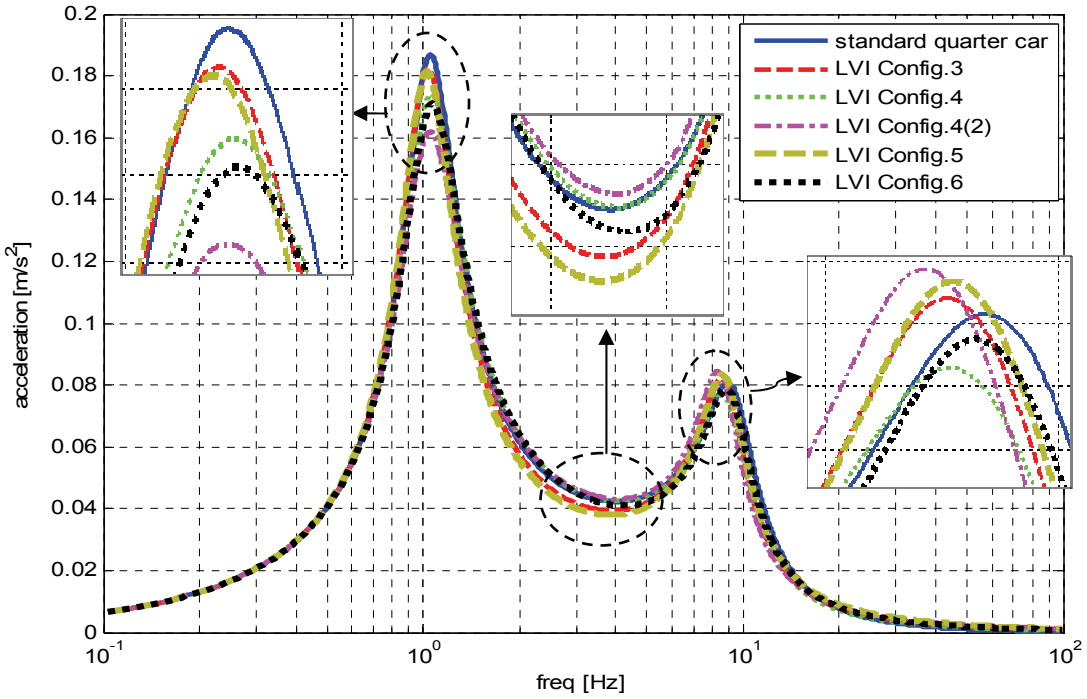

Figure 4.11 Comparison of Performance of LVI Configurations 3 to 6 on Sprung Mass Acceleration

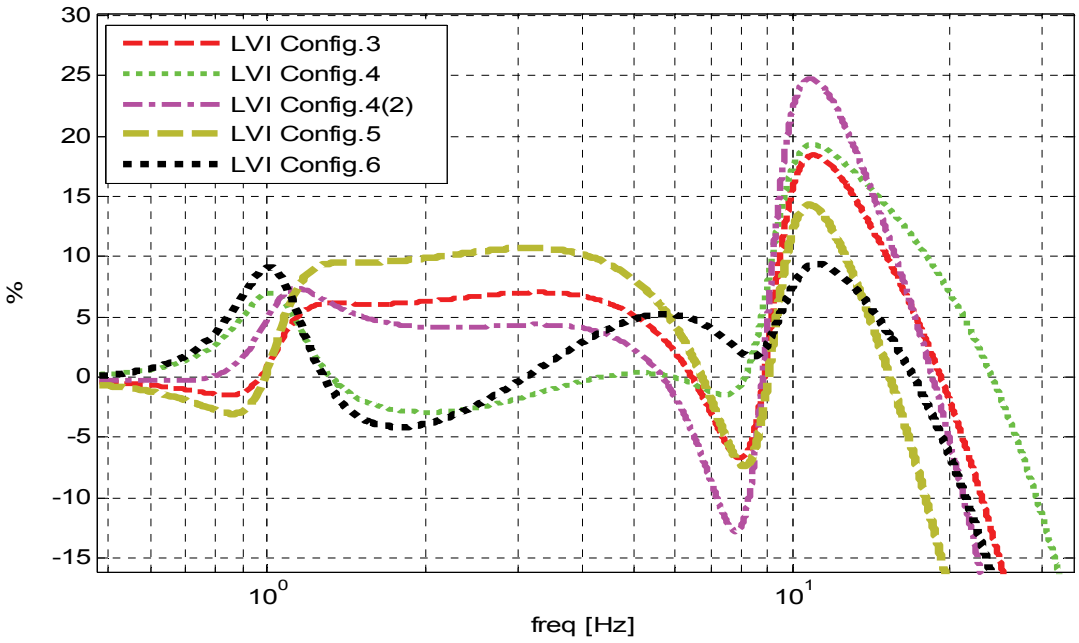

Figure 4.12 Improvement Comparison of LVI Configurations 3 to 6 on Sprung Mass Acceleration

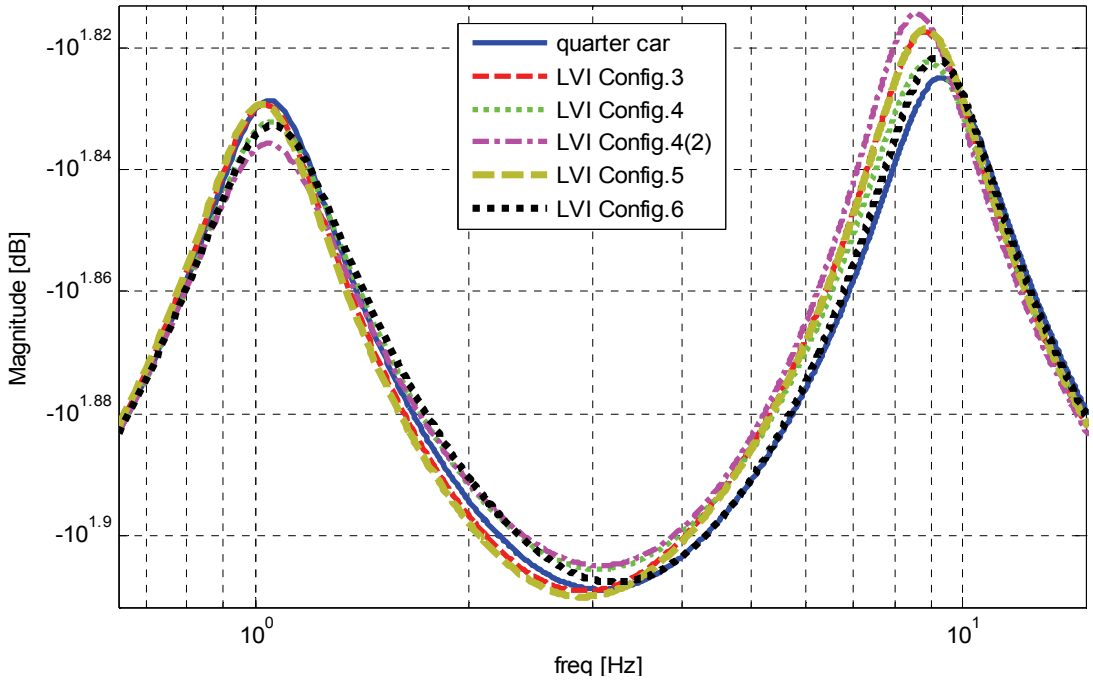

Figure 4.13 Road Holding Comparison of LVI Configurations 3 to 6

4.4.3 EFFECT OF LVI MASS

In this part of the study, the effect of increasing mass is investigated for LVI configuration 4 with weighting coefficients of set-2. Three different masses (3, 5 and 8 kg) are used. The results obtained on sprung mass acceleration vs frequency plot are given in Figure 4.14. Also, the improvement plots of configuration 4 with different masses are given in Figure 4.15. It can be seen that the improvement of the 8 kg curve is almost always on top of 3 and 5 kg curves. More improvement can be achieved as the total LVI mass employed is increased.

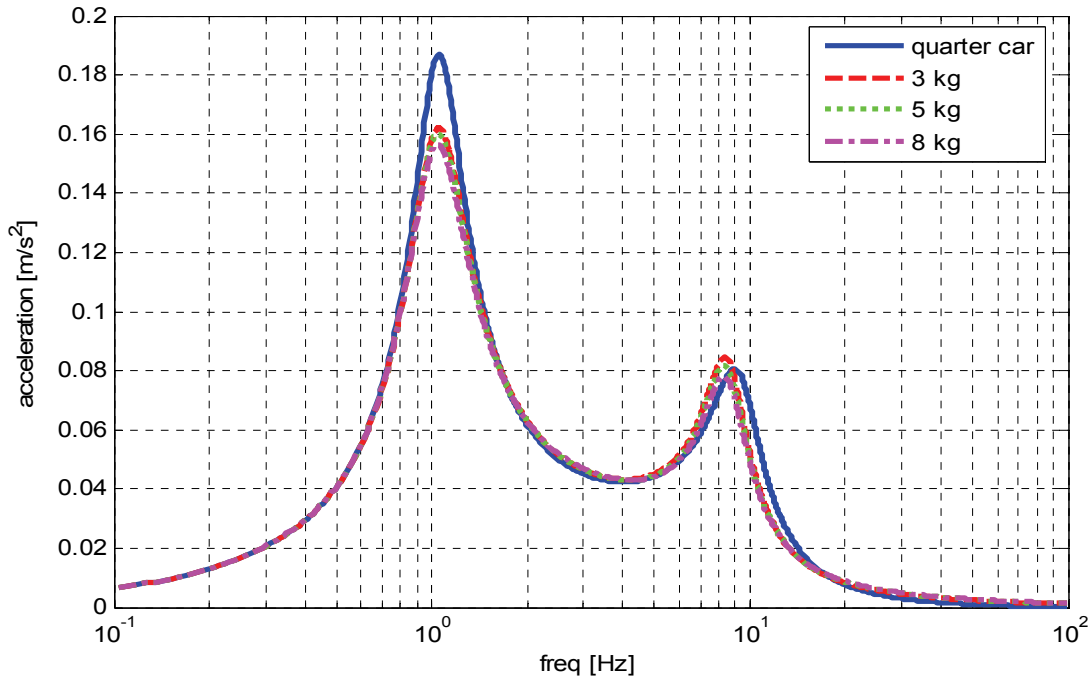

Figure 4.14 Effect of LVI Mass on Sprung Mass Acceleration for LVI Configuration 4 (Set-2)

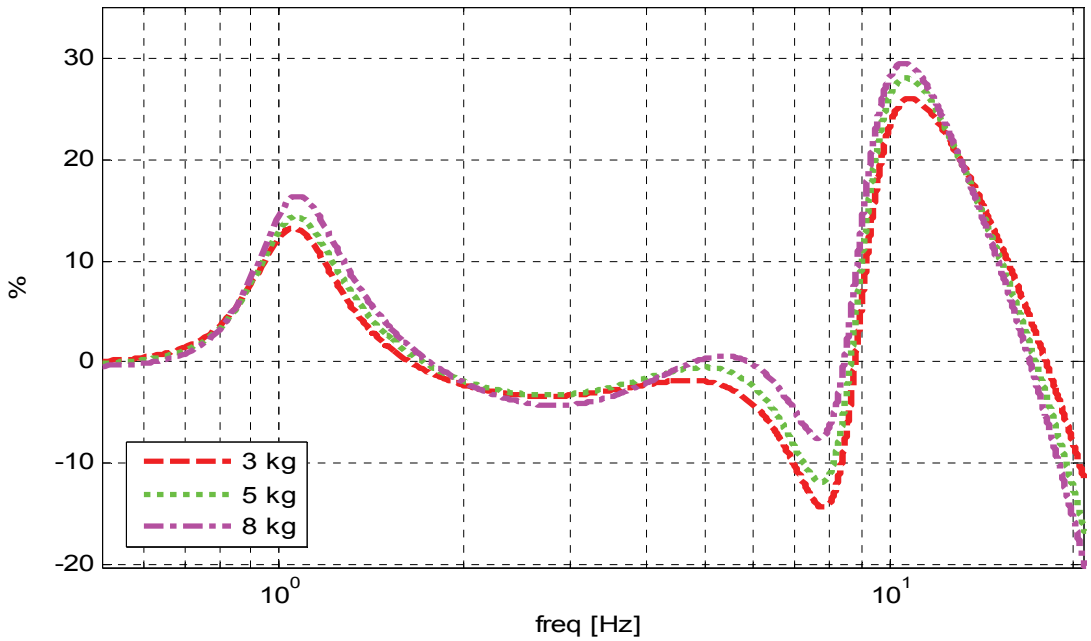

Figure 4.15 Effect of LVI Mass on the Improvement of Sprung Mass Acceleration for LVI Configuration 4 (Set-2)

4.4.4 RESULTS RESPECT TO ISO 2631 STANDARDS

In this part of the study, LVI configuration 4 with two different sets of weighting coefficients and additional mass of 3 kg and standard quarter car model are compared with respect to ISO 2631 ride comfort boundaries. In Figure 4.16 the performances of chain of LVI configuration 4 and quarter-car model are plotted with respect to ISO 2631 ride comfort boundaries for a harmonic input of 0.025 m/s. It can be seen that the standard quarter-car model exceeds the 2.5 hours boundary around the body bounce frequency. However, 2.5 hours boundary is satisfied in LVI configurations. Although set-1 weighting coefficients give more satisfactory results around body bounce frequency, set-2 weighting coefficients show better performance around wheel hop frequency and slightly exceeds the 4 hours boundary. Hence, for travelling 4 hours in the vehicle on which LVI configuration 4 is implemented, without feeling tiredness around the wheel hop frequency, set-1weighting coefficients should be used. If 2.5 hour boundary is more important in all frequency range, then set-2 weighting coefficients should used.

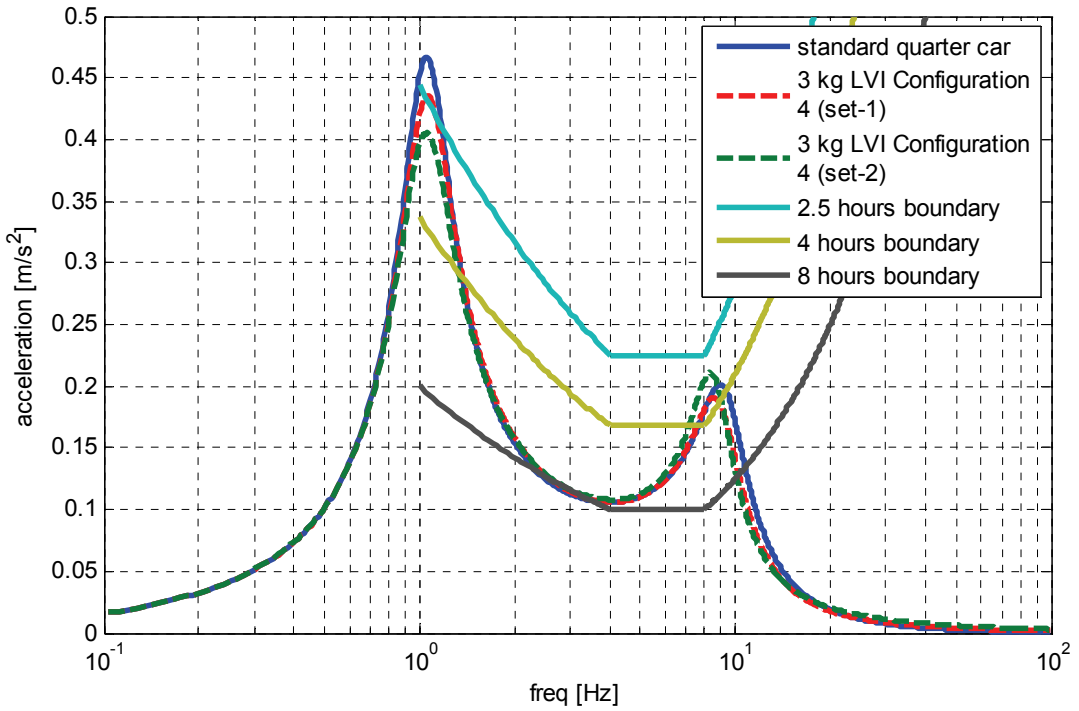

Figure 4.16 Comparison of Chain of LVI Configuration and Quarter-Car Model with Respect to ISO 2631 Curves

CHAPTER 5

RESPONSE UNDER RANDOM ROAD PROFILE

5.1 INTRODUCTION

There exists many studies in the literature about the effects of road roughness on road vehicles. The reason is that it is important to make simulations on the predicted road surfaces in the design stage of road vehicles for reducing the time and cost desired. In former studies, easily generated road surface models were selected such as sine waves. The analysis was verified by constructing specific obstacles and testing the vehicle on them. Since the validity of input, sine wave, was questionable, prediction of vehicle behaviour and the optimum design was difficult [3].

In recent studies, road surface profile is either deterministic or random. If the road profile at any future time can be determined, then it is called deterministic profile. However, for random inputs, the profile at any future time cannot be predicted. For deterministic inputs, road surface profiles are recorded and simulations are made on the recorded profile. Initial assumption in random studies is that road roughness is ergodic. In other words, the wheels on the left and right side of the vehicle are subjected to identical inputs. In this study, the quarter car model is used, therefore only vertical vibrations are considered.

5.2. ROAD SURFACE MODELLING

In this study, first order shaping filter proposed in the project of Kılıç [64] is used with a white noise input. It is known that the power spectral density of the white noise is constant at every frequency of interest. Filter equation is given as follows

$$\dot{y}(t) = -V\beta y(t) + \sqrt{\frac{2V\beta\sigma^2}{\pi}}w(t), \tag{5.1}$$

where $w(t)$ is the white noise input, V is the forward velocity of the vehicle in m/s, σ^2 is the variance of the road irregularities in m^2, β is the breakaway frequency in m^{-1} which depends on the type of the road and $y(t)$ is the road surface displacement in meters.

The values of the coefficients of β and σ^2 depending on different road conditions are given in Table 5.1.

Table 5.1 Road Surface Coefficients [3]

Road Type	$\boldsymbol{\beta}[\boldsymbol{m^{-1}}]$	$\boldsymbol{\sigma}[\boldsymbol{m}]$
Asphalt	0.15	0.0033
Concrete	0.20	0.0056
Rough	0.40	0.0120

5.2 EQUATIONS OF MOTION

It is possible to combine the filter equation with the equations of motion of the quarter car model. The equations of motion for the system that will be investigated under random input conditions can be re-written for the velocity input case. In this part of the study, only single LTMD configuration is considered.

5.2.2 EQUATIONS OF MOTIONS FOR THE QUARTER-CAR MODEL

The mass, damping, stiffness matrices and position vectors of quarter car model are given in the Chapter 1. For the quarter-car model given in Figure 1.1, the equations of motion are:

$$m_{us}\ddot{x}_1 = c_s(\dot{x}_2 - \dot{x}_1) + k_s(x_2 - x_1) + k_t(x_0 - x_1), \tag{5.2}$$

$$m_s\ddot{x}_2 = c_s(\dot{x}_1 - \dot{x}_2) + k_s(x_1 - x_2). \tag{5.3}$$

Leaving the acceleration terms alone gives:

$$\ddot{x}_1 = \frac{c_s}{m_{us}}(\dot{x}_2 - \dot{x}_1) + \frac{k_s}{m_{us}}(x_2 - x_1) + \frac{k_t}{m_s}(y - x_1), \tag{5.4}$$

$$\ddot{x}_2 = \frac{c_s}{m_s}(\dot{x}_1 - \dot{x}_2) + \frac{k_s}{m_s}(x_1 - x_2). \tag{5.5}$$

Choosing a state vector as

$$\{x_{qc}\} = \begin{Bmatrix} \dot{x}_2 \\ \dot{x}_1 \\ x_2 - x_1 \\ x_1 - y \end{Bmatrix}. \tag{5.6}$$

Then equations of motion in state form can be obtained as follows:

$$\{\dot{x}_{qc}\} = [A_{qc}]\{x_{qc}\} + \{B_{qc}\}\dot{y}, \tag{5.7}$$

where

$$[A_{qc}] = \begin{bmatrix} -\frac{c_s}{m_s} & \frac{c_s}{m_s} & -\frac{k_s}{m_s} & 0 \\ \frac{c_s}{m_{us}} & -\frac{c_s}{m_{us}} & \frac{k_s}{m_{us}} & -\frac{k_t}{m_{us}} \\ 1 & -1 & 0 & 0 \\ 0 & 1 & 0 & 0 \end{bmatrix}, \tag{5.8}$$

and

$$\{B_{qc}\} = \begin{Bmatrix} 0 \\ 0 \\ 0 \\ -1 \end{Bmatrix}. \tag{5.9}$$

Inserting the filter equation into the state equation,

$$\{\dot{x}_{qc}\} = [A_{qc}]\{x_{qc}\} - \{B_{qc}\}V\beta y(t) + \{B_{qc}\}\sqrt{\frac{2V\beta\sigma^2}{\pi}}w(t). \tag{5.10}$$

In state space form:

$$\begin{Bmatrix} \{\dot{x}_{qc}\} \\ \dot{y} \end{Bmatrix} = \begin{bmatrix} [A_{qc}] & -\{B_{qc}\}V\beta \\ 0 & -V\beta \end{bmatrix} \begin{Bmatrix} \{x_{qc}\} \\ y \end{Bmatrix} + \begin{Bmatrix} \{B_{qc}\}\sqrt{\frac{2V\beta\sigma^2}{\pi}} \\ \sqrt{\frac{2V\beta\sigma^2}{\pi}} \end{Bmatrix} w(t). \tag{5.11}$$

5.2.3 EQUATIONS OF MOTION FOR THE SINGLE LTMD CONFIGURATION

The mass, damping and stiffness matrices are given in Chapter 2 for the single LTMD configuration (Figure 2.1). Equations of motion for this case are,

$$m_{us}\ddot{x}_1 = c_s(\dot{x}_2 - \dot{x}_1) + c_1(\dot{x}_3 - \dot{x}_1) + k_s(x_2 - x_1) + k_1(x_3 - x_1) + k_t(y - x_1), \quad (5.12)$$

$$m_s\ddot{x}_2 = c_s(\dot{x}_1 - \dot{x}_2) + k_s(x_1 - x_2), \quad (5.13)$$

$$m_1\ddot{x}_3 = c_1(\dot{x}_1 - \dot{x}_3) + k_1(x_1 - x_3). \quad (5.14)$$

Rewriting equations:

$$\ddot{x}_1 = \frac{c_s}{m_{us}}(\dot{x}_2 - \dot{x}_1) + \frac{c_1}{m_{us}}(\dot{x}_3 - \dot{x}_1) + \frac{k_s}{m_{us}}(x_2 - x_1) + \frac{k_1}{m_{us}}(x_3 - x_1) + \frac{k_t}{m_{us}}(y - x_1), \quad (5.15)$$

$$\ddot{x}_2 = \frac{c_s}{m_s}(\dot{x}_1 - \dot{x}_2) + \frac{k_s}{m_s}(x_1 - x_2), \quad (5.16)$$

$$\ddot{x}_3 = \frac{c_1}{m_1}(\dot{x}_1 - \dot{x}_3) + \frac{k_1}{m_1}(x_1 - x_3), \quad (5.17)$$

choosing state vector as

$$\{x_{LTMD}\} = \begin{Bmatrix} \dot{x}_3 \\ \dot{x}_2 \\ \dot{x}_1 \\ x_3 - x_1 \\ x_2 - x_1 \\ x_1 - y \end{Bmatrix}. \tag{5.18}$$

Then equation of motion becomes

$$\{\dot{x}_{LTMD}\} = [A_{LTMD}]\{x_{LTMD}\} + \{B_{LTMD}\}\dot{y}, \tag{5.19}$$

where

$$[A_{LTMD}] = \begin{bmatrix} -\frac{c_1}{m_1} & 0 & \frac{c_1}{m_1} & -\frac{k_1}{m_1} & 0 & 0 \\ 0 & -\frac{c_s}{m_s} & \frac{c_s}{m_s} & 0 & -\frac{k_s}{m_s} & 0 \\ \frac{c_1}{m_{us}} & \frac{c_s}{m_{us}} & -\frac{c_s}{m_{us}} - \frac{c_1}{m_{us}} & \frac{k_1}{m_{us}} & \frac{k_s}{m_{us}} & -\frac{k_t}{m_{us}} \\ 1 & 0 & -1 & 0 & 0 & 0 \\ 0 & 1 & -1 & 0 & 0 & 0 \\ 0 & 0 & 1 & 0 & 0 & 0 \end{bmatrix}, \tag{5.20}$$

$$[B_{LTMD}] = \begin{Bmatrix} 0 \\ 0 \\ 0 \\ 0 \\ 0 \\ -1 \end{Bmatrix}. \tag{5.21}$$

Inserting filter equation (5.1) into system equation as follows

$$\{\dot{x}_{LTMD}\} = [A_{LTMD}]\{x_{LTMD}\} - \{B_{LTMD}\}V\beta y(t) + \{B_{LTMD}\}\sqrt{\frac{2V\beta\sigma^2}{\pi}}w(t). \quad (5.22)$$

In state space form:

$$\begin{Bmatrix}\{\dot{x}_{LTMD}\}\\ \dot{y}\end{Bmatrix} = \begin{bmatrix}[A_{LTMD}] & -\{B_{LTMD}\}V\beta\\ 0 & -V\beta\end{bmatrix}\begin{Bmatrix}\{x_{LTMD}\}\\ y\end{Bmatrix} + \begin{Bmatrix}\{B_{LTMD}\}\sqrt{\frac{2V\beta\sigma^2}{\pi}}\\ \sqrt{\frac{2V\beta\sigma^2}{\pi}}\end{Bmatrix}w(t). \quad (5.23)$$

5.3 BODE PLOTS

The magnitude of frequency response functions of the equations of motion of the system with filter equations are investigated in this part of the study. Since a first order shaping filter is utilized, the effect of velocity and road conditions can be observed.

5.3.1 VELOCITY EFFECT

The effect of velocity on sprung mass acceleration is investigated in this part of the study. The road is assumed to be asphalt. Using the standard quarter car model equations combined with the first order shaping filter gives the following results shown in Figure 5.1. It is observed that as the vehicle velocity increases, the acceleration response of sprung mass also increases. However, the acceleration increment at high speeds is lower than the one at low speeds.

5.3.2 EFFECT OF ROAD CONDITIONS

Three different road conditions are tabulated in Table 5.1. An appropriate velocity for these three road conditions, which is 40 kph, is selected and the effect of road condition is observed on the standard quarter car model. It can be seen from

Figure 5.2 that the sprung mass acceleration strongly depends on road surface conditions. As the road surface become rough, the effect of peaks at both body bounce and wheel hop frequencies becomes more significant.

5.4 OPTIMIZATION UNDER RANDOM ROAD INPUT

In this part of the study, optimization under random road input for different road conditions and velocities are investigated on single LTMD configuration with 5 kg TMD mass. Moreover the optimum results obtained from harmonic road input are tested under random road input and the results of them are compared.

Optimization parameters consists of the concentrated mass m_1, TMD stiffness constant k_1 and damping ratio of TMD. The objective function is defined as the sum of areas under the bode magnitude plot multiplied by selected weighting coefficients.

$$\sum_{i=1}^{n} A_i z_i = A_T. \tag{5.24}$$

Areas are divided according to the frequency ranges given in Table 2.1. The coefficients obtained for the best performance, are given in Table 5.2.

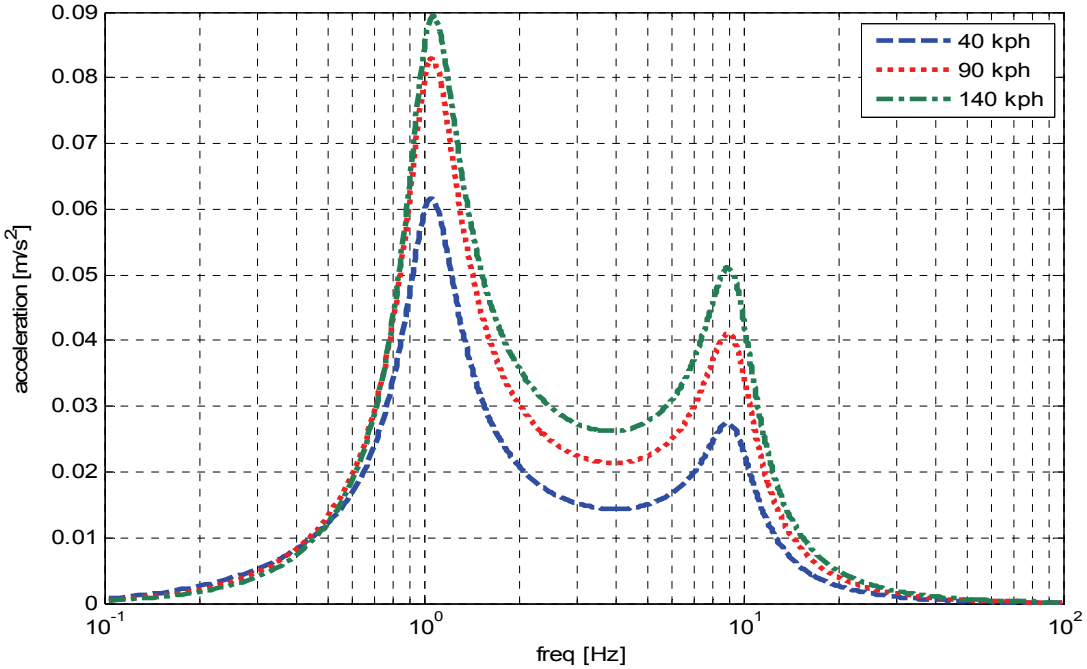

Figure 5.1 Effect of Velocity to the Sprung Mass Acceleration on Asphalt Road (Standard Quarter-Car Model)

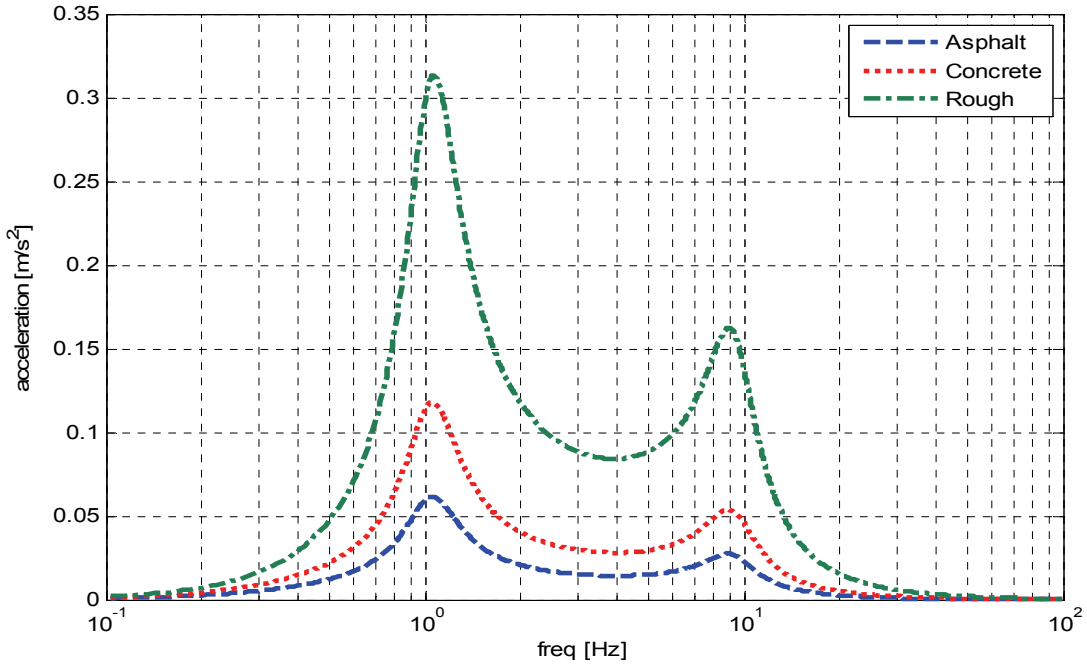

Figure 5.2 Effect of Road Conditions to the Sprung Mass Acceleration at Constant Speed 40 kph (Standard Quarter-Car Model)

Table 5.2 Weighting Coefficients for Random Input

Coefficients	Single LTMD
z_1	1
z_2	1
z_3	1
z_4	4
z_5	7
z_6	7
z_7	6
z_8	4
z_9	4
z_{10}	3
z_{11}	1
z_{12}	0

A lower limit to the damping ratios of TMDs is again imposed in order not to deteriorate performance of the system at frequencies lower than the natural frequency of the TMDs.

The statement of the optimization problem is:

$$\text{minimize} \qquad A_T = \sum_{i=1}^{n} \left(z_i \int_{fr_i} |a(\omega)| d\omega \right), \tag{5.25}$$

subject to

$$m_1 \leq 5\ kg, \tag{5.26}$$

$$0.3 \leq \xi_{\mathrm{TMD}} < 1. \tag{5.27}$$

5.5 RESULTS

Since the sprung mass acceleration depends on road surface conditions and forward velocity, the optimization is done for three different road conditions and three different velocities. The optimization results of parameters can be seen in Table 5.3. It can be seen in optimization results that the damping ratios reach their minimum value. The stiffness constants of the TMDs are very close to each other for different road conditions and velocities. Optimization result for 0.01 m/s harmonic velocity input is given in Table 5.4. Again very close result is obtained to the random input case.

Table 5.3 Optimization Results for Different Road Conditions and Velocities

Road \ Velocity	**50 kph**	**70 kph**	**90 kph**
Asphalt	$m_1 = 5$ kg $k_1 = 7843$ N/m $\xi = 0.3$	$m_1 = 5$ kg $k_1 = 7848$ N/m $\xi = 0.3$	$m_1 = 5$ kg $k_1 = 7854$ N/m $\xi = 0.3$
Concrete	$m_1 = 5$ kg $k_1 = 7847$ N/m $\xi = 0.3$	$m_1 = 5$ kg $k_1 = 7856$ N/m $\xi = 0.3$	$m_1 = 5$ kg $k_1 = 7868$ N/m $\xi = 0.3$
Rough	$m_1 = 5$ kg $k_1 = 7874$ N/m $\xi = 0.3$	$m_1 = 5$ kg $k_1 = 7909$ N/m $\xi = 0.3$	$m_1 = 5$ kg $k_1 = 7953$ N/m $\xi = 0.3$

Table 5.4 Optimization Results for 0.01 m/s Harmonic Velocity Input

m_1	5 kg
k_1	7838 N/m
ξ_1	0.3

The input to the systems given by Equations (5.11) and (5.23) is the white noise. In frequency magnitude response, the white noise vector generated can be converted into frequency domain using discrete fourier transform. The obtained results plotted under random road input is given in the following figures. In Figure 5.3, the sprung mass accelerations of quarter car model and single LTMD configuration with 5 kg TMD mass are plotted under random road input with a velocity of 90 kph on asphalt road. The single LTMD parameters are taken from Table 5.3 for 90 kph speed on asphalt road. As can be seen from Figure 5.3 the sprung mass acceleration is attenuated around 10 Hz. In Figure 5.4 the comparison of optimizations under random road and harmonic road inputs are made. The optimized parameters of single LTMD configuration are taken for asphalt road at 90 kph speed and harmonic velocity input. Sprung mass acceleration plot is again obtained for asphalt road at 90 kph speed. Results show that the blue plot is on the top of red one (Figure 5.4). Although the optimization for random input is made for asphalt road at 90 kph, the harmonic input optimization results gives the similar results with random road input case. In Table 5.3 the most different values from harmonic optimization result is obtained for rough road at 90 kph speed. Therefore the optimized single LTMD configuration under random road input on rough road at 90 kph is tested with the optimization results obtained from harmonic road input on Figure 5.5. Both optimization results are tested under rough road condition at 90 kph speed but again the results are nearly identical. Therefore, according to these simulation results it can be said that, it is enough to optimize the system under harmonic velocity input.

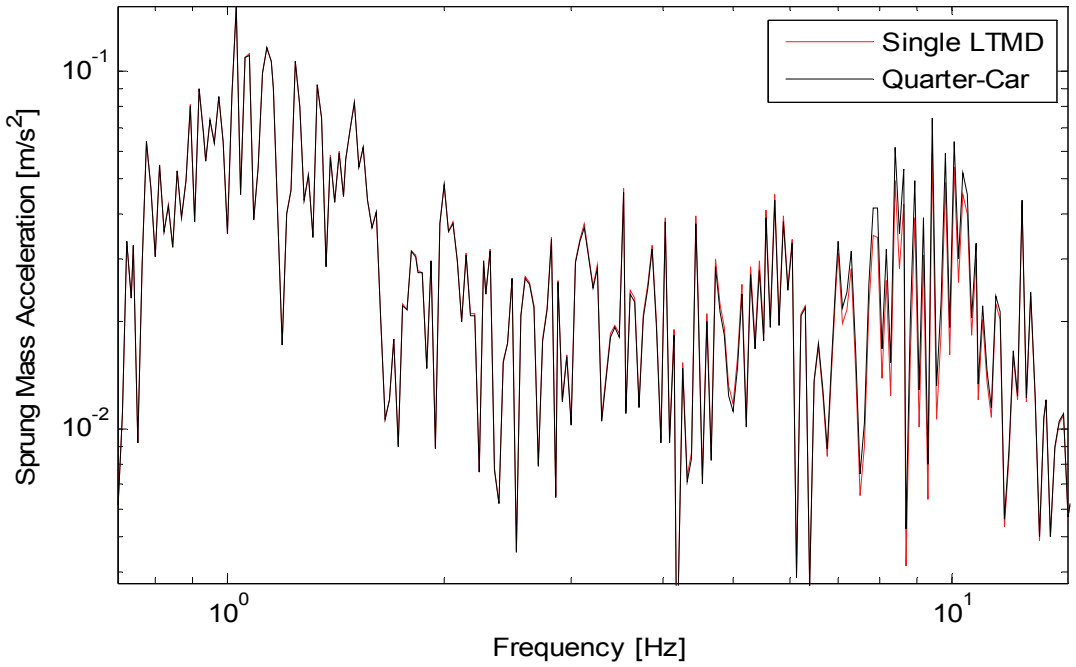

Figure 5.3 Comparison of Sprung Mass Accelerations of Optimized Single LTMD and Quarter Car Model

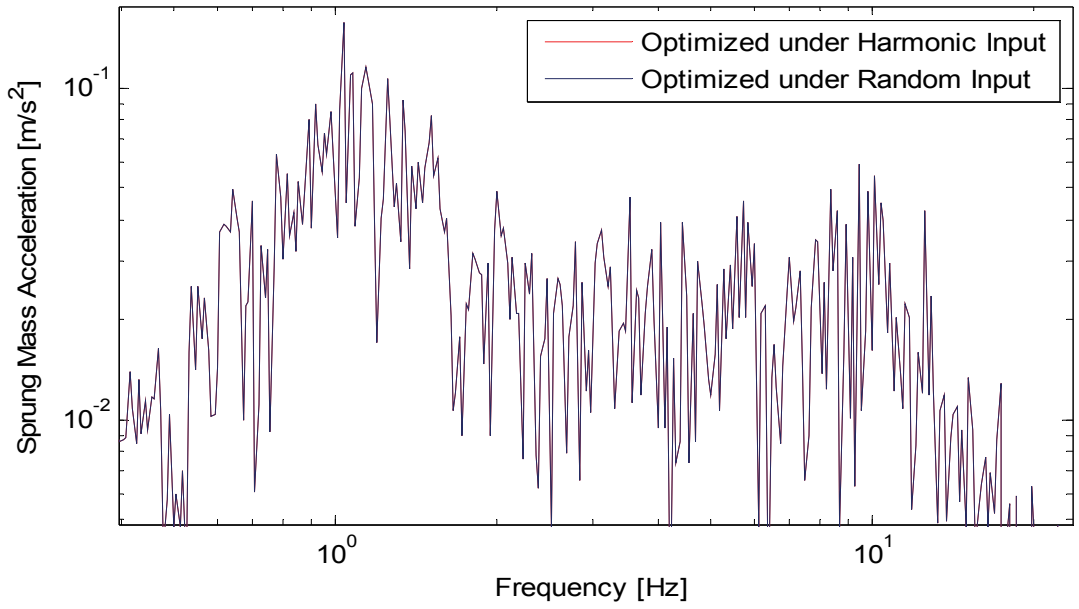

Figure 5.4 Comparison of Optimization Results for Harmonic and Random Road Input (Asphalt)

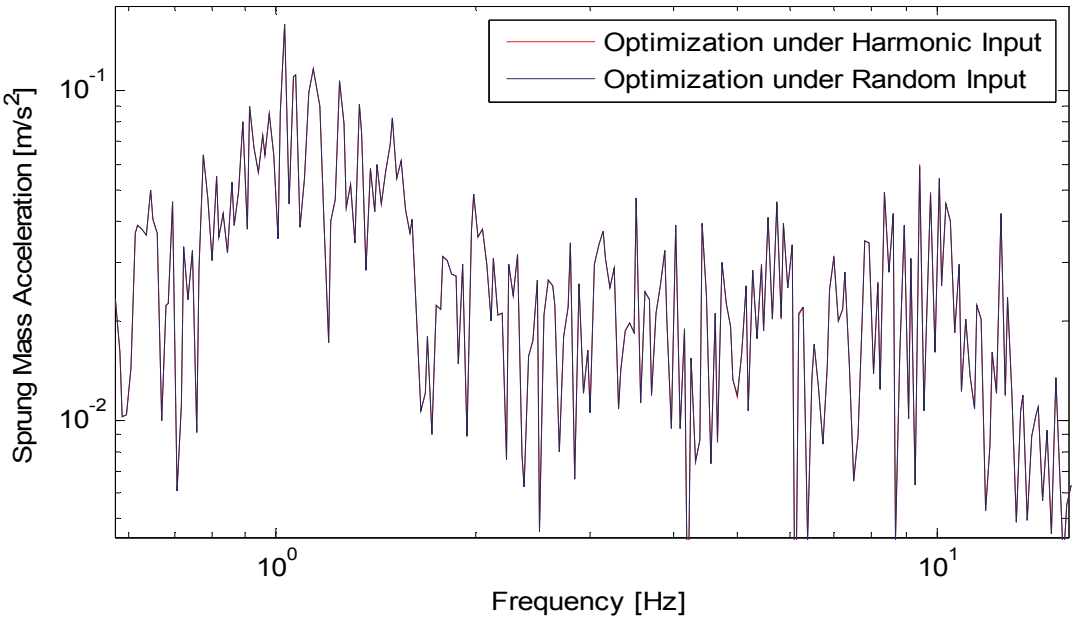

Figure 5.5 Comparison of Optimization Results for Harmonic and Random Road Input (Rough)

CHAPTER 6

THE EFFECT OF PARAMETER CHANGES ON OPTIMIZED SYSTEM

6.1 INTRODUCTION

In chapter 5, the performance of optimum system parameters obtained from harmonic input is tested under random input and it is observed that optimization results obtained under harmonic input are very close to the results obtained under random input. In this chapter, the effect of change of optimized parameters due to aging of TMD and LVI components and manufacturing defects are investigated. Moreover, the effect of change of sprung mass because of additional passengers added on the vehicle is investigated. It is not always easy to manufacture the component parameters exactly as desired. There exists tolerances in the manufacturing process and also manufacturing defects may occur during production. Furthermore, the parameters of components may change in time. Also the optimization is done according to the single driver condition. In the case of more passengers in the car change of sprung mass acceleration should also be investigated. The effects of all of these problems should be concerned before the production; therefore, Monte Carlo simulations used in the following section in order to analyze the optimized systems.

6.2 METHODOLOGY & RESULTS

6.2.1 SINGLE LTMD CONFIGURATION

In Monte Carlo simulations, initially random data with uniform distribution is generated for the values of m_1, k_1 and c_1 values for the configuration of single LTMD which is optimized for 3 kg TMD mass. It is considered that each parameter may vary $\pm 10\%$, due to manufacturing defects and aging. In this study 10000 samples of random data are generated. After the generation of sample data, frequency response function for each data set is calculated and histogram plot of samples are obtained at every frequency in order to get the distribution of samples. Then, these histograms are combined and probability distribution of the resulting frequency response functions is obtained. The variation of sprung mass acceleration according to the change of m_1, k_1 and c_1 values for single LTMD configuration can be seen in Figure 6.1.

It can be seen on Figure 6.1 that the sprung mass acceleration is slightly effected at frequencies around wheel hop. The color spectrum gives the probability of getting an acceleration value at each frequency. Since the distribution of samples around wheel hop frequency is wider, the probability of obtaining a sample data at a specific acceleration decreases. At frequencies other than wheel hop frequency, the distribution of samples is concentrated in a narrow range. Therefore the red color is dominant at those frequencies. Also the plot of optimum values is drawn on the same figure with black color for comparison purposes.

Two probability distribution plots of accelerations at different frequencies are given in Figure 6.2 and Figure 6.3. In Figure 6.2, the distribution is obtained at 2 Hz. It can be seen that at 2 Hz all results concentrate at the same acceleration value. When the thickness of bins are taken as $10^{-3}\ m/s^2$, a single bin is obtained.

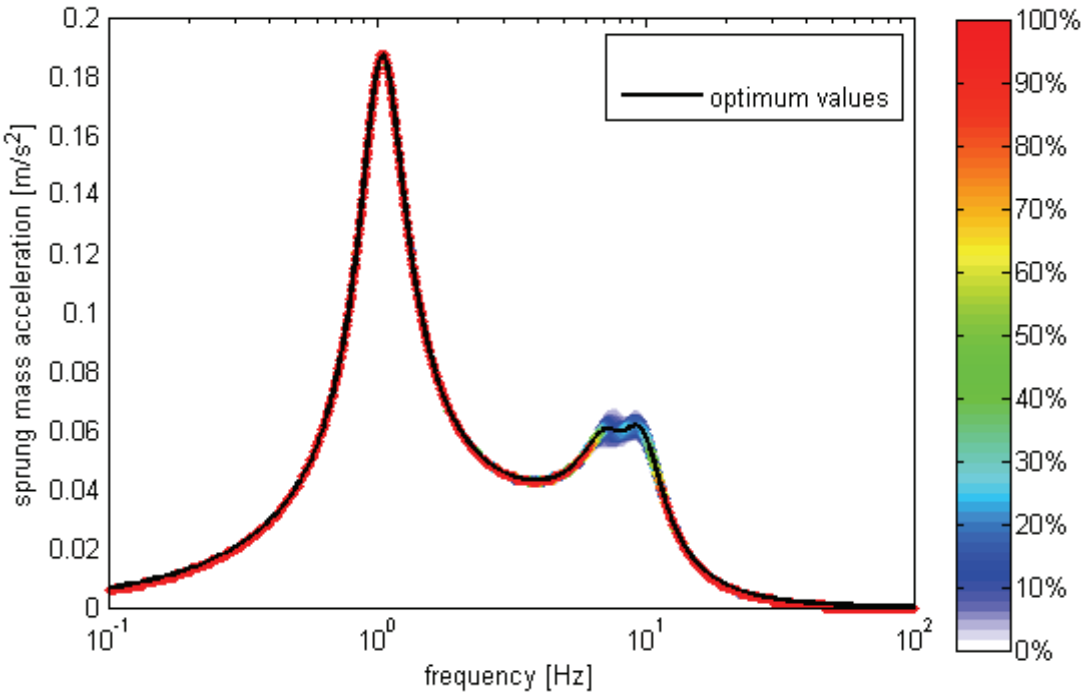

Figure 6.1 Results Obtained for $\pm 10\%$ Change of m_1, k_1 and c_1 on Single LTMD Configuration

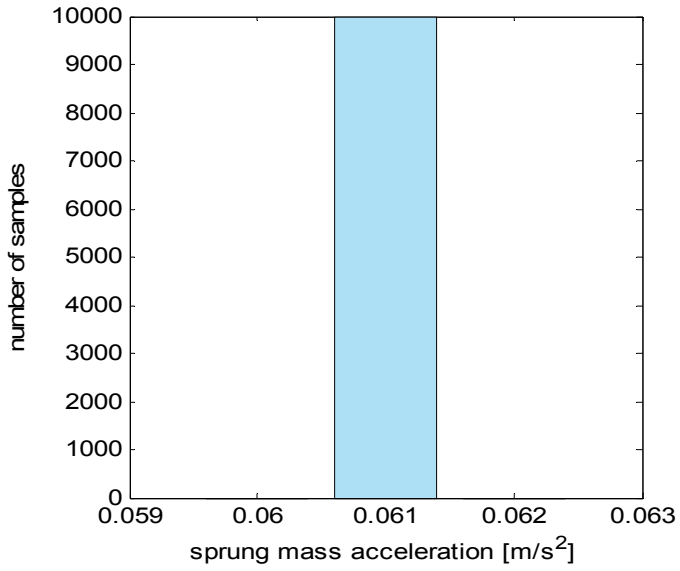

Figure 6.2 The Distribution of 10000 Sample Data at 2 Hz

In Figure 6.3, given is the probability distribution plot calculated at 9 Hz. It can be observed that, the distribution of samples concentrate around the average value, 0.062 m/s^2; therefore, the probability is higher at those points and it decreases as the data deviates from the average value.

In the second stage of analysis, the effect of sprung mass is investigated due to loading condition of the car. It is assumed that the sprung mass of an automobile can increase 40% in full loaded condition. Therefore a random data for sprung mass is generated between 320 kg and 448 kg to observe the variation in sprung mass acceleration. When the results are plotted the distribution obtained is given in Figure 6.4. Also the original plot when the sprung mass is 320 kg is plotted on the same figure with black color. As can be seen from Figure 6.4, the first peak which belongs to the sprung mass resonance, shifted to lower frequencies as expected. At frequencies higher than body bounce, the sprung mass acceleration decreases as the sprung mass increases. Moreover, the probability of the sprung mass acceleration at low and at high frequencies can be observed from the color distribution. In Figure 6.5, the performance of single LTMD configuration with optimum m_1, k_1 and c_1 values obtained by optimization using 320 kg sprung mass is plotted at fully loaded condition and compared with fully loaded quarter car model. Results show that suppression at wheel hop frequency continues at fully loaded condition as well.

In the last stage of the study on the single LTMD configuration, the sprung mass ($+40\%$) and optimized parameters ($\pm 10\%$) are changed at the same time. In other words the manufacturing defects, aging and change in loading conditions are investigated together. It is observed in Figure 6.4 that increase of sprung mass decreases the sprung mass acceleration around wheel hop frequency. Moreover, on Figure 6.6, although both optimization parameters and sprung mass are changed together, the optimum plot has higher acceleration values at frequencies higher than body bounce. This result shows that change in sprung mass has the highest effect on

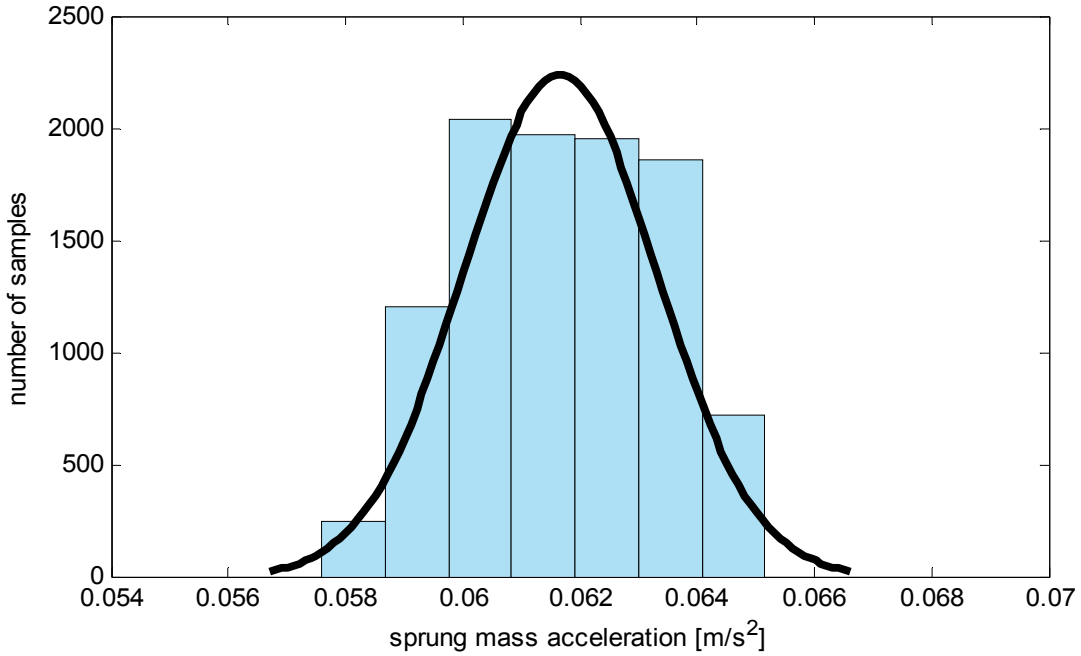

Figure 6.3 The Distribution of 10000 Sample Data at 9 Hz

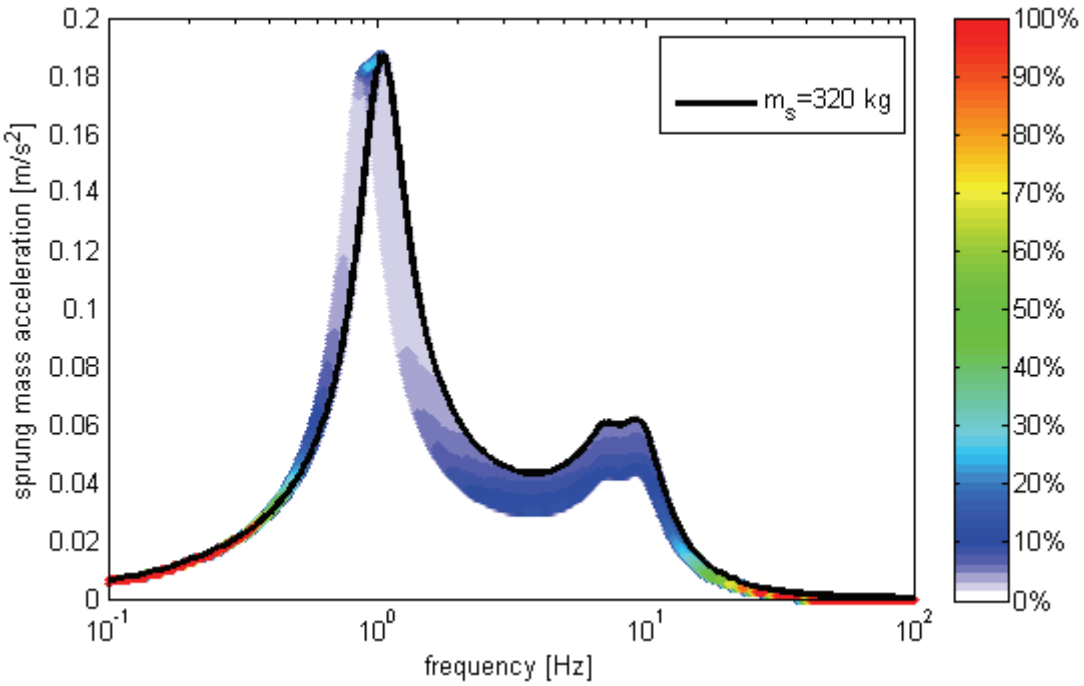

Figure 6.4 Results Obtained for 40% Change of m_s on Single LTMD Configuration

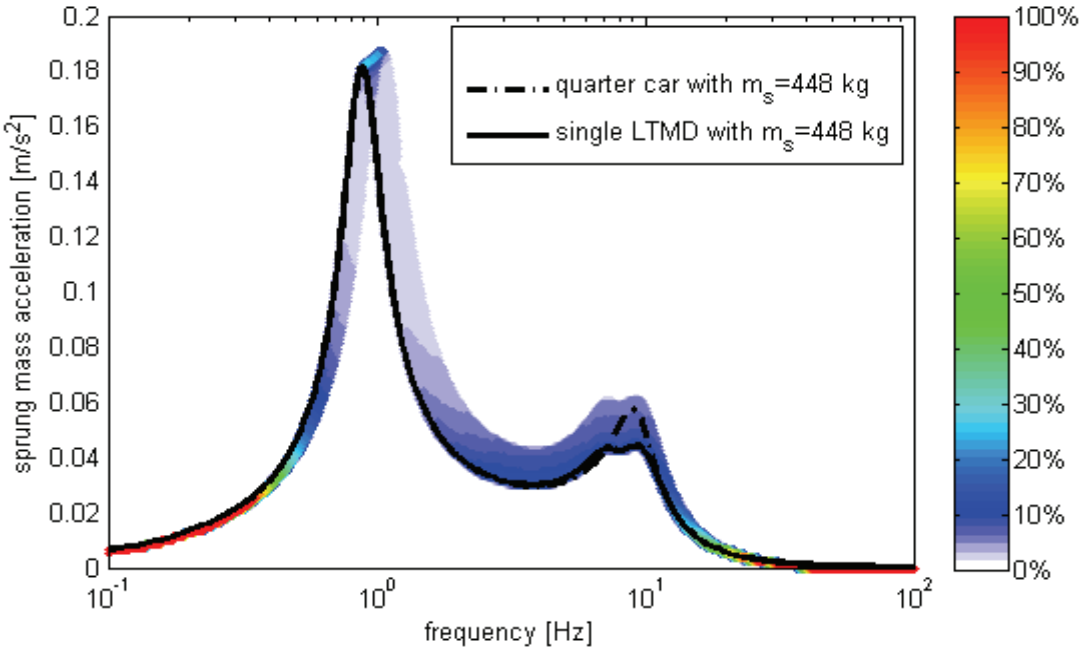

Figure 6.5 Comparison of Single LTMD and Quarter-Car Model on Fully Loaded Condition

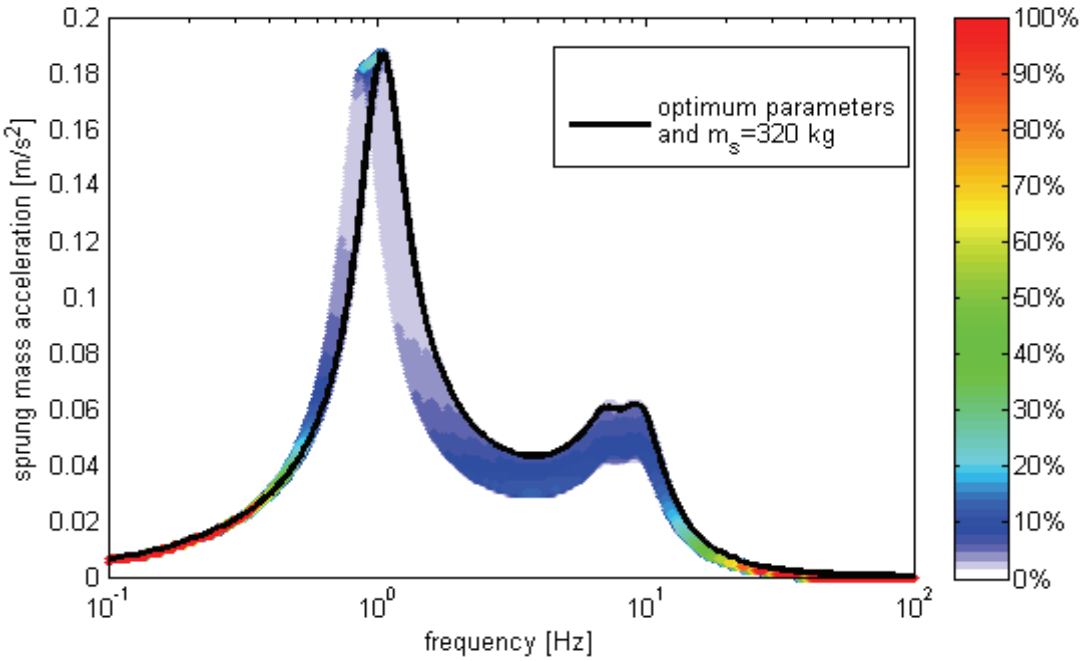

Figure 6.6 Results Obtained for $\pm 10\%$ Change of m_1, k_1 and c_1 and 40% Change of Sprung Mass on Single LTMD Configuration

sprung mass acceleration. Moreover, the optimum results identifies the upper and lower boundaries for the sprung mass acceleration at frequencies higher and lower than the body bounce, respectively .

6.2.2 CHAIN OF LTMD CONFIGURATION

In chain of LTMD configuration with n=3, and total TMD mass of 3 kg, Monte Carlo simulation is made. Firstly the mass, damping and stiffness values of TMDs are changed $\pm$10% from their optimum values which are given in Chapter 2, and 10000 random data with uniform distribution is generated. The obtained result is given in Figure 6.7. It is observed that, the parameter change of mass, damping and stiffness values of TMDs effect the sprung mass only around wheel hop frequency as in the case of single LTMD configuration. However, the probability distribution of results are different in the single LTMD and the chain of LTMD configurations. The probability of distribution around the optimum curve is higher in chain of LTMD configuration than the one obtained in single LTMD configuration. Therefore one can conclude that chain of LTMD configuration is less sensitive to the manufacturing defects and aging.

Moreover it is known that the sprung mass variation may occur approximately 40% on fully loaded condition. Hence both mass, damping and stiffness values of TMDs and sprung mass are changed at the same time and random data is created similar to the previous study. It can be seen on Figure 6.8 that the curve plotted using optimum values, identifies the upper and lower boundaries at frequencies higher than and lower than the body bounce frequency, respectively.

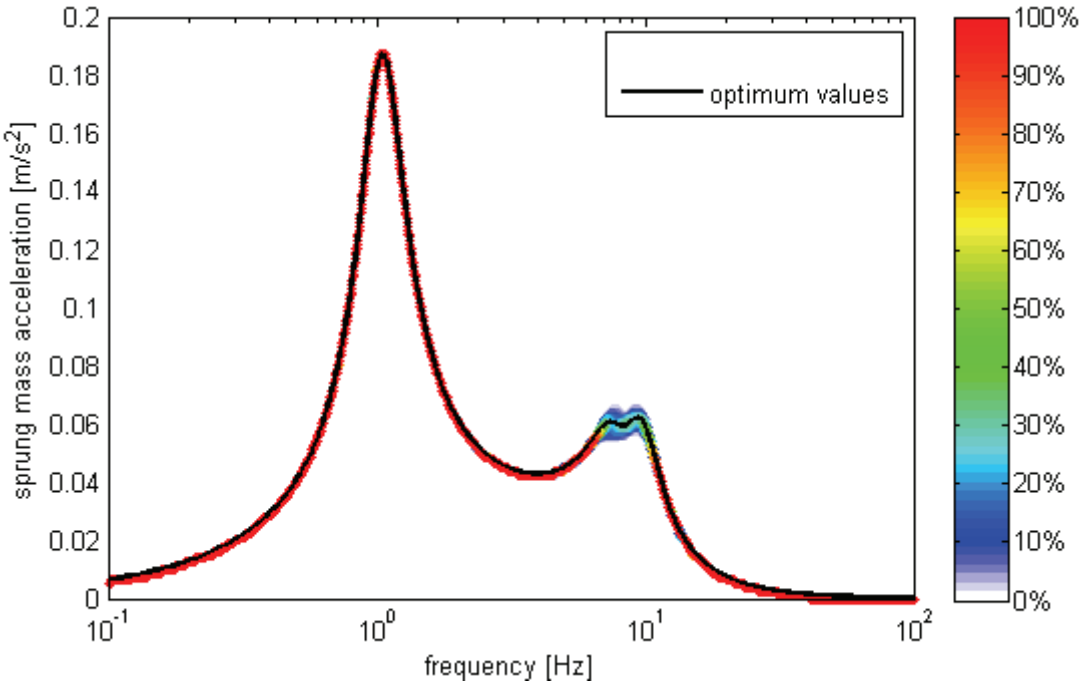

Figure 6.7 Results Obtained for ±10% Change of Mass, Damping and Stiffness values of TMDs on Chain of LTMD Configuration (n=3)

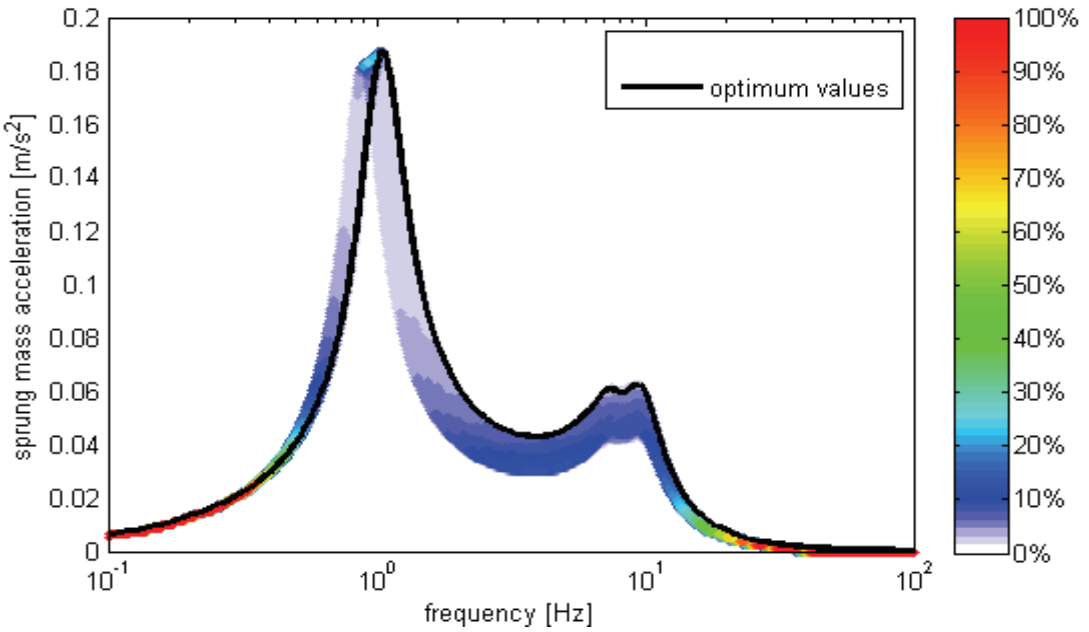

Figure 6.8 Results Obtained for ±10% Change of Mass, Damping and Stiffness values of TMDs and 40% Change of Sprung Mass on Chain LTMD Configuration

6.2.3 LVI CONFIGURATION 4

Finally, Monte Carlo simulations are performed for LVI configuration 4 (set-1) with a total additional mass of 3 kg. In the first case random data is generated for m_1, m_2, α_1 and α_2 in a range of $\pm 10\%$ from their optimum values which are given in Table 4.2. In Figure 6.9 it can be seen that system is less sensitive to the parameters m_1, m_2, α_1 and α_2. Only slight changes are observed around 1.2 Hz and 9 Hz but they are not significant.

In the second case, the change in suspension parameters (k_{s1}, k_{s2}, c_{s1} and c_{s2}) are also added to the Monte Carlo simulation. The variation from optimum values are assumed as $\pm 10\%$. The results are given in Figure 6.10. It can be seen that, the suspension parameter change, mostly effects the sprung mass acceleration at body bounce frequency. Also at frequencies between body bounce and wheel hop, slight effect of suspension parameter change can be observed. But at each frequency, the results obtained from random data are collected around curve drawn by optimum values.

In third case, in addition to the previous cases, the sprung mass is also changed. It is assumed that the variation of sprung mass can be 40% in fully loaded condition. It can be seen in Figure 6.11 that, the optimum curve gives the upper boundary of the probabilities at frequencies higher than body bounce due to sprung mass change. On the other hand at body bounce frequency, due to changes in suspension parameters, probabilities around optimum curve are small.

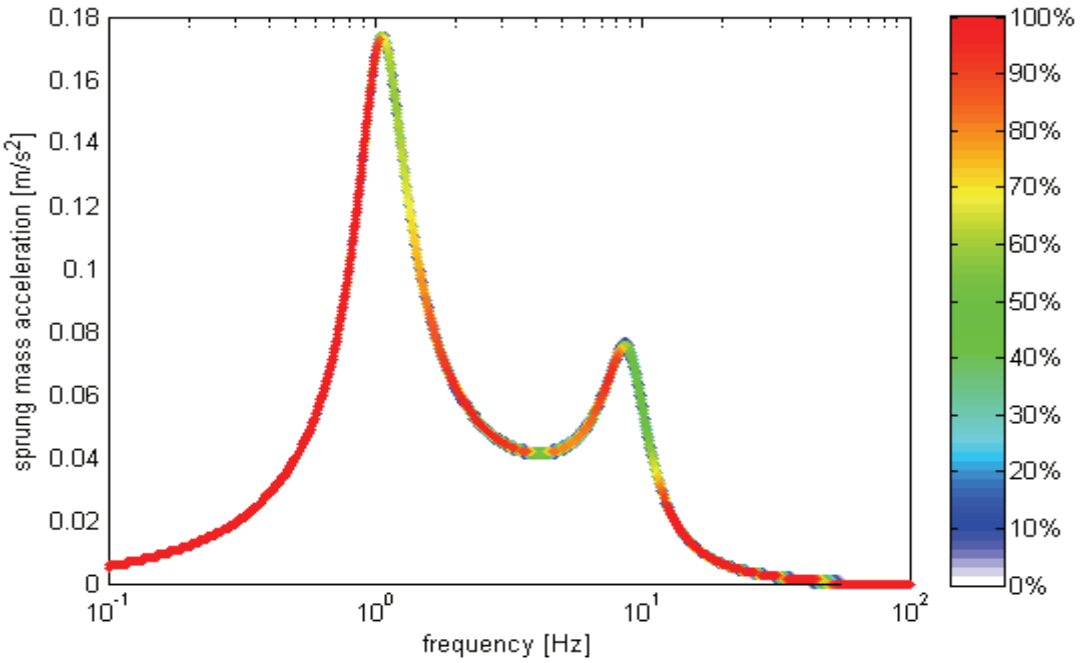

Figure 6.9 Results Obtained for $\pm 10\%$ Change of $m_1, m_2,\ \alpha_1$ and α_2 on LVI Configuration 4

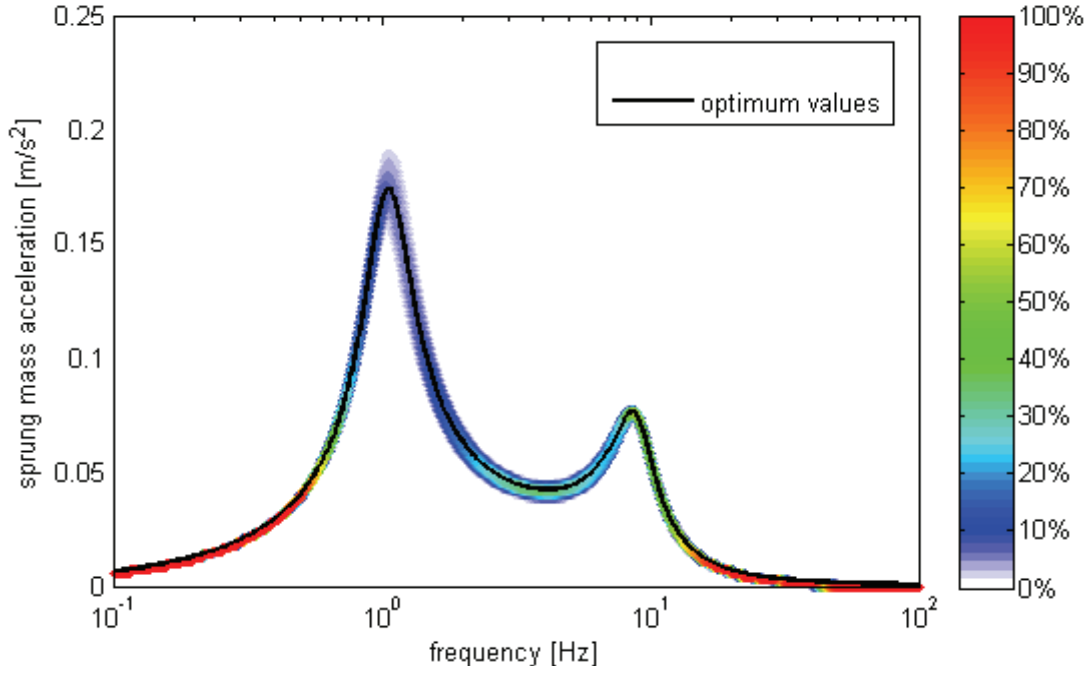

Figure 6.10 Results Obtained for $\pm 10\%$ Change of $m_1, m_2, \alpha_1, \alpha_2, k_{s1}, k_{s2}, c_{s1}$ and c_{s2} on LVI Configuration 4

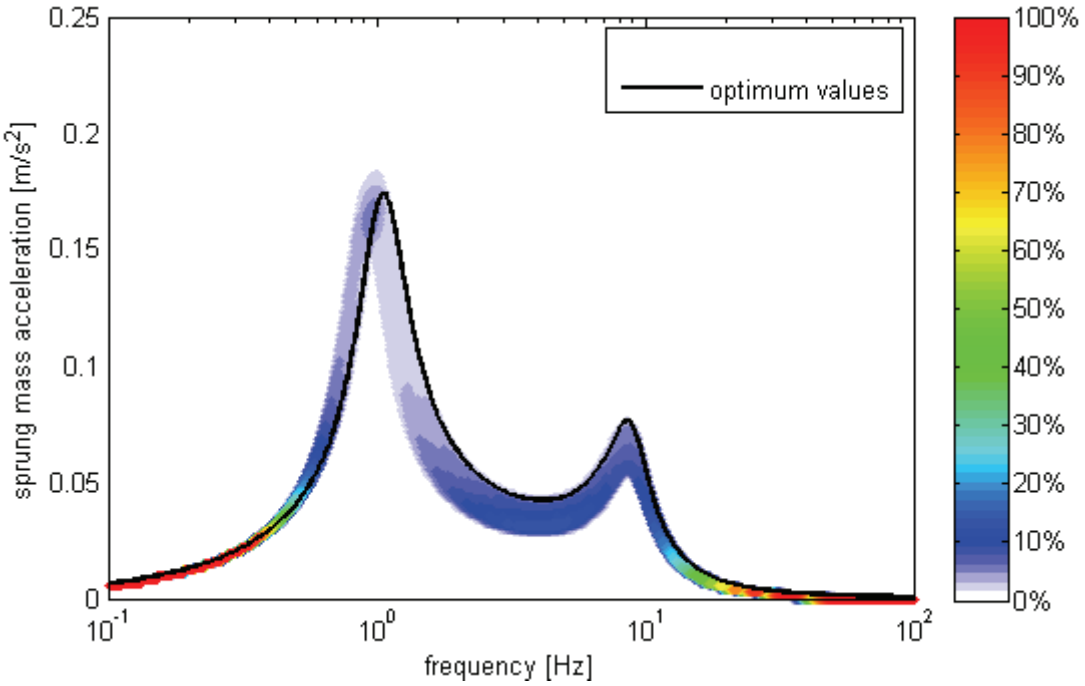

Figure 6.11 Results Obtained for $\pm 10\%$ Change of $m_1, m_2, \alpha_1, \alpha_2, k_{s1}, k_{s2}, c_{s1}, c_{s2}$ and 40% Change of Sprung Mass on LVI Configuration 4

CHAPTER 7

CONCLUSION AND FUTURE WORK

7.1 CONCLUSION

In this study two types of passive vibration isolators are implemented on quarter car model and their effect on ride comfort is investigated. In conclusion, the following observations can be made:

- Tuned mass dampers are implemented on the unsprung mass rather than the sprung mass because a higher mass ratio can be obtained for the former case. It is obvious that a higher mass ratio will give more satisfactory results.

- Sprung mass acceleration is reduced around the wheel hop frequency on TMD implemented configurations since the energy of the unsprung mass is absorbed and dissipated by the TMD at the resonance frequency of the unsprung mass. As a result the transmitted force from the unsprung mass to the sprung mass is reduced and less acceleration is obtained on the sprung mass around the wheel hop frequency.

- Due to the nature of TMDs, unimportant performance deterioration occurs at frequencies lower than the natural frequency of the mass on which the TMD is mounted.

- RTMDs show better performance than LTMDs due to the higher inertia effect. However, the disadvantage of RTMDs is the spacing problem while smaller arm length decrease the effect of RTMD. Therefore, it is better to implement LTMDs on automobiles.

- The performance deterioration in single LTMD configuration at frequencies slightly higher and slightly lower than the wheel hop frequency, can be reduced by using chain of LTMD configuration.

- One has more flexibility while optimizing chains of LTMD system. TMDs can be tuned to different frequencies while optimizing the system and the system response can be reduced at any desired frequency around wheel hop frequency.

- The disadvantage of the chain of LTMD is that the system becomes more complex. The single LTMD can be implemented directly on the unsprung mass without changing the suspension parameters. On the other hand, the suspension should be redesigned during the implementation of the chain of LTMD system.

- LVI configurations reduce sprung mass acceleration around the body bounce frequency, which cannot be obtained if any configuration of TMDs are applied.

- Although the system becomes more complicated in the 2-DOF LVI models compared to the single DOF models, significant improvement in ride comfort is achieved.

- Configurations using type-1 LVI give slightly better performance due to opposite direction of motion of additional mass with respect to the unsprung mass.

- The optimization under random input is not necessary. Optimum parameters obtained under harmonic input is very close to the optimum parameters obtained under random input.

- Chain of LTMD configuration is less sensitive to the parameter changes than single LTMD configuration.

7.2 FUTURE WORK

In order to improve the study, some suggestions can be listed as follows:

- Active TMDs can be used to improve the ride comfort further.

- LVI added configurations can be modeled considering the geometric nonlinearity introduced by the rotation angle in order to get more accurate results.

- Friction dampers can be added to the TMDs in order to increase energy dissipation.

- Different kind of vibration absorbers or isolators can be used to reduce sprung mass acceleration such as centrifugal pendulum vibration absorbers.

- The application of TMDs and LVIs can be investigated on other systems where addition of higher masses is practical: reducing vibrations of machine tools, buildings, bridges etc.

REFERENCES

[1] Karnopp, D. (1995), "Active and Semi-Active Vibration Isolation", *Transactions of American Society of Mechanical Engineers*, Vol. 117, pp. 177–185.

[2] Yilmaz, C., Hulbert, G. M., and Kikuchi, N. (2006), "Reducing Tire-Induced Noise and Vibration," *Tire Science and Technology*, TSTCA, Vol. 34, No. 2, pp. 135-147

[3] Ünlüsoy, Y.S. (2006), *ME513 Vehicle Dynamics Lecture Notes*, Department of Mechanical Engineering, Middle East Technical University

[4] Ivovich, V.A., Savovich, M.K. (2001), "Isolation of Floor Machines by Lever-Type Inertial Vibration Corrector", *Proceedings of the Institution of Civil Engineers - Structures & Buildings,* Vol. 146, Issue 4, pp. 391-402.

[5] Liedes, T., (2009), "Improving the Performance of the Semi-Active Tuned Mass Damper", Ph.D. Thesis, Department of Mechanical Engineering, University of Oulu, Finland

[6] Setareh, M., Ritchey, J.K. and Baxter, A.J. (2006), "Pendulum Tuned Mass Dampers for Floor Vibration Control", *Journal of Performance of Constructed Facilities,* Vol.20, Issue 1, pp.64-73.

[7] Varadarajan, N. and Nagarajaiah, S. (2004), "Wind Response Control of Building with Variable Stiffness Tuned Mass Damper Using Empirical Mode

Decomposition/Hilbert Transform", *Journal of Engineering Mechanics,* Vol.130, No.4, pp 451-458.

[8] Soong, T.T. and Spencer B.F. (2002), "Supplemental Energy Dissipation: State-of-Art and State-of-the-Practice", *Engineering Structures,* Vol.24, No.3, pp. 243-259(17).

[9] Gerges, R.R and Vickery B.J. (2003), "Wind Tunnel Study of the Across-Wind Response of a Slender Tower with a Nonlinear Tuned Mass Damper", *Journal of Wind Engineering and Industrial Aerodynamics,* Vol.91, Issue 8, pp. 1069-1092.

[10] Lee, C.L., Chen, Y.T., Chung, L.L. and Wang Y.P. (2006), "Optimal Design Theories and Applications of Tuned Mass Dampers", *Engineering Structures,* Vol.28, pp. 43-53.

[11] Kareem, A. and Kline, S. (1995), "Performance of Multiple Mass Dampers under Random Loading", *Journal of Structural Engineering*, Vol.121, No.2, pp. 348-361.

[12] Petti, L. and Iuliis, D.M. (2009), "Robust Design of a Single Tuned Mass Damper for Controlling Torsional Response of Asymmetric-Plan Systems", *Journal of Earthquake Engineering,* Vol.13, No.1, pp. 108-128.

[13] Sgobba, S. and Marano, G.C. (2010), "Optimum Design of Linear Tuned Mass Dampers for Structures with Nonlinear Behaviour", *Mechanical Systems and Signal Processing",* Article in Press

[14] Sadek, F., Mohraz, B., Taylor, A.W. and Chung, R.M. (1997), "A Method of Estimating the Parameters of Tuned Mass Dampers for Seismic

Applications", *Earthquake Engineering and Structural Dynamics,* Vol. 26, pp. 617-635.

[15] Kareem, A. and Kijewski, T. (1999), "Mitigation of Motions of Tall Buildings with Specific Examples of Recent Applications", *Wind and Structures,* Vol.2, No.3, pp. 201-251.

[16] Kwok., K.S.C. and Samali, B. (1995), "Performance of Tuned Mass Dampers under Wind Loads", *Engineering Structures,* Vol.17, pp. 655-667.

[17] Konno, T. and Yoshida, M., (1989), "Examples of Practical Applications of Dampers, (4) Higashima Sky Tower", *Struct.,* Vol.32 (In Japanese).

[18] Kwon, H.C., Kim, M.C. and Lee, I.W. (1998), "Vibration Control of Bridges under Moving Loads", *Computers and Structures,* Vol.66, No.4, pp. 473-480.

[19] Lin, C.C., Wang, J.F. and Chen, B.L. (2005), "Train-Induced Vibration Control of High Speed Railway Bridges Equipped with Multiple Tuned Mass Dampers", *Journal of Bridge Engineering,* Vol. 10, No.4, pp. 398-414.

[20] Lin, Y.Y., Cheng, C.M. and Lee, C.H. (2000), "A Tuned Mass Damper for Suppressing the Coupled Flexural and Torsional Buffeting Response of Long-Span Bridges", *Engineering Structures,* Vol.22, pp. 1195-1204.

[21] Matsumoto, Y., Nishioka, T., Shioriji, H. and Matsuzaki, K. (1978), "Dynamic Design of Footbridges", *Int. Assoc. Bridge Struct. Eng.,* P-17/78, 1-15.

[22] Koo, J.H. (2003), "Using Magneto-Rheological Dampers in Semiactive Tuned Vibration Absorbers to Control Structural Dynamics", PhD Thesis,

Department of Mechanical Engineering, Virginia Polytechnic Institute and State University, Virginia, USA.

[23] Shultz, N.A. (2005), "Motion Control of Long Span Horizontal Structures", Ms Thesis, Department of Civil and Environmental Engineering, Massachusetts Institute of Technology, USA.

[24] Hunt, J. B. (1979), *Dynamic Vibration Absorbers*, Mechanical Engineering Publications, Ltd., London.

[25] Collette, C., Horodinca, M. and Preumont, A. (2009), "Rotational Vibration Absorber for the Mitigation of Rail Rutting Corrugation", *Vehicle System Dynamics,* Vol.47, No.6, pp. 641-659.

[26] Yan, T.H., Pu, H.Y., Xu, C., Li, Q., Lin, R.M. and Chen, X.D. (2010), "Dynamic Absorber Design for Actuator Arm of Hard Disc Drives to Improve Impact Resistance", *Mechanics Based Design of Structures and Machines,* Vol.38, No.1, pp. 50-73.

[27] Yan, T.H. and Lin, R.M. (2004), "Dual-Mass Dynamic Absorber for the Head Actuator Assembly in Hard Disc Drives", *Mechanics Based Design of Structures and Machines,* Vol.32, No.2, pp. 119-132.

[28] Bakioglu M. and Aldemir, U. (2008), "Energy Distribution in a Flexible Marine Structure with Passive Mass Damper", *International Journal of Mechanics and Solids",* Vol. 3, No.2, pp. 169-184.

[29] Wang, M., Zan, T., Yang, Y. and Fei, R. (2010), "Design and Implementation of nonlinear TMD for Chatter Suppression: An Application in Turning

Processes", *International Journal of Machine Tools and Manufacture,* Vol.50, Issue 5, pp. 474-479.

[30] Marra, J.J., Jupiter Fla, (1994), Tuned Mass Damper for Integrally Bladed Turbine Rotor, U.S. Patent 5,393,922.

[31] Rana, R. and Soong, T.T. (1998), "Parametric Study and Simplified Design of Tuned Mass Dampers", *Engineering Structures,* Vol. 20, No.3, pp.193-204.

[32] Li, C. (2000), "Performance of Multiple Tuned Mass Dampers for Attenuating Undesirable Oscillations of Structures under the Ground Acceleration", *Earthquake Engineering and Structural Dynamics,* Vol.29, pp. 1405-1421.

[33] Avila, S.M. and Gonçavles, P.B. (2009), "Optimal Configurations of Composite Multiple Mass Dampers in Tall Buildings", *J. Braz. Soc. Mech. Sci & Eng.,* Vol. 31, No.1, pp.75-81.

[34] Igusa, T. and Xu, K. (1994), "Vibration Control Using Multiple Tuned Mass Dampers", *Journal of Sound and Vibration",* Vol. 175, No.4, pp. 491-503.

[35] Jangid, R.S. (1999), "Optimization Multiple Tuned Mass Dampers for Based-Excited Undamped Systems", *Earthquake Engineering and Structural Dynamics,* Vol.28, pp. 1041-1049.

[36] Nishimura, I, Kobori, T., Sakamoto, M., Koshika, N., Sasaki, K. and Ohrui, S. (1992), "Active Tuned Mass Damper", *Smart Mater. Struct.* Vol.1, pp. 306-311.

[37] Pinkaew, T. and Fujino, Y. (2001), "Effectiveness of Semi-Active Tuned Mass Dampers Under Harmonic Excitation", *Engineering Structures,* Vol. 23, pp.850-856.

[38] Chen, S.R. and Wu, J. (2008), "Performance Enhancement of Bridge Infrastructure Systems: Long-Span Bridge, Moving Trucks and Wind with Tuned Mass Dampers", *Engineering Structures,* Vol.30, pp. 3316-3324.

[39] Muluka, V. (1998), "Optimal Suspension Damping and Axle Vibration Absorber for Reduction of Dynamic Tire Loads", MS Thesis, The Department of Mechanical Engineering, Concordia University, Montreal, Canada.

[40] Rao, M.D. (2003), "Recent Applications of Viscoelastic Damping for Noise Control in Automobiles and Commercial Airplanes", *Journal of Sound and Vibration*, Vol.262, pp. 457-474.

[41] Bianchini, E. (2005), "Active Vibration Control of Automotive Steering Wheels", *Society of Automotive Engineers,* 2005-01-2546.

[42] Black, M.D. and Rao, M.D., (2004), "Evaluation and Reduction of Steering Column Vibration of a rear Wheel Drive Sedan", *Int. J. Vehicle Noise and Vibration,* Vol.1 No.1, pp.122-141.

[43] Botti, J., Venizelos, G. and Benkaza, N. (1995), "Optimization of Power Steering System Vibration in Passenger Cars", *Society of Automotive Engineers,* 951253

[44] Sahinkaya, Y. (1996), "A Novel Steering Vibration Stabilizer", *Society of Automotive Engineers,* 960930.

[45] Goetchius G.M., Oakland, MI (2006), "Constrained Layer Viscoelastic Laminate Tuned Mass Damper and Method of Use", U.S. Patent 2006 / 0169557 A1

[46] Freitag, J., Gerhardt, F., Hausner, M. and Wittmann C., Schaeffler Symposium 2010.

[47] Cerri, J, Norwalk, OH, Weilnau, J. Huron, OH, (2006), "Multi-Directional Tuned Mass Damper with Unique Assembly", U.S. Patent 2006 / 0012090 A1.

[48] Formula 1 Latest, http://www.formula1latest.com/category/mass-dampers, Last visited date 20/06/2010.

[49] Formula 1, http://www.formula1.com/news/headlines/2006/8/4830.html, Last visited date 20/06/2010.

[50] Flannelly W. G. (1967), Dynamic Antiresonant Vibration Isolator, U.S. Patent 3,322,379

[51] Goodwin, J.H. (1965), Vibration Isolators, U.S. Patent 3,202,388

[52] Halwes D.R. (1981), Total Main Rotor System Analysis: Bell Helicopter Textron, NASA, Contractor Report No. 165667, Langley Research Center, Hampton Virginia.

[53] Strydom, J.P.D., Heyns, P.S., Niekert, J.L. (2002), "Development of a Vibration-Absorbing Handle for Rock Drills", *The Journal of the South African Institute of Mining and Metallurgy,* pp.167-172.

[54] Rita, A. D., McGarvey, J. H., Jones, R. (1978), "Helicopter Rotor Isolation Evaluation Utilizing the Dynamic Antiresonant Vibration Isolator", *Journal of the American Helicopter Society*, Vol. 23, No. 1, pp. 22-29.

[55] Jones, R. and McGarvey, J.H. (1976), "Helicopter Rotor Isolation Evaluation Utilizing the Dynamic Antiresonant Vibration Isolator", *SAE,* Document Number: 760894.

[56] Braun, D., (1982), "Development of Antiresonance Force Isolators for Helicopter Vibration Reduction", *Journal of the American Helicopter Society*, Vol. 27, No. 4, pp. 37–44

[57] Desjardins, R. A. and Hooper, W. E., (1980), "Antiresonant Rotor Isolation for Vibration Reduction", *Journal of the American Helicopter Society*, Vol. 25, No. 3, pp. 46–55

[58] Corcoran, P.E. , Ticks, G.E. (1984), "Hydraulic Engine Mount Characteristics", *SAE*, Document Number: 840407.

[59] Flower, W.C., (1985), "Understanding Hydraulic Mounts for Improved Vehicle Noise, Vibration and Ride Qualities, *SAE*, Document Number: 850975

[60] Ivovich, V.A and Onischenko, V.Y. (1990), *Vibration Protection in Engineering*. Mashinostroenie, Moscow, Russia.

[61] Nelson, F.C (1991), "Shock Vibration Isolation: Breaking the Academic Paradigm", *ASME PVP, Seismic and Vibration Isolation, No.5, pp. 1-6*

[62] Yilmaz, C. and Kikuchi, N. (2006), "Analysis and Design of Passive Band-stop Filter-type Vibration Isolators for Low-frequency Applications", *Journal of Sound and Vibration*, Vol. 291, pp. 1004-1028.

[63] Yilmaz, C. and Kikuchi, N. (2006), "Analysis and Design of Passive Low-Pass Filter-Type Vibration Isolators Considering Stiffness and Mass Limtiations", *Journal of Sound and Vibration*, Vol. 293, pp. 171-195

[64] Kılıç, V. (2003), "Generation of Deterministic Data From Signals of Known Power Spectral Density", *ME 513 Vehicle Dynamics Term Project*, Middle East Technical University.

APPENDIX

PATTERN SEARCH

Pattern Search is an optimization routine of MATLAB® and it does not require any gradient information of the objective function. It directly searches the points around the current point where the objective function is lower than the current point. If a point is found where the objective function value is lower than the current point, this point becomes the current point in the next iteration. At every successful iteration algorithm multiplies mesh size by 2 and at every unsuccessful iteration algorithm divides mesh size by 2. Optimization continues until mesh size becomes lower than a certain value. It can be utilized in systems on which the objective function is not differentiable or is not continuous. Following example obtained from MATLAB® Help File which defines how the Pattern Search works more clearly.

Assuming an initial point for an objective function:

$$x_0 = [2.1 \;\; 1.7] \tag{A.1}$$

At the first step the mesh size is 1 and the Pattern Search computes the objective function at the following mesh points:

$$[1 \;\; 0] + x_0 = [3.1 \;\; 1.7] \tag{A.2}$$

$$[0\ \ 1] + x_0 = [2.1\ \ 2.7] \quad \text{(A.3)}$$

$$[-1\ \ 0] + x_0 = [1.1\ \ 1.7] \quad \text{(A.4)}$$

$$[0\ \ -1] + x_0 = [2.1\ \ 0.7] \quad \text{(A.5)}$$

If the objective function is less than the initial point at any mesh point, then algorithm chooses that point as the current point and mesh size is multiplied by 2.

Assuming that at the point [1.1 1.7] the objective function value is less than the value at the initial point. Then this iteration is successful and mesh size in the second iteration becomes 2.

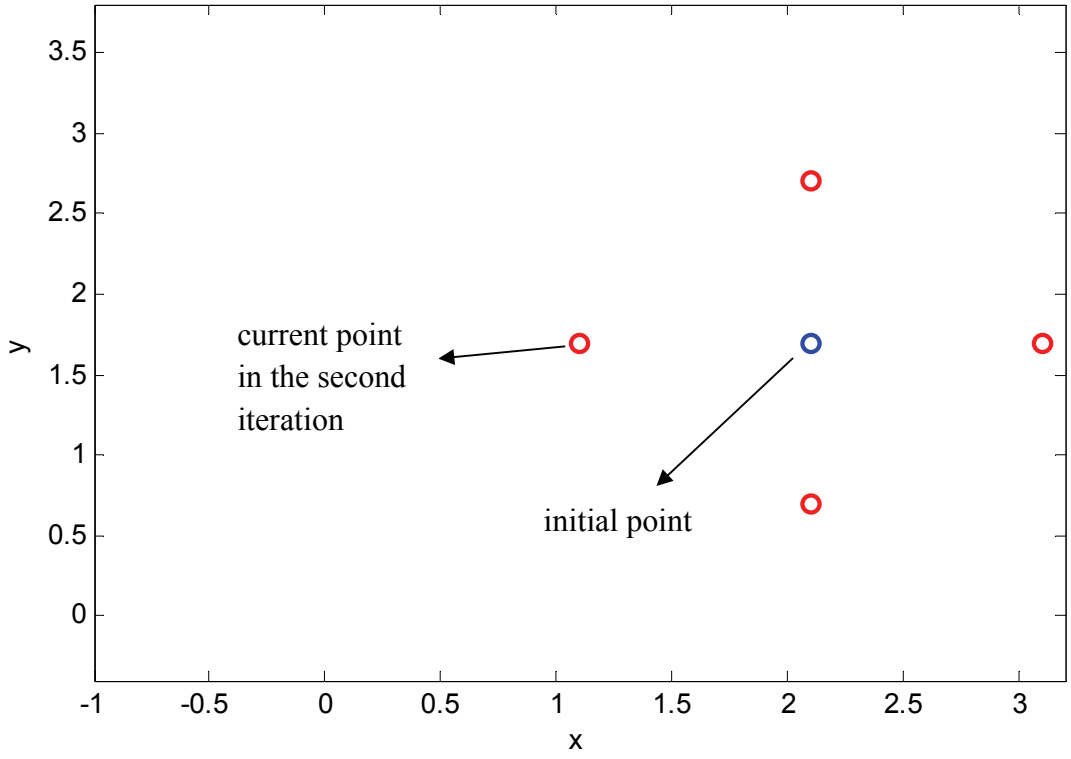

Figure A.1 Mesh Points Around the Initial Point

The current point in the second iteration is:

$$x_c = [1.1 \;\; 1.7] \tag{A.6}$$

The mesh in the second iteration include the following points:

$$[2 \;\; 0] + x_c = [3.1 \;\; 1.7] \tag{A.7}$$

$$[0 \;\; 2] + x_c = [1.1 \;\; 3.7] \tag{A.8}$$

$$[-2 \;\; 0] + x_c = [-0.9 \;\; 1.7] \tag{A.9}$$

$$[0 \;\; -2] + x_c = [1.1 \;\; -0.3] \tag{A.10}$$

Assuming that the value of the objective function at all mesh points is higher than the current point, then the current point remains the same and mesh size is divided by 2.

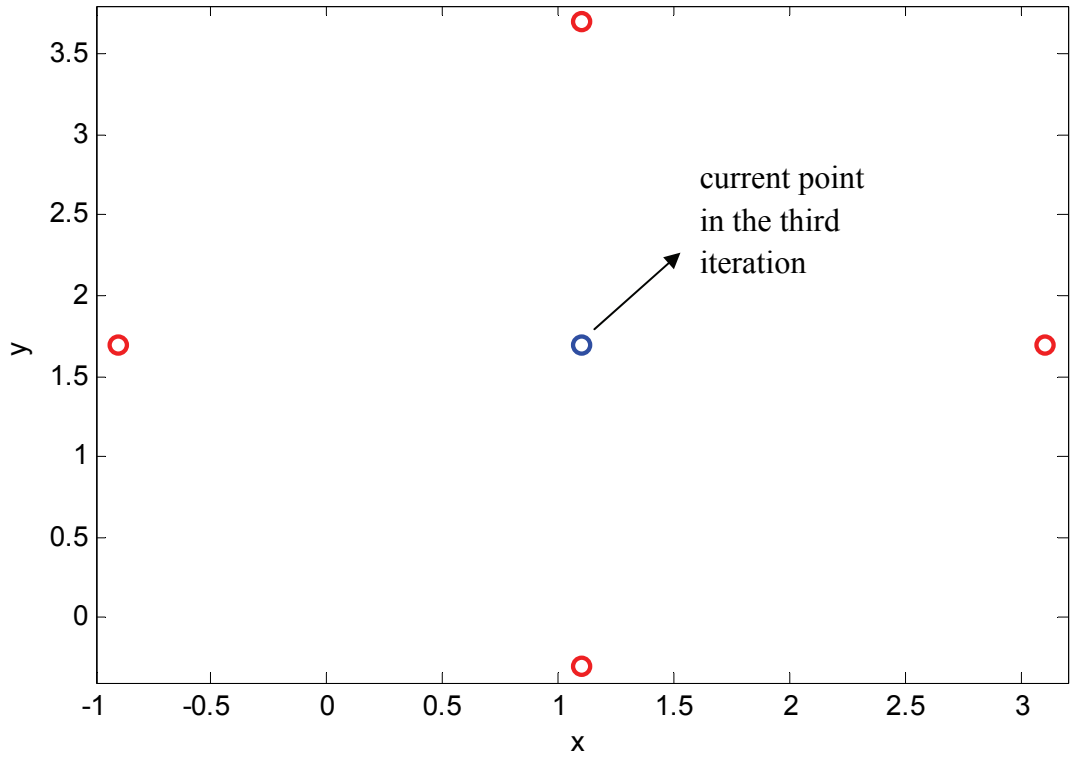

Figure A.2 Mesh Points Around the Current Point in Second Iteration

In the third iteration mesh points are as follows:

$$[1\ \ 0] + x_c = [2.1\ \ 1.7] \tag{A.11}$$

$$[0\ \ 1] + x_c = [2.1\ \ 1.7] \tag{A.12}$$

$$[-1\ \ 0] + x_c = [0.1\ \ 1.7] \tag{A.13}$$

$$[0\ \ -1] + x_c = [2.1\ \ 0.7] \tag{A.14}$$

Algorithm continues the iterations until the mesh size is lower than a predefined limit.

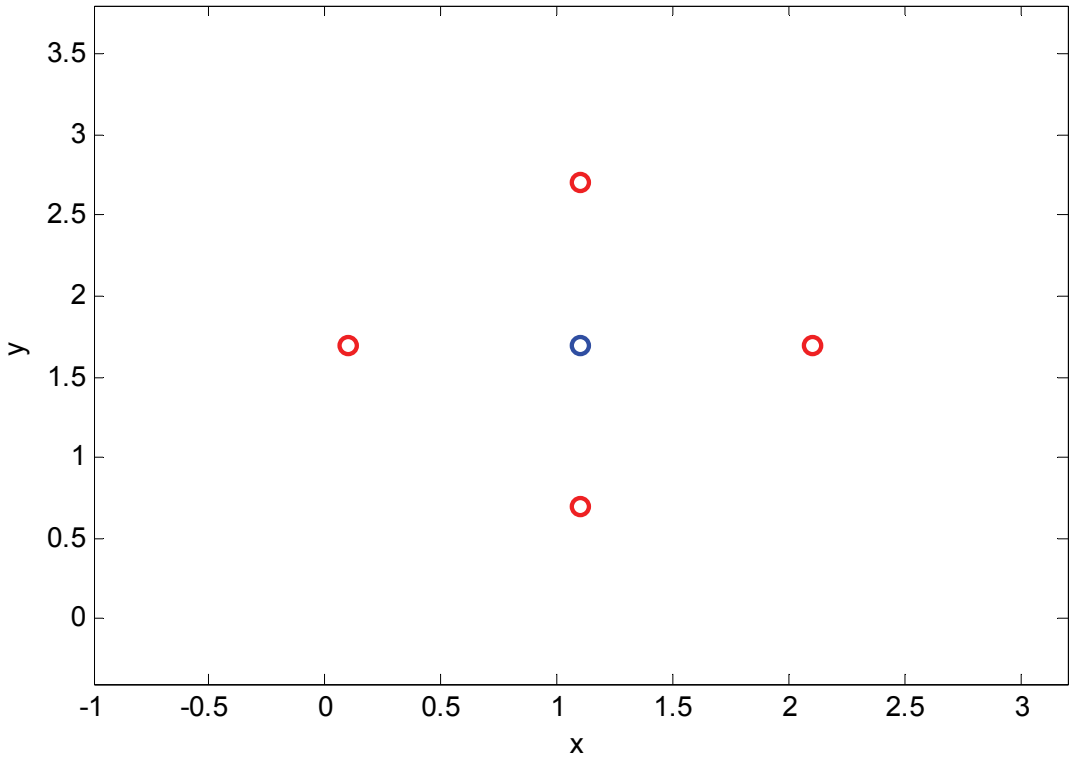

Figure A.3 Mesh Points Around the Current Point in Third Iteration